KTH Industrial Engineering and Management

Aqua Ammonia as Secondary Fluid in Ice Rink Applications

Brianna Kilberg

Master of Science Thesis

KTH School of Industrial Engineering and Management
Energy Technology TRITA-ITM-EX 2020:538
Division of Applied Thermodynamics and Refrigeration
SE-100 44 STOCKHOLM

<table>
<tr><td> 
KTH Industrial Engineering and Management</td><td colspan="2">Master of Science Thesis
TRITA-ITM-EX 2020:538

Aqua Ammonia as Secondary Fluid in Ice Rink Applications

Brianna Kilberg</td></tr>
<tr><td>Approved
2020-09-24</td><td>Examiner
Björn Palm</td><td>Supervisor
Monika Ignatowicz
Jörgen Rogstam</td></tr>
<tr><td></td><td>Commissioner</td><td>Contact person</td></tr>
</table>

Abstract

Refrigerant management is crucial in the attempts to slow climate change. Emissions from the refrigeration sector are primarily due to poor management and unsafe destruction of refrigerants currently in circulation. Safe refrigerant management and improving system operating efficiency can result in a reduction of emissions. Ice rinks are some of the most energy-intensive public buildings, providing both heating and cooling. The major share of energy in an ice rink is the refrigeration system, which consumes about 43%. There are more than 360 ice rinks in Sweden as of 2018 and the most common type of refrigeration system is an indirect system. With the push for natural fluids, aqua ammonia is becoming a more appealing option as a secondary fluid in ice rinks because of its minimal negative impact on the environment and favorable thermophysical properties. The main drawbacks of the fluid are its toxic characteristics and material compatibility. However, since the first use in 2007, there has been an increase to 34 of the total ice rinks in Sweden that have aqua ammonia as a secondary fluid.

Thermophysical properties are used to calculate refrigeration design parameters, including secondary fluid concentration and pumping power required. The properties of aqua ammonia have not been experimentally tested within this century to the extent presented in this thesis. Existing data is either derived from measured values taken several decades ago or has been calculated. The novelty of this thesis project stems from the unique and more accurate results measured through laboratory work and from the ability to determine the impact of the newly measured values in ice rink refrigeration design. A total of 11 varying concentrations of aqua ammonia were tested for density, dynamic viscosity, specific heat capacity, thermal conductivity, and corrosion of 7 metal specimens. The solutions tested ranged from 2 wt-% to 30 wt-%, correlating to freezing points from -2°C to -84°C. The measurements for density resulted in values similar to reference values, ranging in a difference of only 0.3% to 1.7%. Dynamic viscosity results followed nearly the same trend as references with changing temperature and solution concentration, with values varying from 0.8% to 17% different than references. Specific heat capacity measurements proved significantly different than reference values. The trend is opposite of the reference, leading to drastically different values, especially at lower temperatures and higher solution concentrations. The difference in values ranges from 0.1% to 28%. Thermal conductivity results show similar trends, but higher values than expected. The difference between measured values and reference values range from 0.1% to 13%. Corrosion results show that copper and brass have the highest corrosion rates of 16.2 mm/yr and 1.84 mm/yr, respectively. The most compatible specimen was stainless steel, followed by carbon steel, with maximum corrosion rates of 0.041 mm/yr and 0.11 mm/yr, respectively. Brass connections commonly used in industry were also tested and resulted in corrosion rates ranging from 69.6 g/yr to 112 g/yr, which accounts for about 1% and 1.5% of the connections' total weight lost per year. Compiling the laboratory measurements taken during the completion of this thesis project results in a more complete and accurate list of thermophysical properties for aqua ammonia that has never existed before.

These updated thermophysical properties for aqua ammonia, along with measured properties for other secondary fluids, were used to calculate operational parameters in a hypothetical ice rink refrigeration system. The results show that aqua ammonia is favorable with high COP and low pumping power, and therefore low pressure drop. Ammonia is most comparable to $CaCl_2$ and K-formate for most results. The changes in calculated COP between old reference data and new measured data were less than a 1% decrease when plotting versus the temperature of the ice surface and with a set pump control (ΔT) for cooling capacities of 200kW and 300kW. The change in heat transfer coefficients was more significant, with a range of about a 9% to 27% decrease in either the U-pipe under the rink floor or in a plate of the heat exchanger. Even though these heat transfer coefficient values are lower than previously calculated, the required pumping power is also lower using updated properties: 40% lower at a secondary fluid temperature of -10°C. Even though the change in heat transfer coefficients is larger with experimental values, the impact on COP is minimal.

The takeaway from this project is that aqua ammonia is a favorable secondary fluid compared to calcium chloride and ethylene glycol, the two most commonly used secondary fluids in ice rink refrigeration. A system using aqua ammonia would have a 45% and 47% lower pumping power requirement compared to calcium chloride and ethylene glycol, respectively. The system would also have a 4.7% and 11.6% higher COP when compared to systems with calcium chloride and ethylene glycol, respectively. The significantly lower pumping power will lower total energy demand of the ice rink, thus decreasing operation costs.

Abstrakt

Köldmediehantering är avgörande i försöken att sakta ner klimatförändringen. Utsläppen från kylsektorn beror främst på dålig hantering och osäker destruktion av köldmedier som för närvarande är i omlopp. Säkrare hantering av köldmedium och förbättrad systemdriftseffektivitet kan leda till ett minskat utsläpp. Ishallar är några av de mest energiintensiva offentliga byggnaderna som ger både uppvärmning och kylning. Den största andelen energi i en ishall är kylsystemet som förbrukar cirka 43%. Det finns mer än 360 isbanor i Sverige från och med 2018 och den vanligaste typen av kylsystem är ett indirekt system. Med trycket på naturliga vätskor blir ammoniakvatten ett mer tilltalande alternativ som en köldbärare i ishallar på grund av dess minimala negativa påverkan på miljön och gynnsamma termofysikaliska egenskaper. Köldbärares främsta nackdelar är dess toxiska karaktär och materialkompatibilitet. Sedan den första användningen 2007 har det dock skett en ökning till 34 av de totala ishallar i Sverige som har ammoniakvatten som köldbärare.

Termofysikaliska egenskaper används för att beräkna parametrar för kyldesign, inklusive köldbärares koncentration och pumpeffekten som krävs. Ammoniakvattens egenskaper har inte testats experimentellt under detta sekel i den utsträckning som presenteras i detta exjobb. Befintliga data härleds antingen från uppmätta värden som tagits för flera decennier sedan eller har beräknats. Nyheten härrör i detta exjobbsprojekt från de unika och mer exakta resultat som mätts genom laboratoriearbetet och från förmågan att bestämma effekten av de nyligen uppmätta värdena i kylskåpsdesign. Totalt 11 olika koncentrationer av ammoniakvatten testades med avseende på densitet, dynamisk viskositet, specifik värmekapacitet, värmeledningsförmåga och korrosion av 7 metallprover. De testade lösningarna varierade från 2 vikt-% till 30 vikt-%, korrelerade med fryspunkter från -2 ° C till -84 ° C. Mätningarna för densitet resulterade i värden som liknar referensvärdena, med en skillnad på endast 0,3% till 1,7%. Dynamiska viskositetsresultat följde nästan samma trend som referenser med förändrad temperatur och lösningskoncentration, med värden som varierade från 0,8% till 17% annorlunda än referenser. Specifika värmekapacitetsmätningar visade sig vara väsentligt annorlunda än referensvärden. Trenden är motsatt referensen, vilket leder till drastiskt olika värden, särskilt vid lägre temperaturer och högre koncentrationer. Skillnaden i värden varierar från 0,1% till 28%. Värmeledningsförmåga visar liknande trender, men högre värden än förväntat. Skillnaden mellan uppmätta värden och referensvärden sträcker sig från 0,1% till 13%. Korrosionsresultat visar att koppar och mässing har de högsta korrosionshastigheterna på 16,2 mm / år respektive 1,84 mm / år. Det mest kompatibla exemplet var rostfritt stål, följt av kolstål, med maximala korrosionshastigheter på 0,041 mm / år respektive 0,11 mm / år. Mässinganslutningar som vanligen används i industrin testades också och resulterade i korrosionshastigheter från 69,6 g / år till 112 g / år, vilket motsvarar för cirka 1% och 1,5% av anslutningarnas totala viktförlust per år. Att sammanställa laboratoriemätningarna som gjorts under slutförandet av detta projekt resulterar i en mer fullständig och noggrann lista över termofysikaliska egenskaper för ammoniakvatten som aldrig funnits tidigare.

Dessa uppdaterade termofysikaliska egenskaper för ammoniakvatten, tillsammans med uppmätta egenskaper för andra köldbärare, användes för att beräkna driftsparametrar i ett hypotetiskt kylsystem. Resultaten visar att ammoniakvatten är gynnsam med hög COP och en låg pumpeffekt och därmed ett lågt tryckfall. Ammoniakvatten är mest jämförbart med CaCl2 och K-formiat för de flesta resultat. Förändringarna i beräknad COP mellan gamla referensdata och nya uppmätta data var mindre än 1% minskning vid planering jämfört med isytans temperatur och med en inställd pumpkontroll (ΔT) för kylkapacitet på 200 kW och 300 kW. Förändringen i värmeövergångstal var mer signifikant, med ett intervall på cirka 9% till 27% minskning i antingen U-röret under golvet eller i en platta på värmeväxlaren. Även om dessa värmeövergångstal är lägre än tidigare beräknat, är den erforderliga pumpeffekten också lägre med hjälp av uppdaterade egenskaper: 40% lägre vid en köldbärarestemperatur på -10 ° C. Även om förändringen i värmeövergångstal är större med experimentella värden, är påverkan på COP minimal.

Slutsatser från detta projekt är att ammoniakvatten är en lämplig köldbärare jämfört med kalciumklorid och etylenglykol, de två vanligaste köldbärare i ishallskylning. Ett system som använder ammoniakvatten skulle ha ett pumpeffektbehov på 45% respektive 47% jämfört med kalciumklorid respektive etylenglykol. Systemet skulle också ha en 4,7% och 11,6% högre COP jämfört med system med kalciumklorid respektive etylenglykol. Den betydligt lägre pumpeffekten kommer att sänka det totala energibehovet för ishallar, vilket minskar driftskostnaderna.

Keywords

Ice rink, secondary fluid, aqua ammonia, ammonia water, thermophysical properties, corrosion, pressure drop, pumping power, refrigeration

Acknowledgements

Foremost, I would like to thank Monika Ignatowicz at the Applied Thermodynamics and Refrigeration Division at Royal Institute of Technology (KTH) for her continual support for the duration of the project. Monika's expertise, especially in the laboratory, made this thesis possible. Thank you for preparing all the numerous ammonia solutions, keeping the lab stocked with everything I could need, and for completing and/or managing the upkeep and repair of crucial equipment.

Next, I would like to express my sincere gratitude to Jörgen Rogstam of Energi & Kylanalys AB (EKA). Thank you for proposing this project and allowing me to work on it. This project would not be possible without your guidance and continuous outlook of the bigger picture. Thank you for funding this project through EKA and to the rest of the EKA employees who attended project status updates and provided feedback.

Thank you to the professors of the Applied Thermodynamics and Refrigeration department that helped introduce me to this project and to Björn Palm for his time in evaluating this work.

I would also like to thank my classmates of the InnoEnergy SELECT program and other students working in the KTH department of Applied Thermodynamics and Refrigeration for their encouragement and for creating a positive, enjoyable atmosphere during the completion of this project.

Of course, I would not be where I am without the continuous support of my family and friends. Thank you for being there for me, even if it is far in geographical terms.

Table of Contents

List of Figures

List of Tables

Nomenclature

A_s	amplitude of blank in DSC methodology	W
A_s	amplitude of sample in DSC methodology	W
A_{s_i}	initial surface area	cm^2
$CaCl_2$	calcium chloride	-
CC	cooling capacity	kW
CFC	chlorofluorocarbon	-
CO_2	carbon dioxide	-
C_p	specific heat capacity	$J \cdot g^{-1} \cdot K^{-1}$
DSC	differential scanning calorimetry	-
EG	ethylene glycol	-
E_p	pumping power	kW
F-gases	fluorinated greenhouse gases	-
GHG	greenhouse gases	-
Gt CO2 eq.	gigatons CO_2 equivalent	-
GWP	global warming potential	-
h	convection heat transfer coefficient	$W \cdot m^{-1} \cdot K^{-1}$
HCFC	hydrochlorofluorocarbon	-
HFC	hydrofluorocarbons	-
k	thermal conductivity	$W \cdot m^{-1} \cdot K^{-1}$
K	constant used for calculating corrosion rate	-
K-acetate	potassium acetate	-
K-formate	potassium formate	-
m_{empty}	mass of empty pycnometer	g
m_f	mass of metal specimen after corrosion test	g
m_{full}	mass of full pycnometer	g
m_i	mass of metal specimen before corrosion test	g
m_s	mass of sample in DSC test	g
NH_3	ammonia	-
ODP	ozone depletion potential	-
P_{comp}	compressor power	W
PFC	perfluorocarbons	-
P-h diagram	pressure-enthalpy diagram	-
PHE	plate heat exchanger	-
PG	propylene glycol	-

P_{pump}	pumping power	W
$\dot{Q}$	heating power	kW
$\dot{Q}_2$	cooling capacity	W
SCF	scale calibration factor	-
t	duration of test	hr
T	temperature	°C (or K)
ΔT	- temperature difference	K
T_c	calibration temperature	°C
T_f	freezing point temperature	°C
TPS	transient plane source	-
T_{ref}	reference temperature	°C
T_{room}	room temperature	°C
T_s	sample temperature	°C
$u(x_1)$	instrument uncertainty of pycnometers	cm^3
$u(x_2)$	instrument uncertainty of balance	g
$u_c(y)$	combined uncertainty	$g \cdot m^{-3}$
V	volume	cm^3
$\dot{V}$	volumetric flowrate	$m^3 \cdot s^{-1}$
V_{cor}	corrected volume	cm^3
V_{ct}	volume at calibration temperature	cm^3
VCRS	vapor-compression refrigeration system	-
wt-%	measure of concentration; weight percentage	-
x_1	measured volume from pycnometers	cm^3
x_2	weight measurements from balance	g
y	calculated density	$g \cdot m^{-3}$
α	coefficient of mean linear thermal expansion	K^{-1}
β	heating rate	$K \cdot s^{-1}$
$\eta_{20,REF}$	reference values for refractive index at 20°C	-
$\eta_{D,20}$	refractive index reading from scale at 20°C	-
$\eta_{D,room}$	refractive index reading from scale at room temperature	-
μ	dynamic viscosity	mPa·s
ρ	density	$kg \cdot m^{-3}$
ρ_{air}	density of air	$kg \cdot m^{-3}$
ρC_p	volumetric heat capacity	$kJ \cdot m^{-3} \cdot K^{-1}$

1 Introduction

1.1 Climate Change and Refrigeration

It is evident that the climate is drastically changing due to human impact on the earth and its atmosphere. Global efforts are being made to limit and eventually reverse this impact. An example of the cooperation amongst different nations is the Paris Agreement, which is an arrangement between around 127 countries, or parties, to combat climate change and keep the global temperature rise during this century to less than 2°C from pre-industrial levels (UNFCCC, 2017). Other similar agreements or regulations that have been passed are the Montreal and Kyoto Protocols, which set ozone depletion and global emission reduction goals, and the F-Gas Regulation and MAC Directive, which control emissions from fluorinated greenhouse gases (F-gases) within the European Union (EU). F-gases are manmade gases that contain fluorine and can be categorized into three main types: hydrofluorocarbons (HFCs), perfluorocarbons (PFCs), and sulfur hexafluoride (SF_6). F-gases were developed to replace chlorofluorocarbon (CFCs) and hydrochlorofluorocarbon (HCFCs) gases with high ozone depletion potential, but they have extremely high global warming potential. There are now goals and regulations to reduce the use of F-gases in existing systems and eliminating their use in new equipment to eventually eliminate global warming from these gases. In addition to the F-gas Regulation in Europe, the Kigali Amendment of the Montreal Protocol also aims to reduce use of HFCs in participating countries, specifically by 80% over the next 30 years ("Montreal Protocol," 2019).

One of the main uses of HFCs is in the refrigeration industry, specifically in equipment for refrigeration, heat pumps, and air conditioning (European Commission, 2016). The refrigeration sector accounts for 7.8% of global greenhouse gas (GHG) emissions coming from around 3 billion systems in operation across the globe today (Didier et al., 2017). Emissions of the refrigeration sector come from both direct and indirect sources. Direct emissions refer to the actual release of the refrigerants being used in the system that can occur during charging, maintenance, dismantling or through leaks during operation. Indirect emissions are associated with the energy produced in order to operate the systems. Indirect emissions primarily come from electricity generation to power the systems and can also come from fuel consumption, such as in the case of the automotive air conditioning. Of the total amount of emissions from the refrigeration sector, about 37% are direct emissions of CFCs, HCFCs, and HFCs and 63% are indirect emissions mainly consisting of CO_2 (Didier et al., 2017).

In order to evaluate and compare the impact of different GHGs on the environment, the global warming potential (GWP) index was created. GHGs are difficult to compare directly because each can have a different lifetime and radiative efficiency, or their ability to absorb energy in the atmosphere, but the GWP takes both of these factors into account. The GWP is a measure of the amount of energy a certain mass of gas will absorb over a certain amount of time relative to the amount of energy the same mass of CO_2 will absorb (US EPA, 2016). It is common to use the timeframe of 100 years when calculating GWP but can have its disadvantages since some gases have a lifetime shorter than 100 years, such as HFCs. However, using a shorter timeframe could lead to overestimations of the impact of gases with shorter lifetimes. Radiative forcing, a type of measure for radiative efficiency, can be used to measure the current effects of GHGs in the atmosphere from past emission releases, while GWP is used to predict the impact of the GHGs being emitted today as well as in the future. Figure 1 shows the amount of radiative forcing for a few types of GHGs exclusively related to the refrigeration sector.

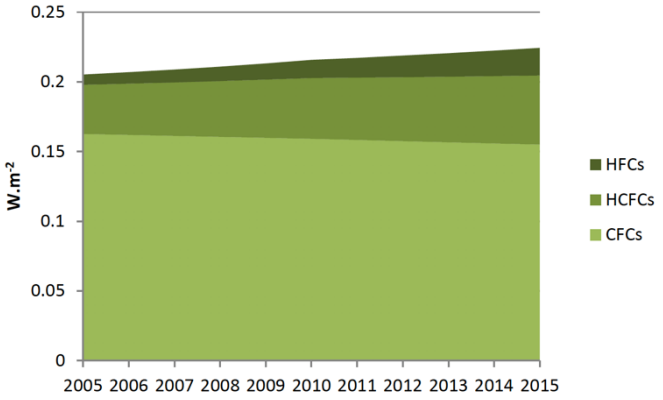

Figure 1: Changes in total radiative forcing in the refrigeration sector from 2005-2015 (Didier et al., 2017).

The refrigeration sector is estimated to grow mostly due to the increased need and availability of cooling systems in developing countries. The importance of international treaties or agreements is crucial to limit the emissions from the refrigeration sector, especially with this expected growth. Figure 2 shows the predicted HFC emissions per year from the refrigeration sector until 2050 with the implementation of the Kigali Amendment and without. According to this graph, following the Kigali Amendment could decrease total emissions by a maximum of 51% from 2020 to 2050, which would cumulatively be about a 30-40 $GtCO_2$ eq (Didier et al., 2017).

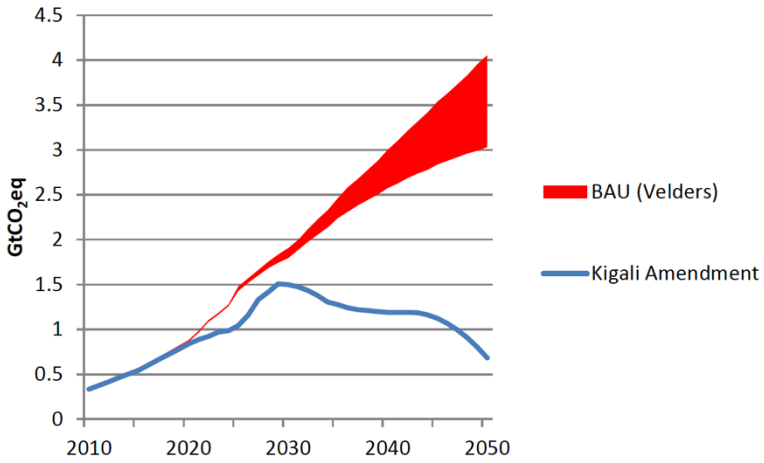

Figure 2: Predicted HFC emissions from the refrigeration sector with and without the Kigali Amendment (Didier et al., 2017).

Similarly, Project Drawdown reports similar possible savings of $GtCO_2$ eq. Project Drawdown is a research organization that identifies and analyzes the most viable climate change solutions. Out of 80 identified solutions, refrigerant management was ranked first in terms of reduced gigatons of CO_2 eq from 2020 to 2050 (Steyer, 2017). The project estimates that nearly 90 $GtCO_2$ eq of emissions can be avoided through the management and safe destruction of refrigerants already in circulation. Furthermore, an additional 25 to 78 GtCO2 eq of emissions can be avoided by phasing out HFCs according to the Kigali Agreement (*Refrigerant Management*, 2017). Although a majority of these predicted reductions in emissions relate directly to the handling of refrigerants already being used, it is important to note that a significant amount of emissions can also be saved by significantly reducing the use of HFCs. Alternative refrigerants to HFCs could include synthetic fluids with low GWP and ozone depletion or natural refrigerants.

A method to reduce the use of harmful refrigerants would be to utilize indirect refrigeration systems. These systems require a lower refrigerant charge in the primary refrigeration cycle and rely on a secondary fluid to transfer the lower temperatures to the designated areas. Indirect systems have a lower risk for harmful or dangerous leaks since there is less primary refrigerant to be released. Furthermore, secondary fluids directly impact the efficiency of and energy required by the refrigeration system. For example, the secondary fluid should have low viscosity in order to reduce the pumping power needed to circulate the fluid. The thermophysical properties should be such so that heat transfer between the secondary fluid and the primary refrigerant and the area to be cooled is effective as well as efficient. Indirect systems are most efficient when utilizing a proper secondary fluid, hence the secondary fluid choice is crucial.

1.2 Project Objective

The purpose of this thesis is to provide previously unavailable or nonexistent information on the implementation of aqua ammonia as a secondary fluid in indirect refrigeration systems, specifically in ice rinks. This refers to both the determination of thermophysical properties of aqua ammonia as well as a comparison of the utilization of various secondary fluids for the ice rink industry. Historically, aqua ammonia has not been thoroughly studied in aspects relating to its properties, which lead to a lack of reliable data available today. This lack of data means that refrigeration systems with aqua ammonia as a component have been designed while using unverified values, which has become the norm. However, with a push towards natural fluids, it has become apparent that there is much to learn when it comes to designing

systems, and specifically ice rinks, with aqua ammonia as a secondary fluid. This relatively new realization has been the motivation behind the work completed during this thesis. The aim is to verify the thermophysical properties and to use these updated, accurate values to determine the advantages and disadvantages of using aqua ammonia as the secondary fluid in ice rinks compared to other commonly used secondary fluids. The results from this thesis will hopefully be the first step toward a wider acceptance and implementation of aqua ammonia as the secondary fluid in ice rinks.

1.3 Refrigeration Systems

Refrigeration is the extraction of heat from a heat source at a lower temperature to a heat sink at a higher temperature. Three common refrigeration cycles are outlined in this section (Shan K. Wang, 2001).

1.3.1 Vapor-Compression

Vapor-compression refrigeration systems (VCRS) operate by circulating a refrigerant through the system that undergoes phase changes in order to absorb heat from the area to be cooled and releases it elsewhere, dependent on system specifics. Figure 3 is a diagram outlining the main components of a vapor-compression cycle. The refrigerant is compressed as shown in stream 1 to stream 2. The refrigerant enters the compressor as a saturated vapor and is converted to a superheated vapor, which has a higher temperature and pressure. The superheated vapor, stream 2, then passes through a condenser, where heat is removed from the fluid and is converted to a saturated liquid, stream 3. The saturated liquid then passes through an expansion valve where pressure and temperature are decreased. The resulting cold stream 4 then flows through the evaporator, where heat is absorbed from the air or liquid to be cooled. The cycle continues with the refrigerant flowing through the compressor. A VCRS can be either direct, operating by the method described above, or indirect, where a secondary fluid is circulated to absorb heat from the area to be cooled and does not go through the vapor-compression cycle. This system is explained in later sections of this report.

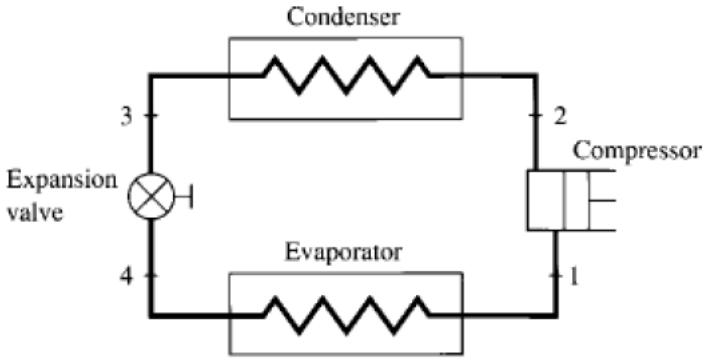

Figure 3: Schematic of a vapor-compression refrigeration cycle (Shan K. Wang, 2001).

The VCRS can be analyzed through a pressure-enthalpy curve, shown in Figure 4. The graph shows the thermodynamics of the cycle at the different stages briefly outlined above. VCRSs are the most common refrigeration system utilized and are in use in many different applications. Applications of the VCRS systems range from domestic, commercial, and industrial refrigeration to food processing and transport refrigeration.

1.3.2 Absorption

An absorption system has similar properties to the VCRS but uses an external heat source to initiate the evaporation phase. The first step in an absorption system, a refrigerant is at a low partial pressure and is evaporated. The gaseous refrigerant extracts heat from a medium to be cooled and is absorbed by an absorbent fluid. A thermal energy input then heats the fluid containing the absorbent and the refrigerant, initiating the evaporation of the refrigerant and continuing the cycle.

1.3.3 Gas Expansion Systems

In expansion systems, mechanical work is used to compress air or another gas to a high pressure. The gas is then expanded, decreasing pressure and temperature, which provides a cooling effect. Gas expansion systems have very similar principles to a VCRS, but the fluid is a gas and does not go through phase changes.

1.4 Operation Principle

A vapor-compression refrigeration system can be designed to provide a cooling effect indirectly. This means that there is a primary fluid undergoing the phase changes in the vapor-compression cycle as well as a secondary fluid that rejects heat to the primary fluid, therefore providing a cooling effect to the desired area. The primary fluid can also be referred to as the primary refrigerant and the secondary fluid can be referred to as the secondary refrigerant, secondary coolant, or brine. This report will use the term secondary fluid.

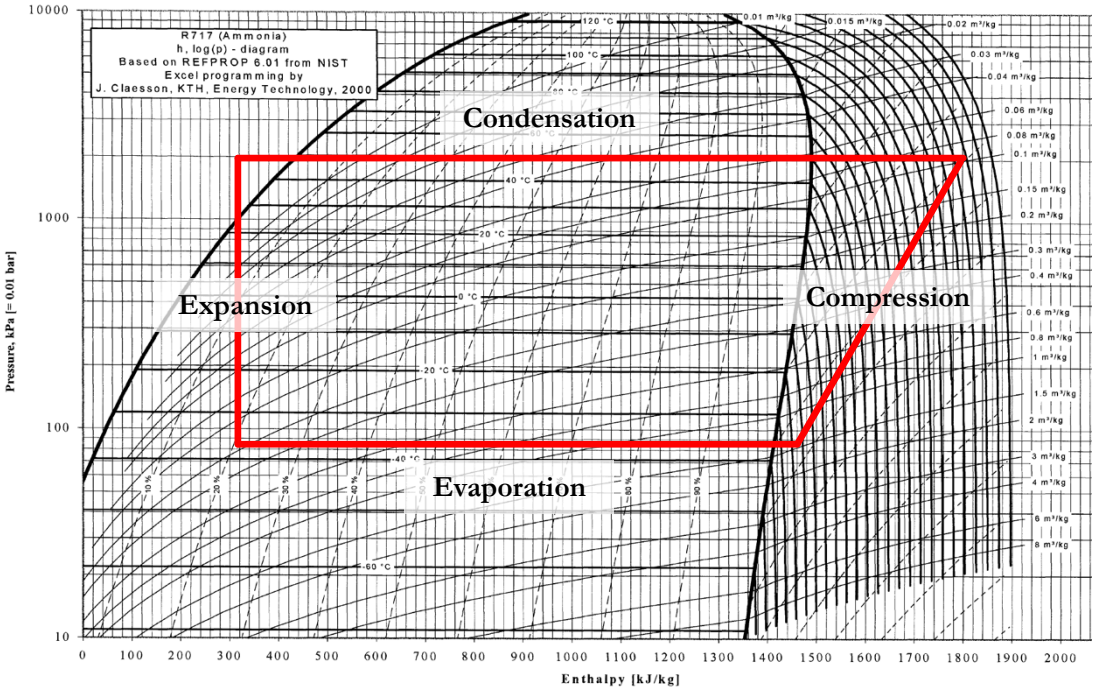

Figure 4: Pressure-enthalpy (P-h) diagram of ammonia with stages of a theoretical refrigeration cycle (Granryd et al., 2009).

An indirect system includes either two or three circuits: one for the primary refrigerant, one for a secondary fluid providing the cooling effect, and an optional circuit for another secondary fluid removing heat from the system. As mentioned, the vapor-compression part of the system consists of a compressor, condenser, expansion valve, and evaporator for the circulation and function of the primary refrigerant. The secondary circuits add circulation pumps and heat exchangers to the overall design of the system. Figure 5 shows a diagram of an indirect system with secondary fluids on the evaporator side of the system.

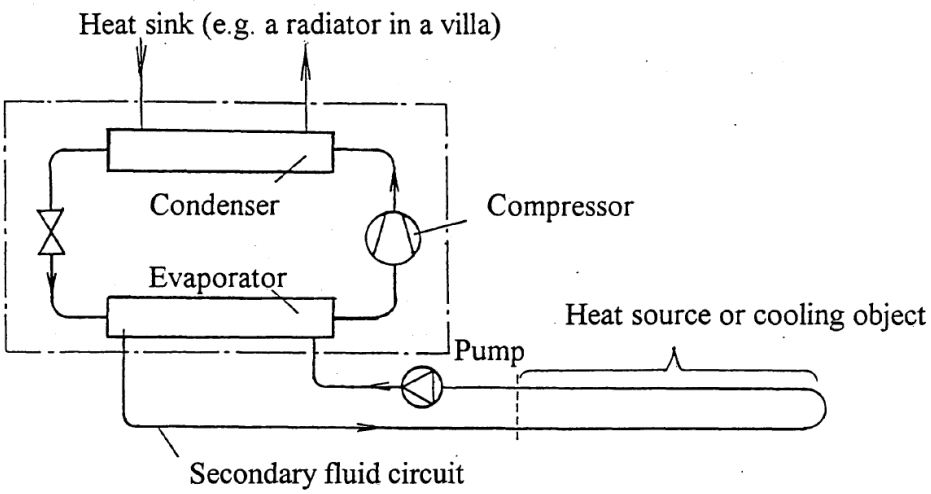

Figure 5: Schematic of an indirect refrigeration system (Granryd et al., 2009).

1.5 Indirect System Advantages and Disadvantages

The main advantage of indirect systems is the ability to reduce the size of the primary refrigeration system. The reduction in size allows for a smaller circulation loop for the primary refrigerant and a compact system that can be located in an isolated machine room. This also results in a lower primary refrigerant charge, which provides safer operating conditions and decreases the impact of potentially damaging leaks of the refrigerant. In some cases, such as ammonia and propane systems, the primary refrigerant charge can be between 5-15% of that for direct systems (Melinder, 2010a, p. 200). Hazardous or flammable natural refrigerants are more easily used in systems that are compact because it decreases risk of harm in the case of a primary refrigerant leak. The smaller operation area allows for easier detection of a leak while also keeping the leak out of contact with people. Furthermore, with smaller circuits required for the primary refrigeration cycle, it is more likely that the piping can be constructed in a manufacturing facility instead of assembled onsite. This possibility is increasingly more important as the shift towards natural refrigerants strengthens.

The main disadvantage of indirect systems is the additional equipment and pumping power required. An additional fluid circulating in the system requires an additional pump, heat exchanger, and piping. This added equipment, as well as the secondary fluid itself, increases the initial cost of the system. The secondary fluid in the system requires additional pumping power, increasing energy consumption. The added heat exchanger increases the temperature difference, which leads to a decrease in evaporation temperature. A decrease in evaporation temperature of around 2-4 K conservatively results in around a 10-15% increase in total energy. However, it has been determined that a properly designed indirect system may have a lower energy consumption annually when compared to direct systems. Part of the reasoning behind this is because an indirect system can adapt easier to variations in ambient temperature (Melinder, 2010a). The selection of the secondary fluid can impact pumping requirements, which is why it is advantageous to choose a fluid that requires less pumping power.

Indirect systems are often used in applications where the area to be cooled is very large or not necessarily located conveniently close to the primary refrigeration cycle. These applications include large butcheries, dairies, food warehouses, ice rinks, air conditioning plants, commercial supermarkets, and ground source heat pumps. This project focuses on the ice rink application.

1.6 Secondary Fluids

Secondary fluids are selected based on various factors, including environmental impact, health and safety, system compatibility, and thermophysical properties. Ideally, the fluid will have minimal or no negative impact on the environment, no risks to the health or safety of humans, no compatibility issues with existing systems and equipment, and suitable thermophysical properties for optimal system operation. Completely satisfying all of these parameters is not possible, hence compromises must be made when choosing the secondary fluid. The importance of the risks of secondary fluids and refrigerants to the environment and to the health and safety of people have been outlined earlier in this report or are self-explanatory. The thermophysical properties that are analyzed when selecting secondary fluids are outlined below and include freezing point, density, dynamic viscosity, specific heat capacity, and thermal conductivity. Although it is not a thermophysical property, one of the following subsections also briefly describes corrosive properties. Corrosion and material compatibility need to be examined to ensure compatibility with existing systems.

Water could be considered a suitable secondary fluid due to its thermophysical properties, specifically its high specific heat capacity and low viscosity. However, water has a high freezing point and corrosive properties. The freezing point of water, 0°C, limits the range of applications since it is common for refrigeration systems to reach a temperature well below 0°C. Since water has the capability to dissolve more substances than any other liquid, it is referred to as the "universal solvent." This capability means that other substances can be added to water to lower the freezing point of the fluid, allowing it to be suitable in more refrigeration applications. Hence, most secondary fluids are water-based (Ignatowicz, 2008). Some commonly used secondary fluids in addition to pure water are hydrocarbons, ammonia, carbon dioxide, glycols, alcohols, and salt solutions (SWEP, n.d.).

1.6.1 Freezing Point

The freezing point of a fluid is the temperature at which ice crystals start to form. This causes complications to the system in terms of pumping the fluid and in the tubes of heat exchangers, in addition to affecting other thermophysical properties. Secondary fluids are mixtures of different freezing point depressants, referred to as additives, such as alcohols, salts, or glycols with water, which decreases the freezing point of the fluid while attempting to maintain other favorable properties of water. A secondary fluid should have a freezing point around 5 to 10 K below the normal operating temperature and should be sufficiently lower than the lowest expected operating temperature (Melinder, 2010a). However, the freezing point of the solution should be chosen carefully because lower freezing points require a secondary fluid with higher additive concentration, which requires higher pumping power and lowers heat transfer. Simply, the freezing point, and therefore solution concentration, should be chosen so that it is certain that no ice crystals will form and isn't unnecessarily low.

1.6.2 Density

Density relates the mass of a solution per unit of volume and changes with the concentration of additive in the secondary fluid. A higher density is preferred when choosing secondary fluids because it results in better heat flow characteristics. Conversely, high density should not result in high viscosity.

1.6.3 Dynamic Viscosity

Viscosity generally refers to the ability of a liquid to flow and can be measured as dynamic (or absolute) viscosity or kinematic viscosity. Dynamic viscosity is a measurement of a liquid's internal resistance to flow and kinematic viscosity is the ratio of a fluid's dynamic viscosity to its density. Dynamic viscosity is used when selecting secondary fluids because it gives the amount of force needed to make the fluid flow at a certain rate (Nieto, 2015). This information, along with the kinematic viscosity, is pertinent when considering the pumping power required to circulate the secondary fluid and when sizing the pump. Hence, the lower the dynamic viscosity, the less pumping power required, which results in energy savings.

1.6.4 Specific Heat Capacity

The specific heat capacity, referred to simply as specific heat in this report, of a liquid is the amount of thermal energy required to increase the temperature of one unit of mass by one unit of temperature. Secondary fluids should have a high specific heat because it requires a lower volumetric flow rate to achieve a certain heating power, which in turn affects the heat transfer coefficient. Volumetric heat capacity is an indicator of the ability of the fluid to convey heat directly through its motion (Melinder, 2007).

1.6.5 Thermal Conductivity

Thermal conductivity is the measure of a fluid's ability to conduct heat. It is ideal for secondary fluids to have high thermal conductivity because it results in better heat transfer between the fluid and heat source and sink of the system. It also decreases the temperature difference between the fluid and the tube walls in the evaporator and heat exchangers, which results in a smaller pressure drop, requiring less pumping power (Melinder, 2010a).

1.6.6 Corrosion

Corrosion is a chemical process that destroys the structure of materials. When the secondary fluid is in contact with certain materials, an electrochemical process can take place where spontaneous oxidation and reduction occurs on the material's surface and causes deterioration (Ignatowicz, 2008). Understandably, a secondary fluid should be chosen that does not corrode any part of the equipment within the system. Corrosion within the system will lead to leaks and potentially more detrimental damage.

1.7 Ammonia in Refrigeration Systems

The main incentive to use ammonia as a primary refrigerant and aqua ammonia as a secondary fluid is that it is a natural compound and has minimal negative impact on the environment while also having favorable thermophysical characteristics. However, there are disadvantages of the solution that keep it from being widely used in industry. This section details the history of use of ammonia and aqua ammonia in industry,

the advantages and drawbacks to using ammonia and aqua ammonia, as well as the extent of their use in the refrigeration industry. For reference, ammonia is the natural compound with the chemical formula of NH_3. Pure ammonia, or anhydrous ammonia, is used as a primary refrigerant, while a solution of ammonia and water is used as secondary fluid, which has a chemical formula of NH_4OH. This solution can be called aqua ammonia, ammonium hydroxide, ammonia water, or aqueous ammonia.

1.7.1 Ammonia as a Primary Refrigerant

Ammonia was first used as a primary refrigerant around 1850 and continued to be used until the 1930s, when chlorofluorocarbons (CFCs), artificial refrigerants, were developed (Riffat et al., 1997). However, by the late 1980s, the harmful ozone-depleting and global warming effects of CFCs were discovered and there was a shift back towards natural refrigerants (Riffat et al., 1997). Ammonia is relatively common in medium to large scale industrial refrigeration systems.

Anhydrous ammonia has been commonly used as a primary refrigerant in medium- to large-scale industrial systems, such as in the food industry and process cooling (Pearson, 2008). Its continued use since the 1930s proves that its thermodynamic properties are ideal in providing the required cooling effect, considering it to be one of the most efficient refrigerants (Linde, n.d.). As a natural refrigerant, ammonia has a GWP and ODP of zero, making it a strong competitor to commonly used HCFCs. Furthermore, it is a readily available, low cost substance (ASHRAE Refrigeration Committee, 2017). These advantages also apply to an ammonia solution with water for secondary fluid applications.

The key disadvantages of ammonia are its toxicity and material compatibility. Anhydrous ammonia is considered to be an extremely hazardous substance by the U.S. Environmental Protection Agency (EPA) and as a dangerous substance by the European Chemical Agency (ECHA). Anhydrous ammonia causes severe burns to the skin and eye damage and is toxic if inhaled and to aquatic life (*Ammonia, Anhydrous - Substance Information - ECHA*, n.d.). Even though it is toxic, ammonia has a pungent odor, which allows for its detection well before being exposed to harmful levels (ASHRAE Refrigeration Committee, 2017). While ammonia is considered to be flammable, ASHRAE classifies the risk as low. Moreover, ammonia is corrosive to some metals, including copper and brass. Therefore, the cost of upgrading or installing a system for use with ammonia might increase with the choice of materials, such as stainless steel.

Despite these disadvantages, ASHRAE supports the use of ammonia as a refrigerant. With well-designed and well-operated systems, ammonia is a safe refrigerant to use while not posing any risks to the environment. Furthermore, using aqua ammonia as a secondary fluid in indirect systems allows for a lower concentration of ammonia, further decreasing the risks it poses.

1.7.2 Aqua Ammonia as a Secondary Fluid

A literature review illustrates the lack of published papers on the use of aqua ammonia as a secondary fluid in indirect refrigeration systems. It appears that aqua ammonia, with respect to the refrigeration sector, has only been studied as a fluid used in absorption coolers. Furthermore, the thermophysical properties of aqua ammonia used to design indirect systems have not been experimentally confirmed. This means that even today, industry is using values from the early 1900s that are either estimated or extrapolated.

The values that are currently used as reference values can be traced back to a limited number of outdated sources. Over the years, books have been published that list the thermophysical properties of aqua ammonia solutions but refer to the same values as previously reported. For example, a book by Jean Timmermans published in 1960, as seen in Figure 6, lists all of the constants previously reported for various binary systems, including aqua ammonia. Experimental data was given preference over extrapolated data and was collected from original sources wherever possible. The references come from years ranging from 1856 to 1955, with a vast majority of the references published prior to 1930 (Timmermans, 1960). Furthermore, most data collected was equilibrium data, freezing temperatures, and density of varying solution concentrations. Relatively, there was a significantly lower quantity of data for viscosity, optics, and thermal constants, some of which are crucial for designing refrigeration systems. This trend was evident over various sources and collections of data, listed in Table 1. Additionally, in the cases where an experimental value was reported, the original source rarely, if ever, stated the experimental methodology used to find the measurement.

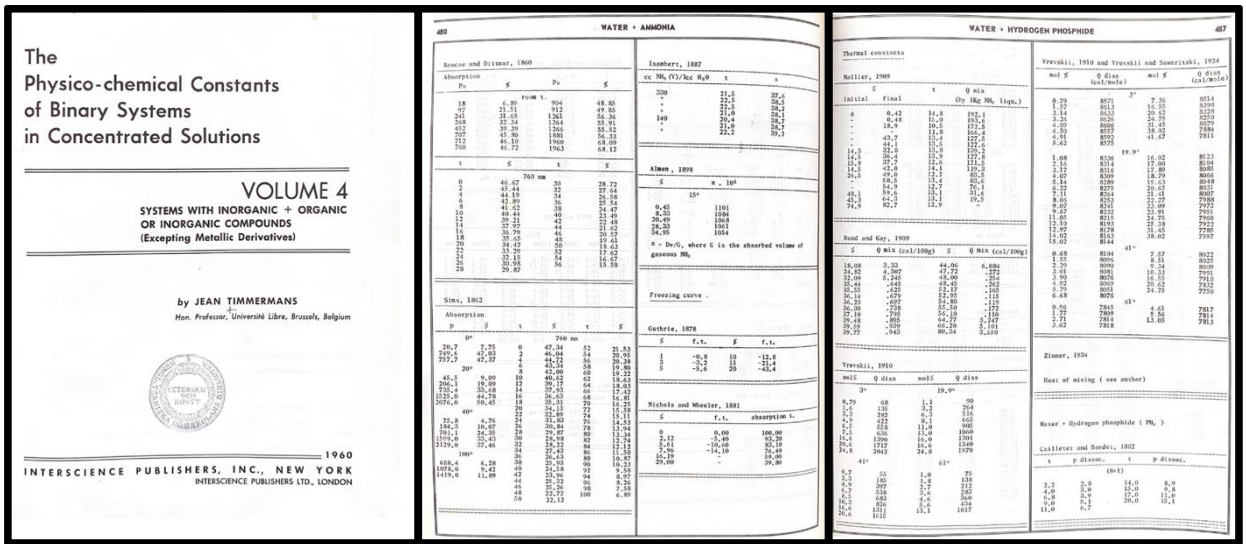

Figure 6: Excerpts from compilation of thermophysical properties of binary systems, specifically aqua ammonia (Timmermans, 1960).

For comparison of results from the experimental work completed for this thesis, the reference values are from tables compiled by Melinder for an International Institute of Refrigeration (IIR) book published in 2010 (Melinder, 2010b). These references were the same as reported in the Engineering Licentiate Thesis by Melinder in 1998 (Melinder, 1998). This list of references compiled during the literature review includes a total of 57 references, ranging from main literary sources of aqueous solution data to references from previously published IIR publications. The selected references used for aqua ammonia density, viscosity, specific heat and thermal conductivity values in the tables are listed in Table 1.

Table 1: List of literary sources for density, viscosity, specific heat capacity, and thermal conductivity data for aqua ammonia solutions (Melinder, 1998).

Reference Number as in Melinder (1998)	Reference for Specific Heat Capacity or Thermal Conductivity	Literature Source
[1]	Density Viscosity Specific Heat Capacity	CRC Handbook of Chemistry and Physics, 67th Edition (1986-87)
[3]	Density Specific Heat Capacity	International Critical Tables of Numerical Data, Physics, Chemistry, and Technology (1928-29)
[4]	Thermal Conductivity	Landolt-Börnstein; Eigenschaften der Materie in Ihren Aggregatzuständen (1960-1971)
[5]	Density Specific Heat Capacity	Landolt-Börnstein; Numerical Data and Functional Relationships in Science and Technology; Vol 1b (1977)
[6]	Density Viscosity	The Physico-chemical Constants of Binary Systems in Concentrated Solutions, Vol. 3-4; J. Timmermans (1960) Density: Mittasch, Kuss, and Schlieter (1926) Viscosity: Pagliani and Batelli (1884)

[21]	Density Viscosity Specific Heat Capacity Thermal Conductivity	Handbuch der Kältetechnik, VI/B; R. Plank (1988)
[36]	Specific Heat Capacity Thermal Conductivity	Thermophysical Properties of Liquid Secondary Refrigerants (Tables and Charts); Å. Melinder (1997)
[52]	Viscosity Specific Heat Capacity Thermal Conductivity	Handbuch der Kältetechnik, VII; R. Plank (1959)

1.8 Ice Rink Refrigeration

A common application of indirect refrigeration systems is indoor ice rinks. The primary refrigeration cycle is carried out in a machine room with the secondary fluid being circulated through distribution pipes that run under the ice slab. A diagram of an indirect system in an ice rink can be seen in Figure 7.

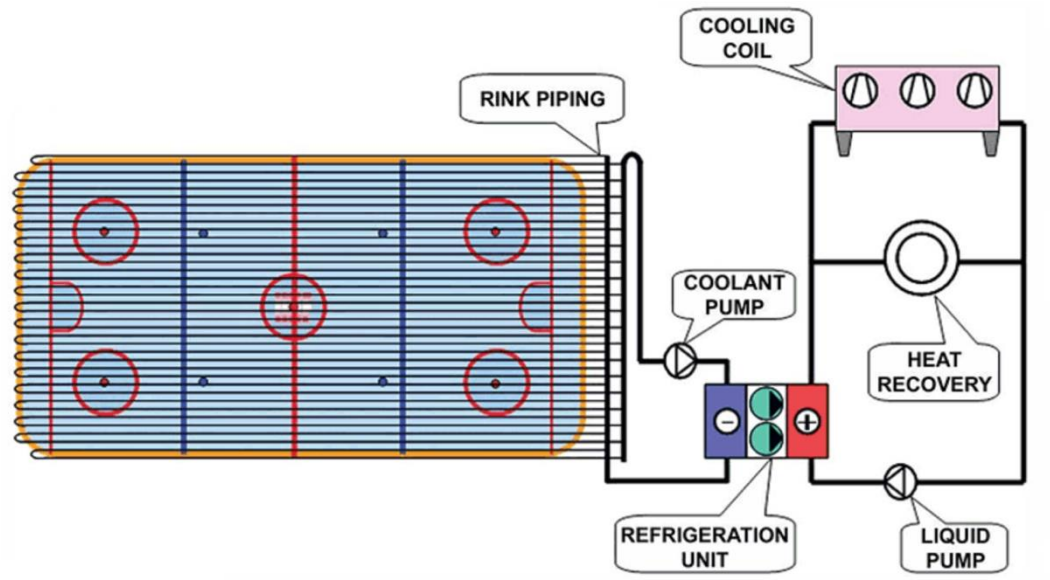

Figure 7: Indirect refrigeration system in an ice rink (IIHF, 2011).

Ice rinks are some of the most energy-intensive public buildings, providing both heating and cooling in addition to ventilation and lighting. The main energy systems in an ice rink are refrigeration, heating/hot water, dehumidification, lighting, and ventilation, as shown in Figure 8. The typical share of energy for each of the main systems indicates that the refrigeration system consumes the majority of the energy out of all the systems at 43%, followed by the heating/hot water at 26% (Jörgen Rogstam, 2017). There are more than 360 ice rinks in Sweden as of 2018, making up a total energy consumption of about 300 GWh per year (Karampour, 2011; *Annual Report*, 2018). The energy-intensive nature of ice rinks is reason to strive for energy efficiency, which can be achieved through the suitable design of operating parameters, including the choice of refrigerant in the primary and secondary loops. The following subsections will provide more details on the areas of energy demand within ice rink buildings.

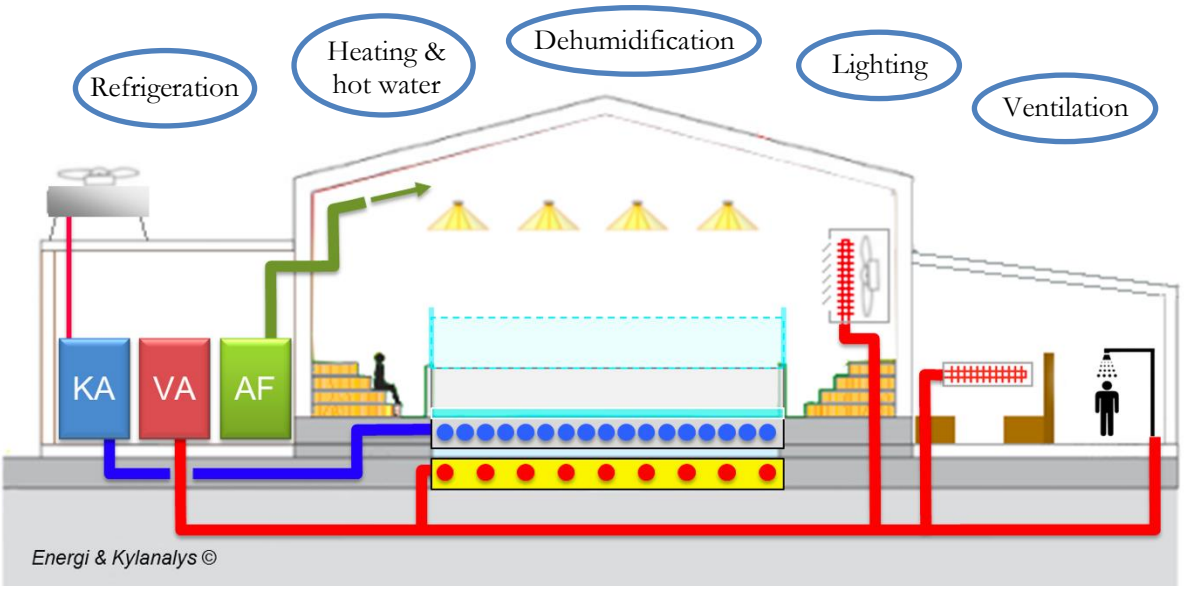

Figure 8: Ice rink diagram highlighting the main energy systems (Jörgen Rogstam, 2017).

1.8.1 Energy Demand: Refrigeration

Ice rink refrigeration is the most crucial area for energy demand. Ice rinks are typically about 30 m by 60 m with an 8.5 m corner radius, as shown in Figure 9. The temperature of the ice can range from -5°C to -3°C depending on the sport and whether the ice is being used for training or a competition (IIHF Facilities Committee, 2016). The typical ice rink has an energy demand of about 1000 MWh per year, 43% of which is attributed to the refrigeration system. The cooling capacity of a refrigeration system required to maintain one indoor rink is typically around 300-350 kW (Jörgen Rogstam, 2017). The refrigeration system is usually an electrically powered vapor-compression indirect system, as detailed in previous sections.

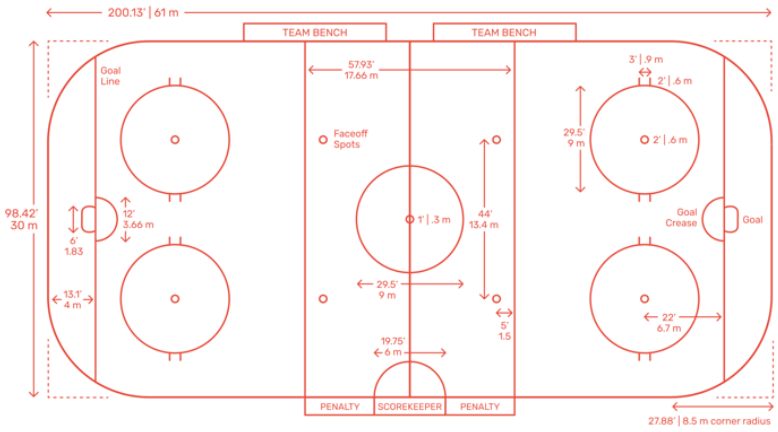

Figure 9: Diagram of a standard ice rink for ice hockey with dimensions (Maddock, 2020).

1.8.2 Energy Demand: Heating

Several areas of ice rink operation require heat, which is ideally supplied by the waste heat from the refrigeration system. These areas are space heating, domestic hot water (DHW), ground frost protection, ice resurfacing, and snow melting pit. Ice rinks have the difficult operating task of keeping the ice at an ideal temperature while also maintaining a comfortable indoor environment for any spectators. On top of this, the facility itself needs to be well maintained and be able to provide necessary services to guests.

Space heating demand applies to all of the air space outside of the ice and is necessary to provide a comfortable climate to any person in the building not participating in the sport. All public areas, such as a lobby and spectator stands, as well as bathrooms, locker rooms, and offices need to be provided with space heating. The spectator stands should be between 10 and 20°C and the other areas, locker rooms and offices, should be at least 20°C (IIHF Facilities Committee, 2016).

Domestic hot water demand refers to all hot water used in bathrooms, locker rooms, and any other faucet in the building. If the facility has a café or restaurant, the kitchen area would also require DHW. The operating schedule and occupancy will determine the heating demand for DHW and varies between rinks.

Ground freeze protection is the heating of the ground below the ice to prevent it from freezing. Without ground heating, frost can build up under the ice slab, causing the surface to become uneven and eventually damaged. To avoid the high cost of fixing the ice slab and to ensure long use of the ice rink, ground frost protection should be incorporated into system design, even in addition to insulation below the ice slab and even if the rink is located in an area that does not typically have ground frost (IIHF Facilities Committee, 2016). Figure 10 shows the cross section of an ice rink floor.

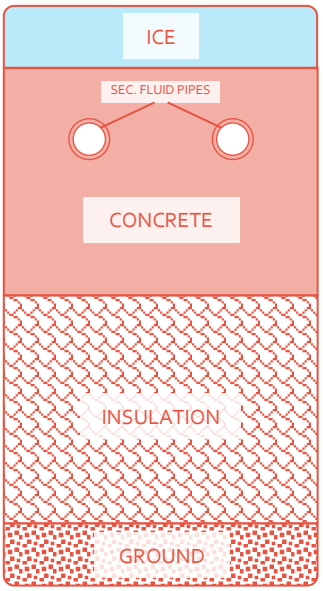

Figure 10: Example of ice rink floor cross section.

Ice resurfacing occurs periodically during operation times in order to maintain a smooth skating surface. An ice resurfacer is a vehicle that drives on the ice, releasing heated water onto the surface. The flood water can be between 30 and 60°C and around 0.4 to 0.8 m^3 of flood water is typically required to cover the entire ice surface (IIHF Facilities Committee, 2016).

A snow melting pit may be included in rink design in order to melt any waste ice or slush during the resurfacing operation.

1.8.3 Energy Demand: Dehumidification

Maintaining an indoor ice rink creates an environment with high humidity; from the exposed ice, to resurfacing and other hot water uses, water in all its physical states is constantly present. Hence, dehumidification is necessary in ice rink buildings and makes up about 6% of the total energy demand (Jörgen Rogstam, 2017). Without dehumidification, the excess moisture in the air can damage the structural integrity of the building by corroding metal structures and rotting wood, promote growth of mold, increase energy consumption, and lower the ice quality, as well as cause fog that can hinder the skaters' view and cause discomfort to spectators. Dehumidification can be achieved by condensation or through absorbent materials.

Dehumidification occurs through condensation by lowering the air temperature to below the dew point with a cooling coil. This leads to the excess water in the air to condense onto the coil, lowering the humidity of the air. It is common for this method to utilize the cooling coil in the HVAC system to dehumidify the air being circulated through the building. A basic diagram of this process is shown in the left part of Figure 11.

Absorption or adsorption is a process that can be utilized to lower the water content in the air. This can be achieved through a desiccant wheel, as shown in the right half of Figure 11. During this process, the desiccant wheel slowly rotates while separate air streams flow through separate parts of the wheel, which contains a material, such as silica gel, that adsorbs the moisture from the air. The cool, humid air flows through the material and exits as warm, dry air. Then as the wheel rotates, the material passes through a warm air stream that absorbs the moisture, revitalizing the adsorbent material and allowing it to adsorb more moisture as it passes again through the cool air stream (IIHF Facilities Committee, 2016).

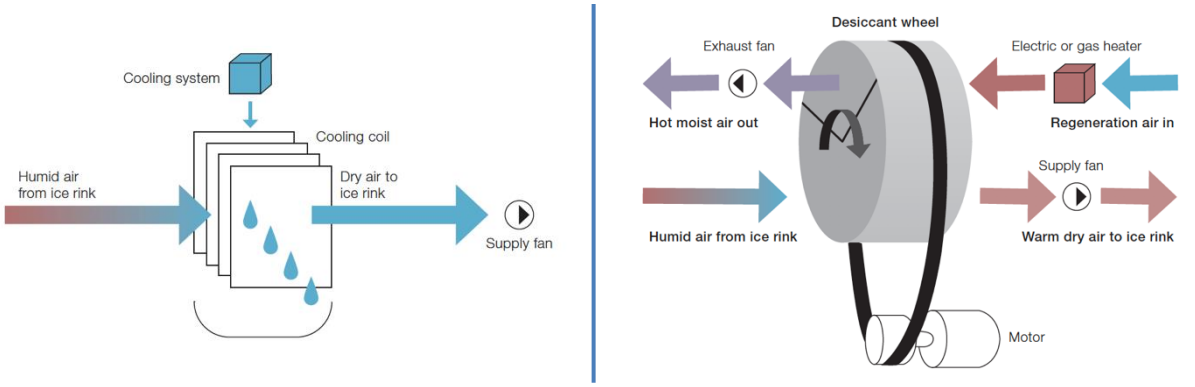

Figure 11: Dehumidification methods - condensation using a cooling coil (left) and absorption or adsorption through a desiccant wheel (right) (IIHF Facilitities Committee, 2016).

1.8.4 Energy Demand: Lighting

The lighting demand in the ice rink is only about 10% of the energy demand (Jörgen Rogstam, 2017). It is recommended that strength of the lighting throughout the building be about 300 lux, with 500 lux possible over the ice for hockey games (IIHF Facilities Committee, 2016). It is important to choose lighting that provides sufficient lux while limiting the increase of heat loads on the ice. This can be managed by choosing different types of light bulbs.

1.8.5 Energy Demand: Ventilation

Proper ventilation ensures good quality indoor air, which is important in maintaining a safe, comfortable environment. Ventilation should be carried out at suitable air change rate so that contaminants do not build up in the air. The ventilation system can also tie together both the heating and dehumidifying requirements, which, when combined, can be referred to as the HVAC (heating, ventilation, air conditioning) system. Fans are used to circulate and refresh the indoor air. The new air can be heated, when required, in order to provide space heating. Additionally, the air can be dehumidified so that dry air is being circulated into the rink to manage indoor humidity. The ventilation system makes up about 9% of the total energy demand (Jörgen Rogstam, 2017).

1.8.6 Aqua Ammonia Use in Ice Rinks

Although ammonia has been used as a primary refrigerant, use of aqua ammonia as a secondary fluid is still not yet widely accepted. For example, of the 368 indoor ice rinks in Sweden, only 34 use aqua ammonia as a secondary fluid (J Rogstam et al., 2019). However, the trend clearly shows an acceptance of and shift towards aqua ammonia as a secondary fluid. While the first systems utilizing aqua ammonia as a secondary fluid in Sweden were installed starting in 2007, the first system of the same type in North America was only installed in 2018 (Garry, 2018). This increased incorporation of aqua ammonia systems replaces the currently most used secondary fluids in Swedish ice rinks – calcium chloride (Mazzotti, 2014). Calcium chloride is the secondary fluid for approximately 94% of ice rinks in Sweden (Jörgen Rogstam, 2017). This fluid has typically been selected due to its good thermal properties and ease of handling. One drawback of calcium chloride solution is it's high corrosivity with some metals. However, aqua ammonia is starting to be chosen over calcium chloride due to even better thermal properties and the ability to achieve a higher overall system efficiency.

2 Experimental Methodology

Several thermodynamic properties of aqua ammonia at varying concentrations were tested in order to revise outdated reference values. As mentioned, the reference values used to evaluate aqua ammonia as a secondary fluid are unreliable due to the fact that the data is either outdated or inaccurately estimated and extrapolated.

2.1 Overview

Multiple solution concentrations were tested for easy comparison of secondary fluids for specific freezing point temperatures. In this case, the solutions that were tested are shown in Table 2 and were tested for freezing point, refractive index, density, dynamic viscosity, thermal conductivity, specific heat capacity, and corrosion rate of various materials.

Table 2: List of aqua ammonia solutions experimentally tested and their freezing temperatures.

Ammonia Concentration in Water (wt-%)	Freezing Point Temperature (°C)
2	-2.34
4.19	-5
7.7	-10
10.9	-15
13.5	-20
15.5	-25
17.7	-30
19.5	-35
21	-40
25	-55
30	-84*

The range of solutions from 4.19 wt-% to 17.7 wt-% was chosen because they are the most common freezing point temperatures required by secondary fluids in refrigeration systems. In order to achieve a higher level of confidence, additional solutions were tested outside of these concentrations: 2 wt-% and 19.5 wt-% to 30 wt-%. The following sections describe the methodologies for the laboratory experiments that were completed.

*The freezing point of 30 wt-% solution was more challenging to determine in the laboratory setting, so the value of -84°C is taken from CRC Handbook (Rumble, 2019).

2.2 Freezing Point Measurement Methodology

The freezing points of the solutions were tested to primarily confirm the concentrations of aqua ammonia. One of the first parameters of secondary fluids selected when designing an indirect system is the freezing point and different fluids are often compared at the same freezing point. Two methods were used to confirm solution concentrations: a deep freezer to measure freezing point temperatures and refractive index.

The former method involves placing 90 cm^3 of each solution in a plastic beaker located in a homemade laboratory apparatus, shown in Figure 12. This apparatus contains 11 thermocouples, one for each of the 9 beakers and 2 for around the outside of the apparatus so that both the samples and ambient temperature of the freezer were monitored. It is designed so that the samples are not in contact with any of the surfaces of the freezer. Once the solutions and thermocouples were set, the apparatus was placed in a deep freezer set for a temperature of at least 10°C lower than the expected freezing point. The temperatures were recorded per second from the thermocouples by a data collection unit and real-time readings were displayed.

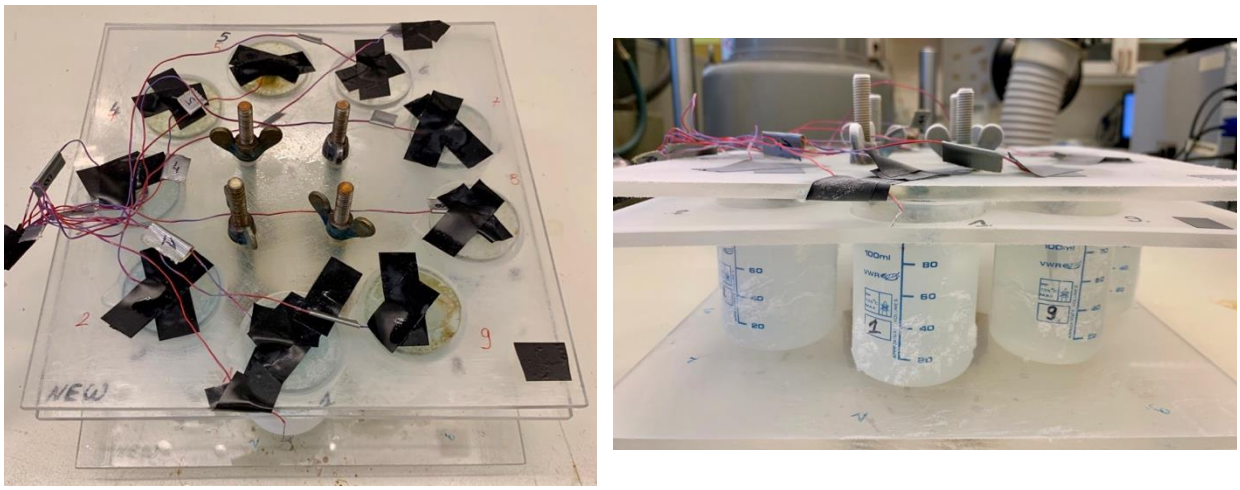

Figure 12: Laboratory apparatus used to test freezing point.

The samples were left in the freezer until the temperatures were steadily reaching the ambient freezer temperature, then they were removed and left to thaw at room temperature. This method allows for the monitoring of the freezing and melting temperatures to accurately determine the real freezing point temperature, which is important as subcooling affects can be seen while the samples freeze.

2.3 Refractive Index Measurement Methodology

Refractive index is defined as the ratio of the velocity light at a certain wavelength in air to the velocity of the light through a substance. Generally, the refractive index changes with changes in molecular weight of solutions (Silla, Arnau, & Tuñón, 2014). Therefore, this measurement was used to determine the concentration of solutions by comparing it to reference values. In addition to the determination of solution concentration from the freezing point, the refractive index of the aqua ammonia solutions was measured to confirm the concentrations.

This testing was completed with an Abbe 5 refractometer, as seen in Figure 13. The samples were individually placed on the instrument's prism and illuminated by the attached light source. Through the eyepiece, it is possible to see two achromatizing prisms, shown in Figure 14. Adjustments were then made by turning the dispersion knob in order to align the prisms at a wavelength of 589 nm, which is used for standard measurements. When the prisms are aligned, the refractive index value can be read through the eyepiece (Bellingham + Stanley, 2008).

After the refractive index value is determined from the refractometer, a correction needs to be applied for the difference of the room temperature from 20°C. The equation used for this correction is as follows:

$$\eta_{D_{20}} = \eta_{D_{room}} + \left(T_{room} - T_{ref}\right) * 0.0001 \qquad \textit{(Equation 1)}$$

$\eta_{D,20}$	: refractive index value from scale at reference temperature at room temperature [-]
$\eta_{D,room}$	: calculated refractive index reading at reference temperature (20°C)
T_{room}	: room temperature [°C]
T_{ref}	: reference temperature (20°C)

Figure 13: Abbe 5 Refractometer (Bellingham + Stanley, 2008).

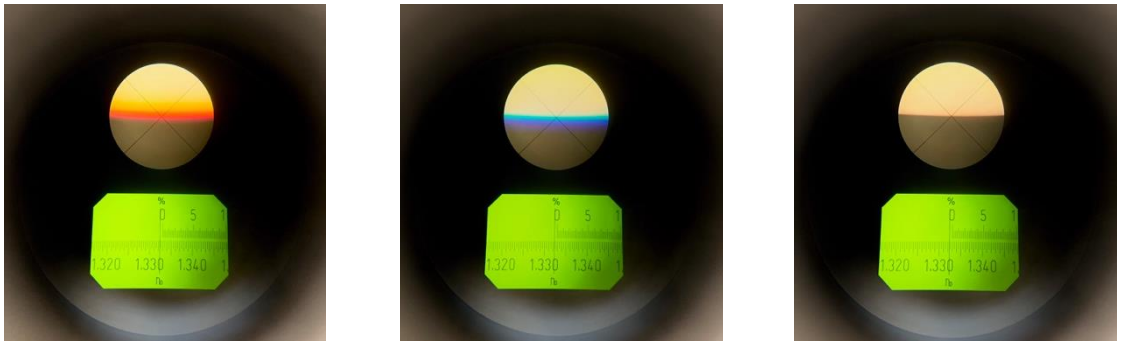

Figure 14: View through refractometer eyepiece showing the two unaligned achromatizing prisms (left and middle) before adjustment and the aligned prisms after adjustment (right).

2.4 Density Measurement Methodology

Following the validation of the aqua ammonia solution concentrations and respective freezing temperatures, the density of each solution was tested. These experiments were performed using two different methods: one using pycnometers and the other using hydrometers, also called areometers.

As the name suggests, the pycnometer method utilizes pycnometers, shown in Figure 15, which are calibrated to a specific volume in cm^3 at temperature of 20°C, accurate to three decimal places. The pycnometer without a thermometer was used for measurements taken at a temperature of 20°C and the pycnometer with a thermometer was used for measurements at temperatures ranging from 10°C to room temperature. For each test, the mass of the clean, empty pycnometer was recorded. Then it was filled with solution and cooled to at least 8°C, if performing temperature-controlled tests. Then the mass of the pycnometer with the solution was recorded, either at room temperature or at 10°C and at every 2°C increase until the solution reached room temperature.

Figure 15: Pycnometers used in the experiments. The pycnometer in the left two photos is used for measuring mass of the solution at a temperature of 20 °C and the pycnometer with the thermometer on the balance in the right photo is used to measure the mass of the solution at a range of temperatures.

To calculate the density of the solutions at room temperature, the following equation was used:

$$\rho = \frac{(m_{full} - m_{empty})}{v} * 1000 \qquad \textit{(Equation 2)}$$

ρ : density [kg/m^3]

m_{full} : mass of full pycnometer [g]

m_{empty} : mass of empty pycnometer [g]

v : pycnometer volume [cm^3]

In order to accurately calculate the density at varying temperatures, a correction of the volume of the pycnometer was calculated based on the material of glass. The coefficient of mean linear thermal expansion of borosilicate glass is used in this correction, (Equation 3. The calculation of the density at each temperature was calculated using (Equation 4. Next the vector method was used to create a curve to calculate the density at varying temperatures. First the difference between the calculated density at 20°C and the reference value at 20°C was determined to calculate an adjusted reference value. This difference was applied to the other temperatures from 10°C to room temperature. Then these values were plotted with a second order polynomial trendline to generate an equation that should be used to accurately calculate density, as shown in Figure 16.

$$v_{cor} = v_{CT} * (1 + (T_S - T_C) * \alpha) \qquad \textit{(Equation 3)}$$

v_{cor} : corrected pycnometer volume [cm^3]

v_{CT} : given pycnometer volume at calibration temperature [cm^3]

T_S : temperature of sample [°C]

T_C : calibration temperature [°C]

α : coefficient of mean linear thermal expansion [K^{-1}]

$$\rho = \frac{(m_{full} - m_{empty})}{v_{cor} * SCF} + \rho_{air} \qquad \textit{(Equation 4)}$$

ρ : density [kg·m^{-3}]

m_{full} : mass of full pycnometer [kg]

m_{empty} : mass of empty pycnometer [kg]

v_{cor} : corrected pycnometer volume [m^3]

SCF : scale calibration factor [-]

ρ_{air} : density of air [kg·m^{-3}]

	5.8	Temp
Sample Δρ at 20°C	929.92	30
	933.82	20
	937.62	10
	940.82	0
	943.12	-10
	944.72	-20
	945.22	-23

Reference Values (Melinder 2010)	935.70	30
	939.60	20
	943.40	10
	946.60	0
	948.90	-10
	950.50	-20
	951.00	-23.3

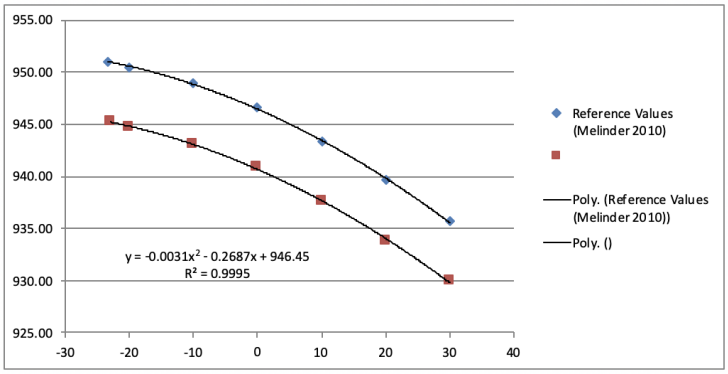

Figure 16: Example of using the vector method to calculate density.

The second method used to test density was to use hydrometers. A hydrometer is an instrument consisting of a closed, long glass tube with a weighted bulb at one end, as shown in **Error! Reference source not found.**. In this case, the tube is calibrated to measure density by placing the hydrometer in graduated cylinder filled with sample solution. The hydrometer floats at a certain level depending on the buoyancy of the liquid and density can measured. The hydrometer can measure density to a certainty of 0.001 g/cm^3. Two types of hydrometers were used, one calibrated at temperature of 15.6°C and one calibrated for 20°C.

Figure 17: Areometer, or hydrometer, used in measuring density, calibrated for 20°C.

2.5 Viscosity Measurement Methodology

A Brookfield DV-2 Pro rotational viscometer was used to determine the viscosity of the different solutions at given shear rates. The instrument used consists of a cylindrical sample chamber and a spindle immersed in the sample, as can be seen in Figure 18. The spindle rotates in the fluid and is driven by a calibrated spring. As the spindle rotates in the fluid, the resistance to the motion, viscous drag of the fluid, is measured through the deflection of the spring with a rotary transducer (Brookfield Engineering Labs, Inc.). Additionally, the sample chamber is temperature controlled to measure the viscosity from temperatures 2°C above the freezing point up to 25°C in 5°C increments for each aqua ammonia solution, allowing for the dynamic viscosity to be measured at a wider temperature range. One exception to this was for the 25 wt-% and 30 wt-% solutions, which were only tested up to 20°C in order to minimize the amount of ammonia degassing from the solution. Another exception to this was in the case of the solution with a freezing point lower than -20°C. The minimum temperature achievable by the unit is -17°C.

Figure 18: Rotational viscometer setup in laboratory showing the sample holder and cylinder (top) and the thermostat bath with the unit ready for testing (bottom).

The data outputs include the shear stress, shear rate, viscosity, percent torque on the spindle, among other values. In order to calculate the viscosity at a given temperature, the shear rate versus shear stress is plotted after the test is finished. A linear fit to the line is determined after removing the necessary data points from the graph, and the slope of the line represents the viscosity in mPa·s. After collecting data at each desired temperature and calculating the respective viscosity, the values can be plotted versus temperature and a fourth order polynomial trendline is used to fit the data and generate an equation to determine dynamic viscosity for temperatures outside the measured range, as seen in Figure 19.

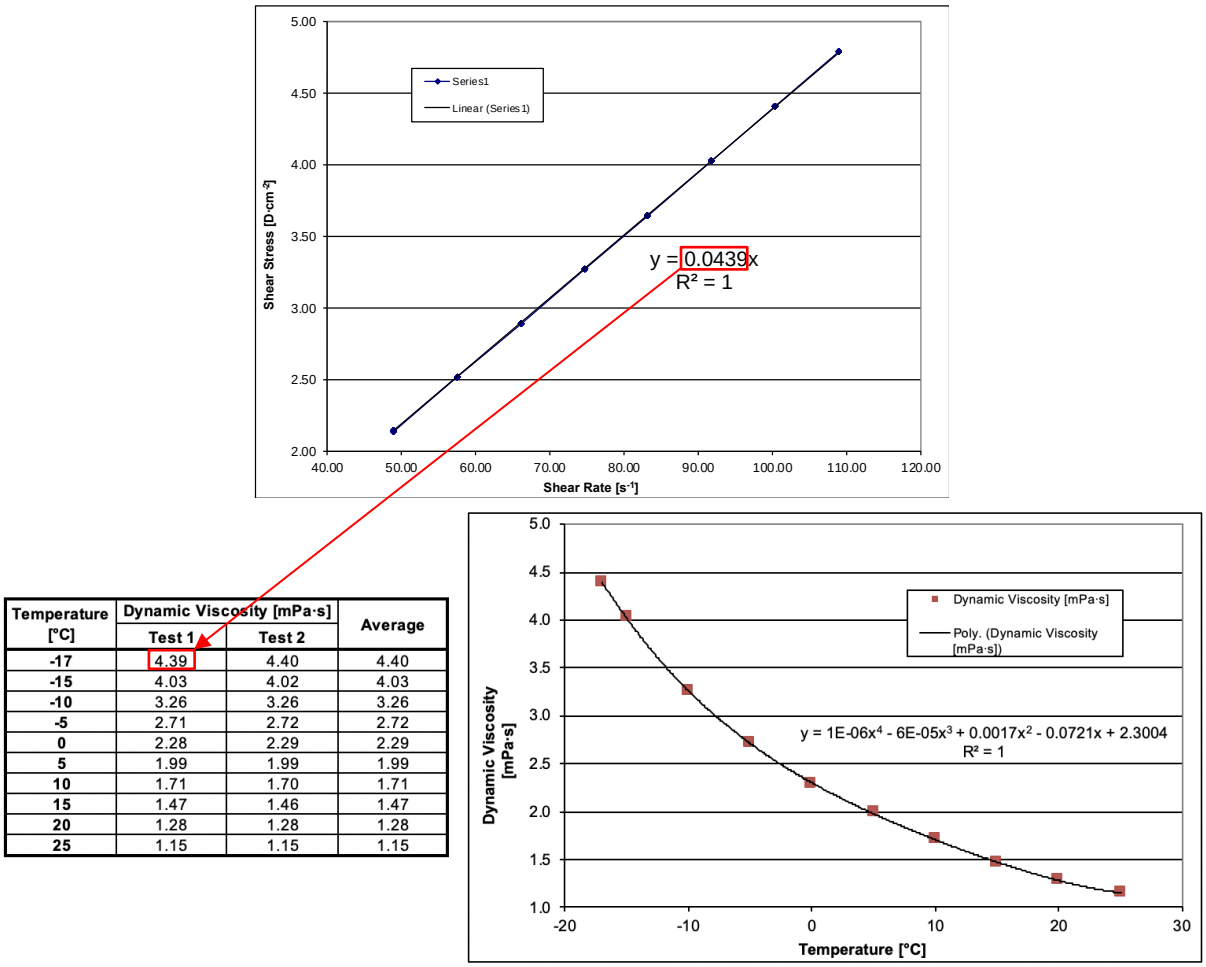

Temperature [°C]	Dynamic Viscosity [mPa·s]		Average
	Test 1	Test 2	
-17	4.39	4.40	4.40
-15	4.03	4.02	4.03
-10	3.26	3.26	3.26
-5	2.71	2.72	2.72
0	2.28	2.29	2.29
5	1.99	1.99	1.99
10	1.71	1.70	1.71
15	1.47	1.46	1.47
20	1.28	1.28	1.28
25	1.15	1.15	1.15

Figure 19: A plot of shear rate vs. shear stress (top) used to determine viscosity measurements which are then used to develop a trend of viscosity at varying temperature (bottom). The example is of 13.5 wt-% aqua ammonia solution.

Limitations of measuring viscosity using this method exist at the higher temperatures, especially with volatile samples such as highly concentrated aqua ammonia. The lowest viscosity that the instrument can measure is 1 mPa·s, which is the viscosity of water at 20°C.

2.6 Specific Heat Capacity Measurement Methodology

A differential scanning calorimeter (DSC) was used in the determination of specific heat capacity using the calorimetric method. In this case a μDSC7 from SETARAM was used with a continuous method, shown in Figure 20. The method involves a blank test with two identical vessels, one reference and one measuring vessel, followed by a test with the sample using the same vessels (SETARAM Instrumentation, 2014). The instrument applies heat to the vessels at a continuous heating rate and records the difference in the amount of heat required to increase the temperature as a function of temperature.

Figure 20: Sample chamber closed and open and μDSC7 unit.

The blank vessel is measured in order to account for an effect the vessel has on the heating of the sample. Therefore, during the calculation of specific heat capacity, the heat measured from the blank is subtracted from the measurement of the sample, as seen in (Equation 5. The scanning heating rate used for this testing was 0.05 K per minute.

Figure 21 shows the program used to run the test, with the continuous heating of the sample displayed by the red line in the top screenshot. The computer program used the raw data collected from the μDSC7 to calculate specific heat capacity for the temperature range of the test. A second or third order regression line was then fit to the data in order to determine the specific heat capacity at a given temperature. The raw data and regression line are shown in the bottom screenshot of

Figure 21.

$$C_p = \frac{(A_s - A_b)}{m_s * \beta}$$ *(Equation 5)*

C_p : specific heat capacity [J·g^{-1}·K^{-1}]

A_s : amplitude of sample [W]

A_b : amplitude of blank [W]

m_s : mass of sample [g]

β : heating rate [K·s^{-1}]

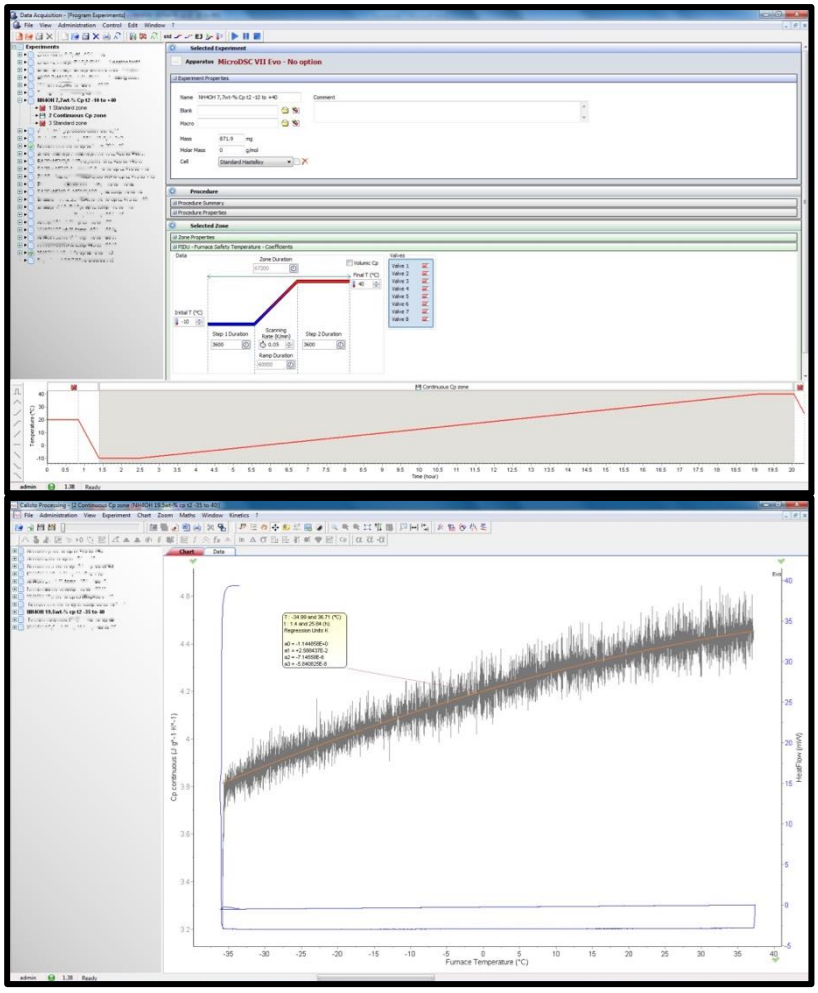

Figure 21: Computer program to run DSC test (top) and resulting data for Cp determination (bottom).

2.7 Thermal Conductivity Measurement Methodology

The Transient Plane Source (TPS) method was used to determine the thermal conductivity of the aqua ammonia solutions. The TPS method is considered to be one of the most precise and convenient techniques used to study thermal transport properties. This method uses a transiently heated plane sensor that consists of a double spiral-shaped electrically conducting nickel foil. This spiral foil is laminated between two sheets of an insulating material, Teflon in this case, and can be seen in Figure 22. The sensor acts as both a heat source and dynamic thermometer by supplying an electric current through the foil to increase the temperature of the sensor, and therefore the sample, while also measuring the resistance increase as a function of time. By recording and analyzing the dynamic features of the temperature increase, the thermal conductivity and diffusivity can be determined from a single transient recording (Hot Disk AB, 2016).

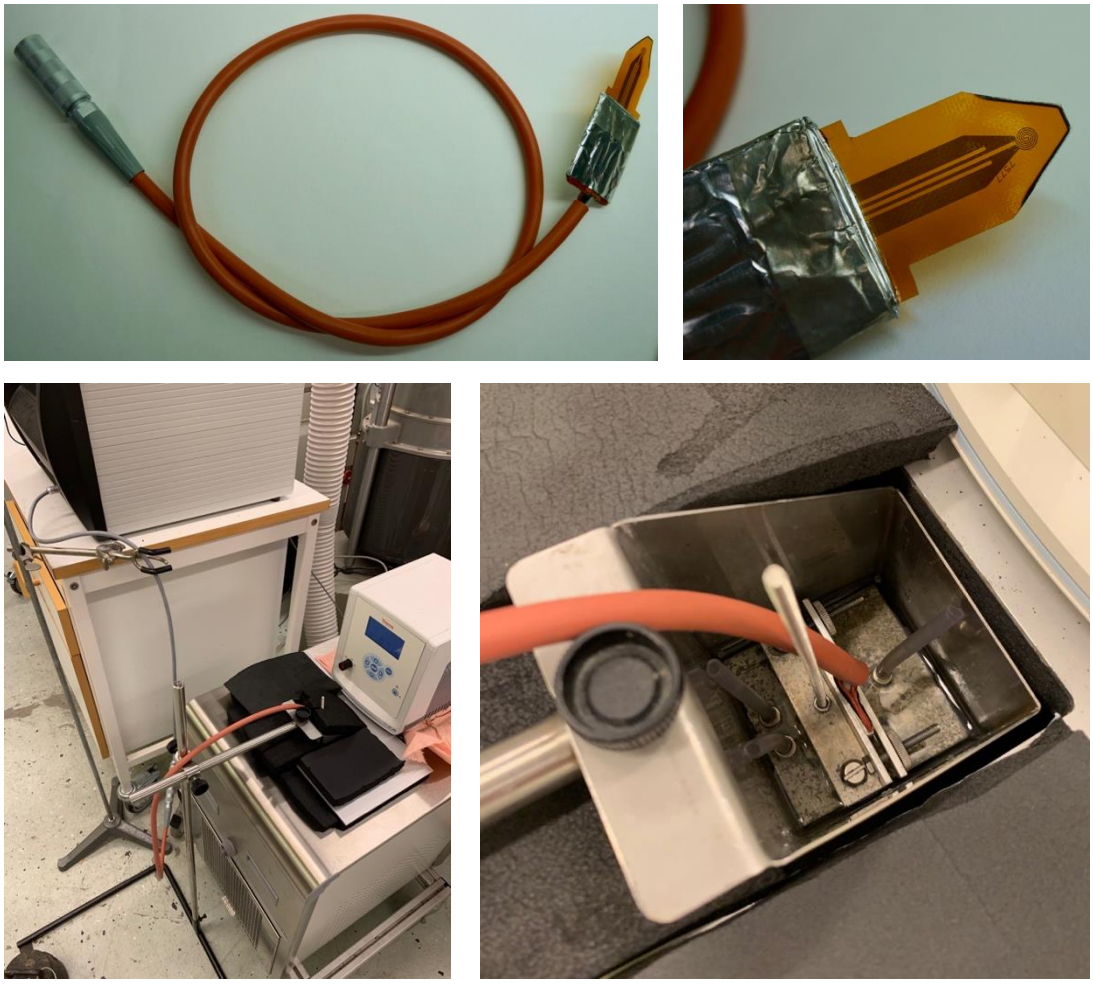

Figure 22: Teflon sensor 7577 used for the TPS tests (top) and instrument setup with sample in thermostat bath connected to Hot Disk Thermal Constant Analyzer TPS-2500S (bottom).

To perform the tests, a program is customized for the ammonia solutions in the accompanying HotDisk software. The program consists of recording the dynamic temperature features at three different powers, in mW, per temperature. The temperatures of the tests range from 2°C higher than the freezing point up to 25°C. Each set of recordings creates a batch of 200 measured points used to calculate thermal transport properties. In order to decrease the error of measurement while post-processing, the density and specific heat capacity are used from the results of the density and DSC tests completed prior. An example of the output data per batch can be seen in Figure 23. Outlying data points from each batch are trimmed to calculate a more accurate value of thermal conductivity. The values for each temperature are compared with values at previous temperatures and incorrect values are removed in order to generate an average, resulting in a value for thermal conductivity at each tested temperature.

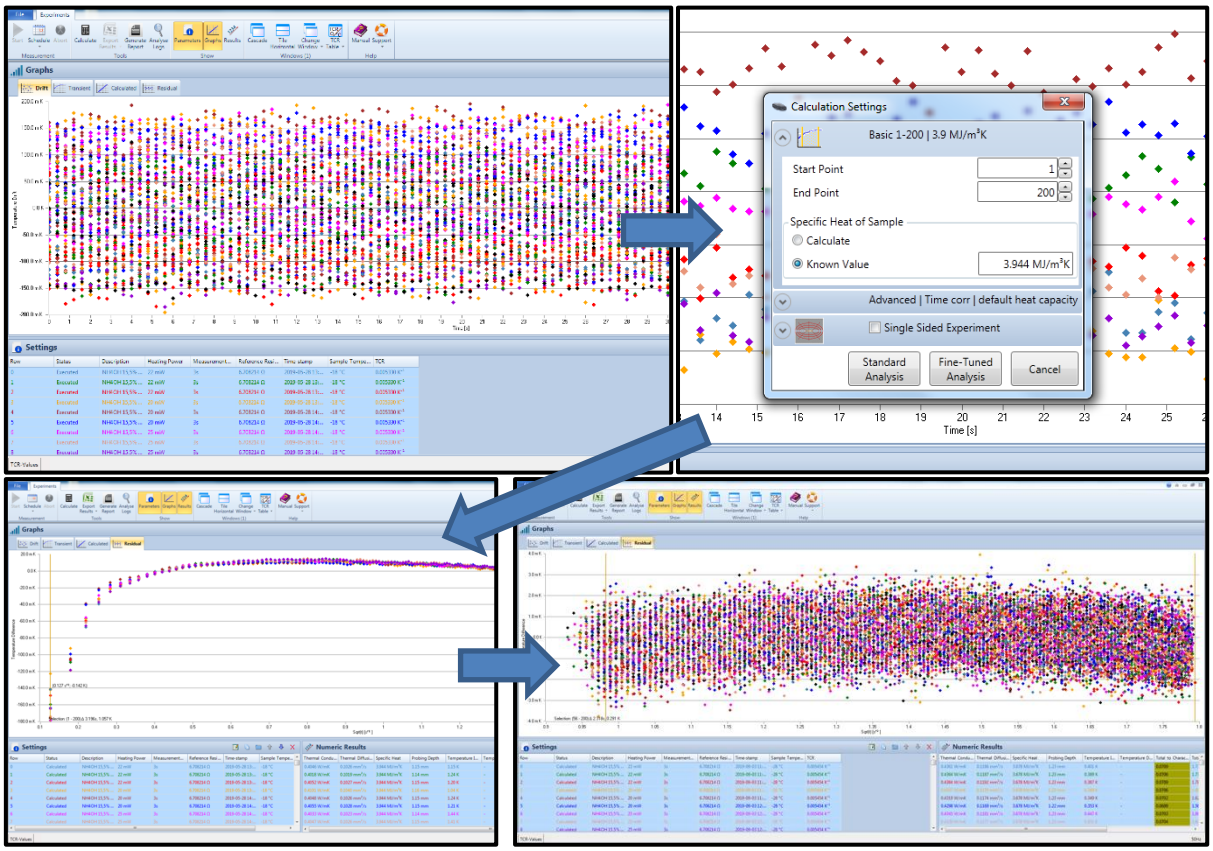

Figure 23: Data processing of data collected from the TPS unit: raw data (top left), calculation settings (top right), untrimmed, calculated data for one temperature (bottom left), and final data for all temperatures (bottom right).

2.8 Corrosion Rate Measurement Methodology

As mentioned previously, corrosion is an important factor when considering aqua ammonia as a secondary fluid to understand compatibility with system components. Corrosion rate tests were carried out for each ammonia solution for varying amounts of time. The test consists of submersing metal specimens in solution for a set amount of time and using the difference in the mass of the specimens before and after submersion to calculate the rate of corrosion. The tests were completed according to the ASTM NACE TM0169/G31-12a standard and the specimens were prepared and measured according to ASTM G1-03 (reapproved 2017) standard. The general procedure for these experiments was to first clean and measure each metal specimen, of which the same size and shape was used where possible, then place one specimen into a closed bottle containing around 100 mL of aqua ammonia solution, as can be seen in Figure 24. The bottles were left closed for a specified amount of time, then the metal specimens were removed, cleaned, and dried before being remeasured. The measurements of each specimen before and after the corrosion period include weighing and measuring its dimensions (length, width, height, etc.). The specimens that were tested are copper 99.95%, brass (65% copper), carbon steel 312, stainless steel 316L, galvanized steel, aluminum 3300 series, and a brass connection commonly used in ice rink refrigeration systems. The brass connections were coated

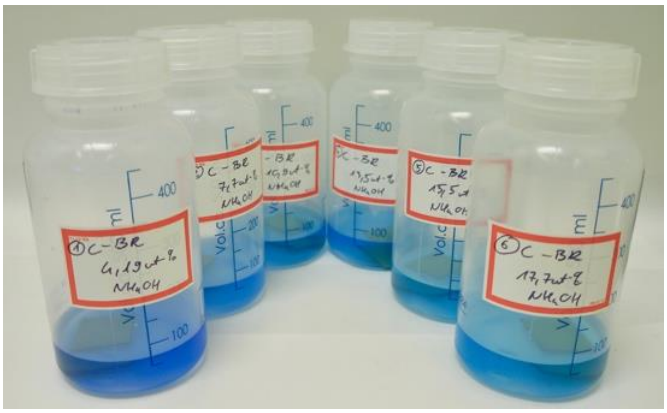

Figure 24: Corrosion test set for each ammonia solution with brass.

on their exterior side since corrosion in real situations will only occur inside the pipe and connections through which the secondary fluid flows, as seen in Figure 25. All specimens were kept in the closed bottle for 7 days, with the exception of the brass connections, which were kept for 30 days.

Figure 25: Brass connections used in corrosion tests and an example of coating the exterior (bottom right).

The difference in mass was used to calculate the rate of corrosion after the tests were completed. The following equation was used in this calculation (ASTM International, 2017):

$$corrosion\ rate = \frac{K * (m_i - m_f)}{A_{S_i} * t * \rho}\ [mm/yr] \qquad \textit{(Equation 6)}$$

K : constant (87600 for mm/yr)

m_i : mass of specimen before test [g]

m_f : mass of specimen after test [g]

A_{S_i} : initial surface area of specimen [cm^2]

t : duration of the test [hr]

ρ : density of specimen [g/cm^3]

2.9 Error calculations

Each laboratory test was calibrated with distilled water prior to completion of the experiments with aqua ammonia. The measurements for distilled water are used in the following calculations of error to determine the accuracy of each experimental method used.

2.9.1 Density Measurement Accuracy

The procedure to determine density involves measuring multiple parameters with laboratory equipment in order to calculate the density values. The pycnometers were weighed three times in the process. The following Table 3 shows the uncertainty of the pycnometers and balance that were used in the determination of the density. (Equation 7 was used in addition to the commonly used average and standard deviation equations in order to account for the propagation of error through mathematical calculations.

Table 3: Accuracy of density experimental method.

Pycnometer [cm³]	25.157
Volume Uncertainty [cm³]	0.01
Weight empty pycnometer [g]	23.3085
Weight full pycnometer [g]	48.0449
Balance Uncertainty [g]	0.001
Density at 20°C [kg/m³]	995.41
Combined Uncertainty [kg/m³]	0.0003996 (0.04%)

$$u_c(y) = \sqrt{\left(\frac{u(x_1)}{x_1}\right)^2 + \left(\frac{u(x_2)}{x_2}\right)^2} \quad ; y = \frac{x_1}{x_2} \qquad \textit{(Equation 7)}$$

$u_c(y)$: combined uncertainty of *y*

$u(x_1)$: instrument uncertainty of pycnometers

$u(x_2)$: instrument uncertainty of balance

y : calculated density value [kg/m³]

x_1 : measured volume value [cm³]

x_2 : measured weight value [g]

2.9.2 Viscosity Measurement Accuracy

The accuracy of measuring viscosity with the method used for this project involves calculations from data collected from the viscometer program. Water was tested at the temperatures listed in Table 4. The raw data collected gives 520 measured values at each temperature. However, some of these values are cut from the usable data, as mentioned previously. The number of measurements used in each calculation are tabulated in Table 4. Also tabulated are the average measurements of viscosity, standard deviation, and different types of error. The instrument uncertainty is used to calculate the final relative error (Lemmon et al., n.d.). The maximum standard error is 0.0003 mPa·s and the relative error is 0.19 mPa·s, hence the values can be considered precise and that further testing will result in similar error.

Table 4: Accuracy of viscosity experimental method.

Temperature [°C]	3	5	10	15	20	25
Number of Measurements [-]	400	380	400	320	260	280
Average [mPa·s]	1.77	1.68	1.46	1.30	1.18	1.06
Standard Deviation [mPa·s]	0.0051	0.0042	0.0023	0.0020	0.0046	0.0041
Standard Error [mPa·s]	0.0003	0.0002	0.0001	0.0001	0.0003	0.0002
Instrument Uncertainty [mPa·s]	0.2	0.2	0.2	0.2	0.2	0.2
Relative Error [mPa·s]	0.11	0.12	0.14	0.15	0.17	0.19
Percent Relative Error [%]	11%	12%	14%	15%	17%	19%

2.9.3 Specific Heat Capacity Measurement Accuracy

The μDSC is an extremely precise instrument. The measurement and calculation of the specific heat capacity of water was used for the calculation of error. The instrument was used in the continuous measurement mode, which means measurements were taken at every temperature over the range of the test at 0.05 K increments. For the calculation of error, the range of measurements for each temperature were considered within ±0.05K of the reported measurements, shown in

Table 5. The low percent relative error validates the results from this test. Additionally, these results were

Temperature [°C]	3	5	10	15	20	25
Number of Measurements [-]	20	20	20	20	20	20
Average [kJ·kg^{-1}·K^{-1}]	4.2511	4.2491	4.2447	4.2409	4.2374	4.2340
Standard Deviation [kJ·kg^{-1}·K^{-1}]	0.0003	0.0003	0.0003	0.0002	0.0002	0.0002
Standard Error [kJ·kg^{-1}·K^{-1}]	0.00007	0.00007	0.00006	0.00005	0.00005	0.00005
Instrument Uncertainty [kJ·kg^{-1}·K^{-1}]	0.04	0.04	0.04	0.04	0.04	0.04
Relative Error [kJ·kg^{-1}·K^{-1}]	0.00941	0.00941	0.00942	0.00943	0.00944	0.00945
Percent Relative Error [%]	0.941%	0.941%	0.942%	0.943%	0.944%	0.945%

from one test, whereas at least two tests were completed for ammonia solutions, increasing certainty of results.

Temperature [°C]	3	5	10	15	20	25
Number of Measurements [-]	20	20	20	20	20	20
Average [kJ·kg^{-1}·K^{-1}]	4.2511	4.2491	4.2447	4.2409	4.2374	4.2340
Standard Deviation [kJ·kg^{-1}·K^{-1}]	0.0003	0.0003	0.0003	0.0002	0.0002	0.0002
Standard Error [kJ·kg^{-1}·K^{-1}]	0.00007	0.00007	0.00006	0.00005	0.00005	0.00005
Instrument Uncertainty	0.04	0.04	0.04	0.04	0.04	0.04

[kJ·kg^{-1}·K^{-1}]						
Relative Error [kJ·kg^{-1}·K^{-1}]	0.00941	0.00941	0.00942	0.00943	0.00944	0.00945
Percent Relative Error [%]	0.941%	0.941%	0.942%	0.943%	0.944%	0.945%

Table 5: Accuracy of specific heat capacity experimental method.

2.9.4 Thermal Conductivity Measurement Accuracy

The program used to carry out the thermal conductivity tests records the values for thermal conductivity at each of the temperatures in

Table 6, along with the standard deviation of the measured values. There is a total of 1800 values measured

Temperature [°C]	**3**	**5**	**10**	**15**	**20**	**25**
Number of Measurements [-]	865	568	284	281	425	1287
Average [W·m^{-1}·K^{-1}]	0.5745	0.5782	0.5840	0.5849	0.5874	0.5946
Standard Deviation [W·m^{-1}·K^{-1}]	0.0030	0.0024	0.0018	0	0.0020	0.0037
Standard Error [W·m^{-1}·K^{-1}]	0.0001	0.0001	0.0001	0	0.0001	0.0001
Instrument Uncertainty [W·m^{-1}·K^{-1}]	0.05	0.05	0.05	0.05	0.05	0.05
Relative Error [W·m^{-1}·K^{-1}]	0.087	0.087	0.086	0.086	0.085	0.084
Percent Relative Error [%]	8.7%	8.7%	8.6%	8.6%	8.5%	8.4%

at each temperature, but varying amounts of the raw data is eliminated during post processing. Water is highly conductive and is more difficult to test, which leads to the elimination of a greater amount of raw data. The standard and relative error were calculated using the output values from the program. The standard error is 0.0001 W·m^{-1}·K^{-1} for nearly all the temperatures, with the exception of 15°C, and the relative error ranges from 0.084 to 0.087 W·m^{-1}·K^{-1}. In the case for 15°C, the average value for thermal conductivity after post processing of the data was the same for each measurement period, resulting in no standard deviation and error. This is the only temperature where values for both should increase slightly with further testing, but the increased standard deviation and errors can be expected to be similar to those at the other temperatures.

Temperature [°C]	**3**	**5**	**10**	**15**	**20**	**25**
Number of Measurements [-]	865	568	284	281	425	1287
Average [W·m^{-1}·K^{-1}]	0.5745	0.5782	0.5840	0.5849	0.5874	0.5946
Standard Deviation [W·m^{-1}·K^{-1}]	0.0030	0.0024	0.0018	0	0.0020	0.0037
Standard Error [W·m^{-1}·K^{-1}]	0.0001	0.0001	0.0001	0	0.0001	0.0001
Instrument Uncertainty [W·m^{-1}·K^{-1}]	0.05	0.05	0.05	0.05	0.05	0.05
Relative Error [W·m^{-1}·K^{-1}]	0.087	0.087	0.086	0.086	0.085	0.084

Percent Relative Error [%]	8.7%	8.7%	8.6%	8.6%	8.5%	8.4%

Table 6: Accuracy of thermal conductivity experimental method.

2.10 Limitations

Certain limitations existed when completing the previously described laboratory work to measure certain thermophysical properties and corrosion rate of aqua ammonia at varying concentrations. One main limitation was that of the equipment used, despite being highly precise. For example, each piece of equipment has a freezing point threshold. The limits are -45°C, -30°C, and -18°C for the measurement of specific heat capacity, thermal conductivity, and dynamic viscosity, respectively. Additional laboratory equipment factors, including repairs and operating procedures, also put a strain on time limitations. The thesis project lasted about 8 months in person, in which all tests needed to be completed. With breakdowns and limited equipment, this time limited the number of results. Furthermore, aqua ammonia is a highly volatile solution, which can limit the accuracy of results as ammonia evaporates from the solution during laboratory test setup and measurement.

3 Experimental Results

This section will highlight the findings of the experimental testing of aqua ammonia. Furthermore, Appendix A contains additional details of experimental methods and/or results.

3.1 Freezing Point Results

Figure 26 shows the freezing point temperature results for 15.5 wt-% aqua ammonia solution as an example. The light blue and dark blue lines in the graphs represent two different samples of 15.5 wt-% aqua ammonia that were both in the freezer during freezing and melting. Using the freezer method, it is common to see evidence of subcooling during the freezing of the samples, which would result in freezing temperatures lower than expected. However, the freezing part of the test shows results that would confirm the expected freezing point of the solution. It is common to analyzing the melting temperatures instead, but in this case, the melting part of the test shows higher than expected freezing point temperatures. Furthermore, the results from the melting process of the test made it more difficult to determine the temperatures at which the samples melted, while the freezing process of the test more clearly shows the temperature at which the samples froze. In Figure 26, the red circles indicate the temperatures at which freezing and melting most likely occurred.

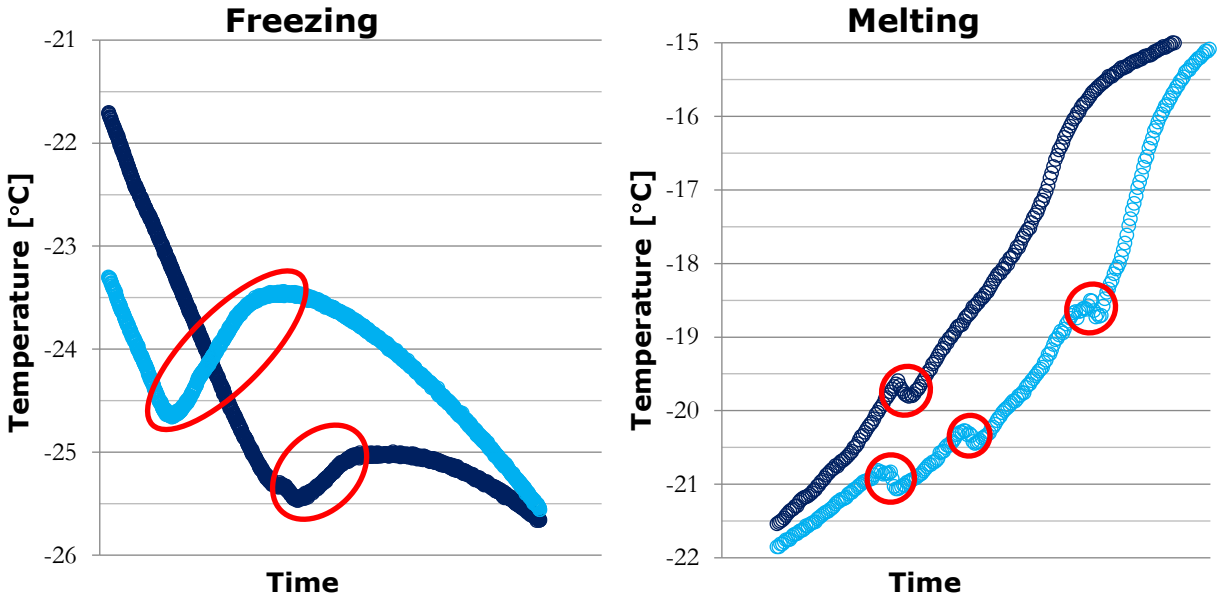

Figure 26: Example of freezing point test results for aqua ammonia 15.5 wt-%, expected freezing point of -25°C. The light and dark blue lines represent different samples of the same concentration.

The method of using a deep freezer to determine freezing point has a lower level of confidence than other available tests, such as refractive index. Due to the difficulty to confirm the freezing points, and hence solution concentration, with the deep freezer, the refractive index method was also utilized with results explained in later sections. Confirming the solution concentration was the first step in the experimental testing and allowed for the following experiments to be completed.

Although the concentration of the solutions was verified with refractive index tests, the results from the freezing and melting tests show agreement with literature values of freezing points for the tested solutions. Even though the melting tests produced less clear melting temperatures, the freezing point determination agrees with the assumed freezing points.

3.2 Refractive Index Results

Table 7 displays the values for refractive index, corrected for 20°C, for each of the tested ammonia water solutions. For the tested solutions that are not a whole number, the reference values used were calculated based on the trendline of the graphed reference values with respect to concentration. The reference values and trendline can be seen in Figure 27, along with the experimental values. The percentage of error in the measured values compared to the reference values range from 0.05% to 0.28%. The percent error is well below the acceptable limit of 2%, which validates of the concentrations being used.

Table 7: Numerical results of refractive index testing of all ammonia solutions. The $\eta_{20,\,REF}$ values are from the CRC Handbook (Rumble, 2019).

Concentration [wt-%]	T_f [°C]	$\eta_{D,\,room}$ [-]	$\eta_{D,\,20}$ [-]	$\eta_{20,\,REF}$ [-]	Error [%]
0 (water)	0	-	-	1.333	-
2.00	-2	1.3330	1.33329	1.3339	0.05
4.19	-5	1.3345	1.33485	1.3352	0.03
7.7	-10	1.3355	1.33587	1.3372	0.1
10.9	-15	1.3375	1.33774	1.3391	0.1
13.5	-20	1.3390	1.33920	1.3406	0.1
15.5	-25	1.3400	1.34025	1.3419	0.12
17.7	-30	1.3420	1.34230	1.3433	0.07
19.5	-35	1.3420	1.34220	1.3444	0.16
21	-40	1.3430	1.34320	1.3454	0.16
25	-55	1.3440	1.34422	1.3480	0.28
30	-84	1.3465	1.34674	1.3502	0.26

The difference in the observed refractive indexes can be attributed to the volatile characteristic of ammonia in water. The solution is exposed to open air during setup of the experiment, which can lead to some evaporation of ammonia from the solution. This is reflected in the values that are lower than expected, in comparison to the reference values. Additionally, the general trend of increasing error with increasing solution can be attributed to the increase in volatility with the increase in solution concentration.

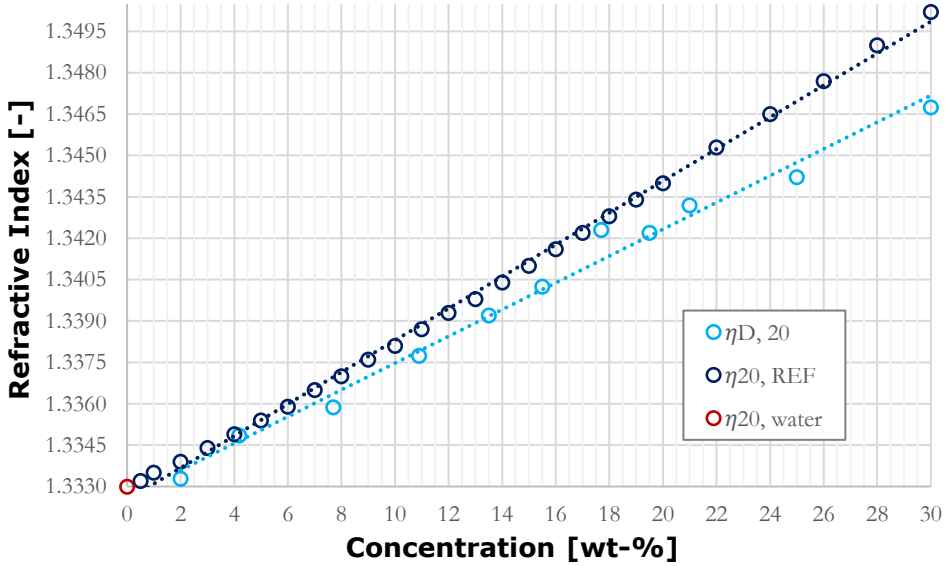

Figure 27: Graph of refractive index laboratory results and reference values, including water.

3.3 Density Results

Figure 28 displays the calculated densities of each solution at varying temperatures from the pycnometer method. The experimental values from the pycnometer method were confirmed with the hydrometer method. The results show a high level of agreement with the reference values. The percent difference between the measured values and references range from 0.3% to 1.7%, which indicates a high level of agreement between measured and reference values. The trend of the change of density with temperature is also in agreement with the reference values. The repeatability of the trends and values validate the experiments. It is logical that these results reflect the reference values, albeit outdated, due to the fact that density was one of the most tested thermophysical properties over the years and has led to a higher validation of results among scientists.

The experimental values are shown in solid lines and the reference values are shown in dashed lines in Figure 28. The marker type of the reference values for each solution concentration matches the markers of the experimental values. With increasing ammonia concentration, density decreases, while decreasing temperature results in higher density. This is expected since pure ammonia has a lower density than pure water.

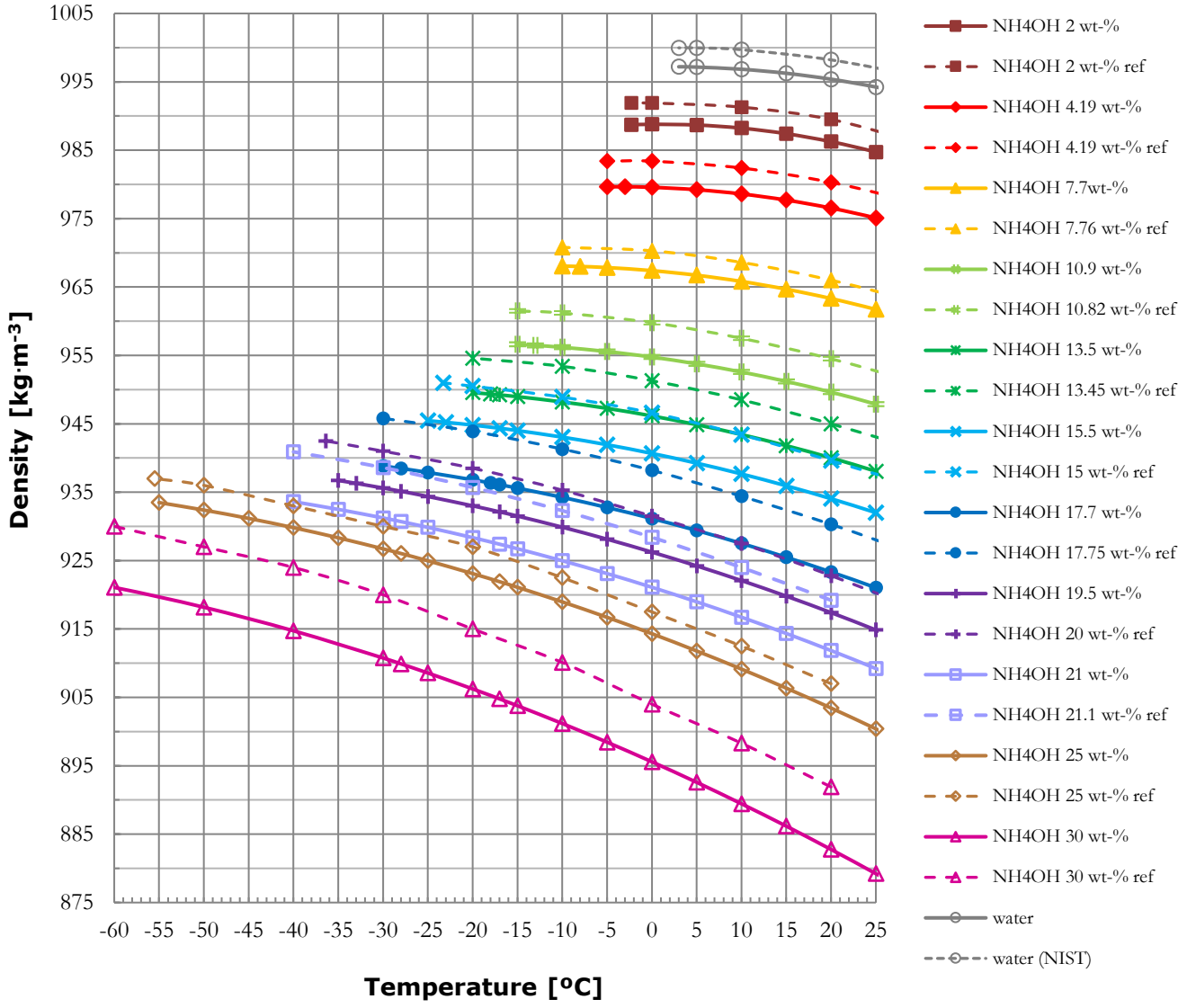

Figure 28: Experimental results for density of aqua ammonia compared to reference values.

3.4 Viscosity Results

Experimental results for dynamic viscosity are displayed in Figure 29. For ease of comprehension, only solutions with freezing point temperatures ranging from -5°C to -30°C were included in this graph. Appendix A contains a graph with the results from all the tested solutions. The general trends that can be seen from this graph are that reference values are consistently lower than experimental values for all solutions, most evidently for temperatures up to 15°C. The results are most similar to reference values with increasing temperatures. Specifically, for the 17.7 wt-% solution, the experimental value at -10°C is 13% higher than the reference value, but is only 4% lower than the reference at 20°C. Additionally, the rates of change of viscosity with temperature are comparable between the experimental and reference data, however the actual viscosity of the solutions was more effected by temperature than previously expected. These results most affect systems operating at low temperatures, as the viscosity will be higher than expected, requiring more energy for pumping.

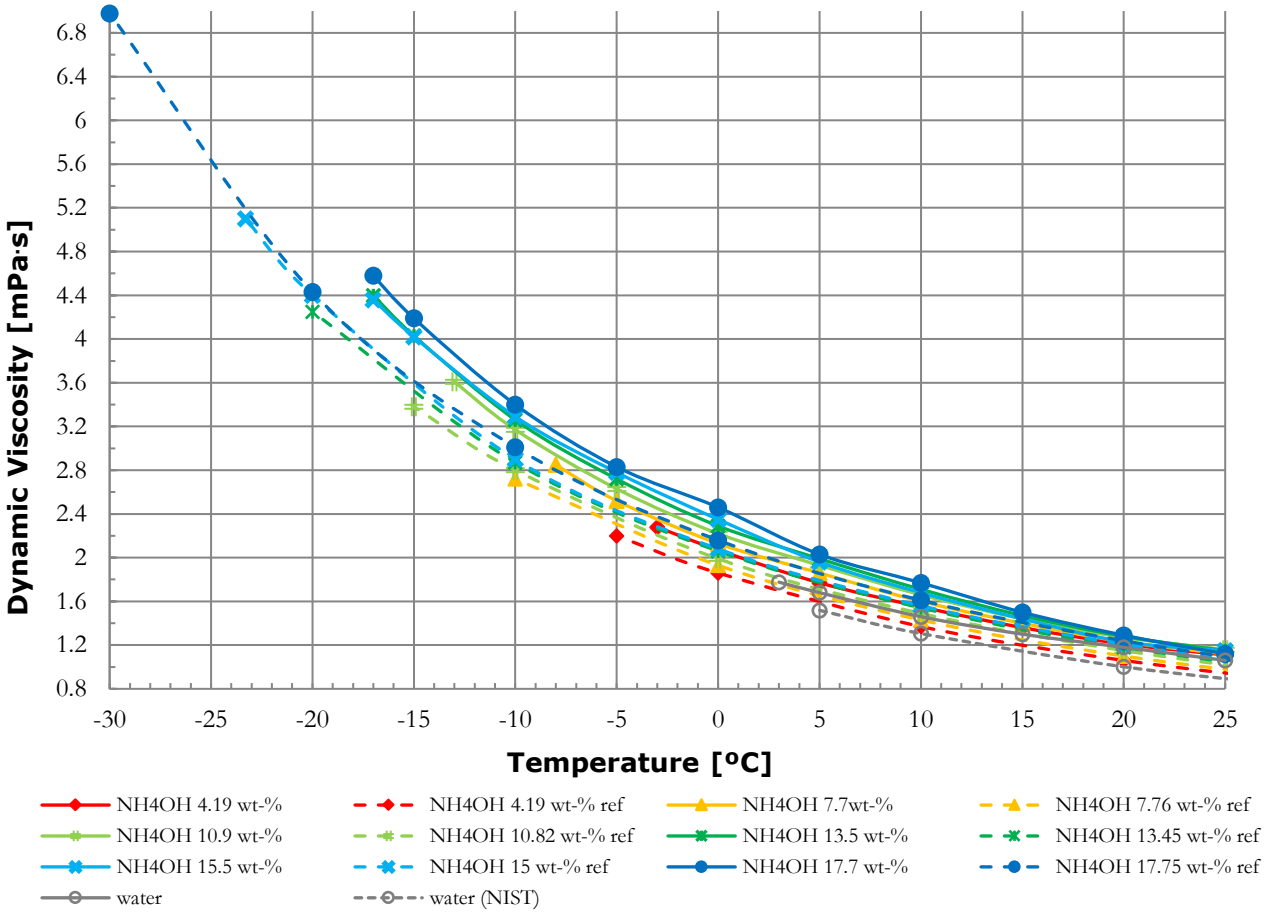

Figure 29: Experimental results for dynamic viscosity of aqua ammonia compared to reference values for solutions with freezing point temperatures ranging from -5 °C to -30 °C (4.19 wt-% to 17.7 wt-%).

Since the lowest measurable value of the instrument is 1 mPa·s, measurements nearing this limit have less certainty than values well above the limit. For example, the measurements at 20°C can show unexpected values. Specifically, in Figure 30 the viscosity of the 25 wt-% solution is greater than the value for both the 21 wt-% and 30 wt-% solutions. This goes against the trend at the rest of the temperatures and what is to be expected but can be attributed to the error of measuring values so close to 1 mPa·s with highly volatile solutions.

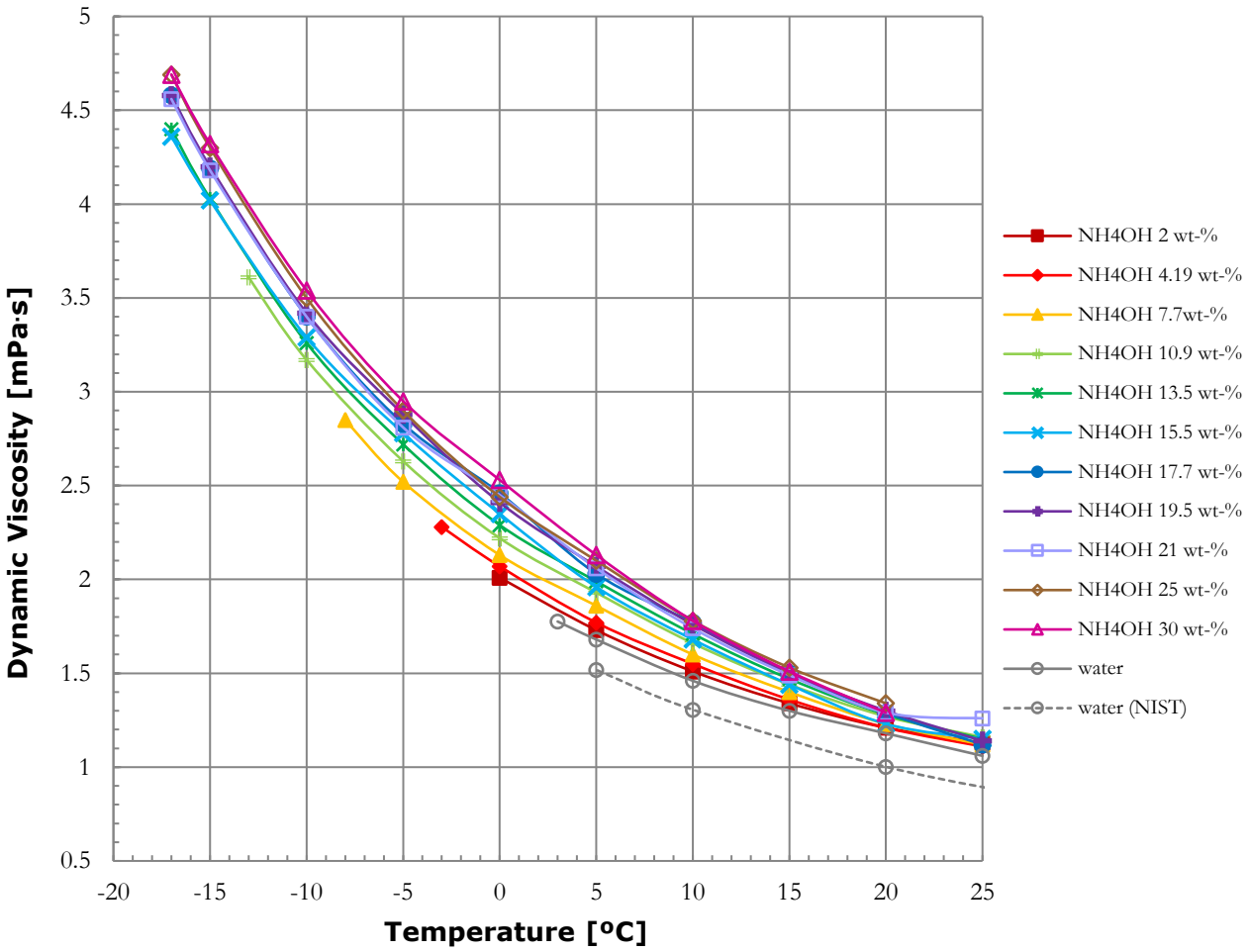

Figure 30: Experimental results for the dynamic viscosity of the aqua ammonia solutions without comparison to reference values.

3.5 Specific Heat Capacity Results

Some of the most unexpected, and thus most noteworthy, results came from the specific heat capacity experiments. Figure 31 displays these results in comparison with reference values. Evidently, the previously estimated and extrapolated values for specific heat capacity are drastically different from the measured values. Not only do the actual values differ, but the effect that temperature has on the specific heat is also opposite to what was previously assumed. The reference values (Melinder, 1998) were generated assuming aqua ammonia would give similar trends to water with varying temperature as it was done in Handbuch der Kältetechnik (Plank, 1959). This assumption, however, is proven to be incorrect based on reliable experimental results.

Furthermore, the results show a change in the trend with changing temperature based on solution concentration. For the solutions with lower than 10.9 wt-% ammonia, the trend is more similar to that of water but with slightly higher values of specific heat. It is worth mentioning these results because they have higher specific heat values than water, even though it has been assumed that any additive to water will decrease the specific heat. However, this experiment proves that up to a certain concentration, adding ammonia to water will increase the specific heat capacity of the fluid.

With the exception of the three lowest concentration solutions tested, the values of specific heat start to be lower than the reference values between 5°C and -10°C. The difference in the reference and measured values at -30°C for 17.7 wt-% solution is 9%. This result can affect system design with respect to calculating the heat transfer coefficient, but not detrimentally. With lower specific heat capacity values than expected, the mass per volume is also affected which can increase the required pumping power. Impacts on real systems are discussed in later sections.

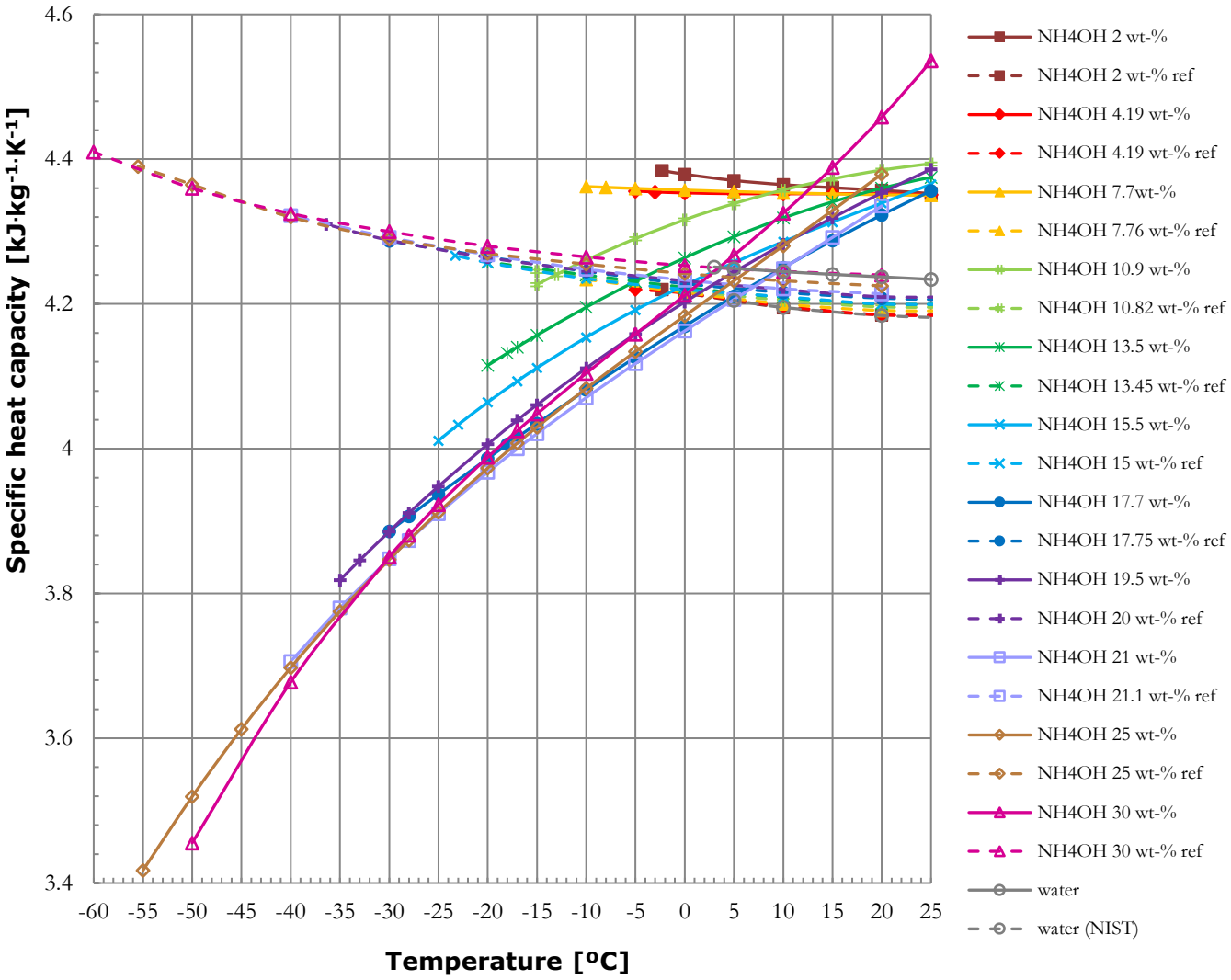

Figure 31: Experimental results for specific heat capacity of aqua ammonia compared to reference values.

In order to more clearly distinguish between the measured data, a smaller temperature range is shown in Figure 32. This graph makes is clearer to observe the behavior of the results for the higher concentration solutions. The higher concentration solutions, starting at a concentration of 17.7 wt-%, show polynomial trendlines to the third order more clearly at temperatures above 0°C. The solutions with lower concentrations seem more in line with second order polynomial trends for the full range of temperatures shown. Furthermore, the results stray from assumed trends at high concentrations. For example, 30 wt-% solution results in a higher specific heat capacity than 25 wt-% and 21 wt-% solutions for temperatures above -30°C. With increasing temperature, the specific heat also becomes higher than 19.5 wt-% and 17.7 wt-% solutions. A similar situation is present when comparing 17.7 wt-% and 19.5 wt-% solutions as well. It would be assumed that the higher concentration solution would have lower specific heat capacity, but the results show otherwise. A reason for these unexpected results in comparison with each other could be partially attributed to the high volatility of the solutions at higher concentrations.

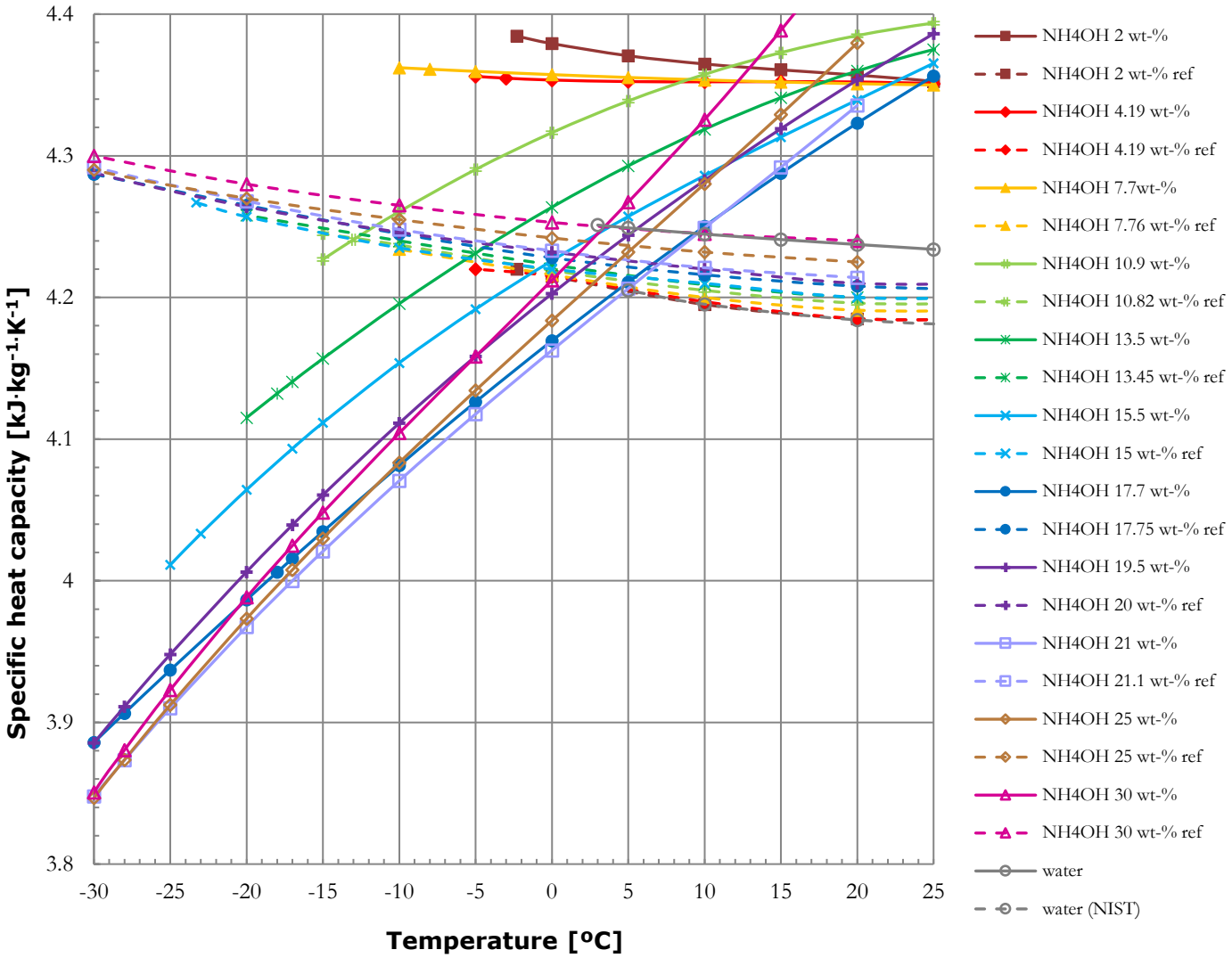

Figure 32: Experimental results for specific heat capacity of aqua ammonia, with reference values, for a temperature range from -30 ºC to 25 ºC.

Furthermore, the trends found can be somewhat validated from some references, shown in the figures below. Figure 33 is a comparison of reference data (Melinder, 1998) with the new experimental data. The digital version of the graph (top right graph) was created by estimating the values from the graph in the hardcopy book (top left image). The reference values in Melinder (1998) come from 5 different sources, listed in

Table 8. These 5 sources were graphed with differing line types and without line markers. The labels 1-5 were used to distinguish between references and can be seen in the table as well as in the legend. The wt-% of the ammonia solutions from the reference values are listed in parentheses following the reference number.

The experimental data completed during this project are shown in the top right and bottom graphs of Figure 33 with solid lines and star line markers. The experimental data shown is for solutions of 10.9 wt-%, 19.5 wt-%, and 30 wt-% for a more direct comparison with literature data. The bottom graph shows the same data as the top right graph, but with a larger range for specific heat to better show the trend of changing specific heat with temperature of the experimental results. Although the values of specific heat for the different concentrations and temperatures are not the same between the references and new experimental values, the increasing specific heat capacity with temperature trend is similar. Since this trend is the opposite of what was reported in Melinder (1997), shown as the solid line curves in the lop left graph of Figure 33, validity is added to the new experimental values.

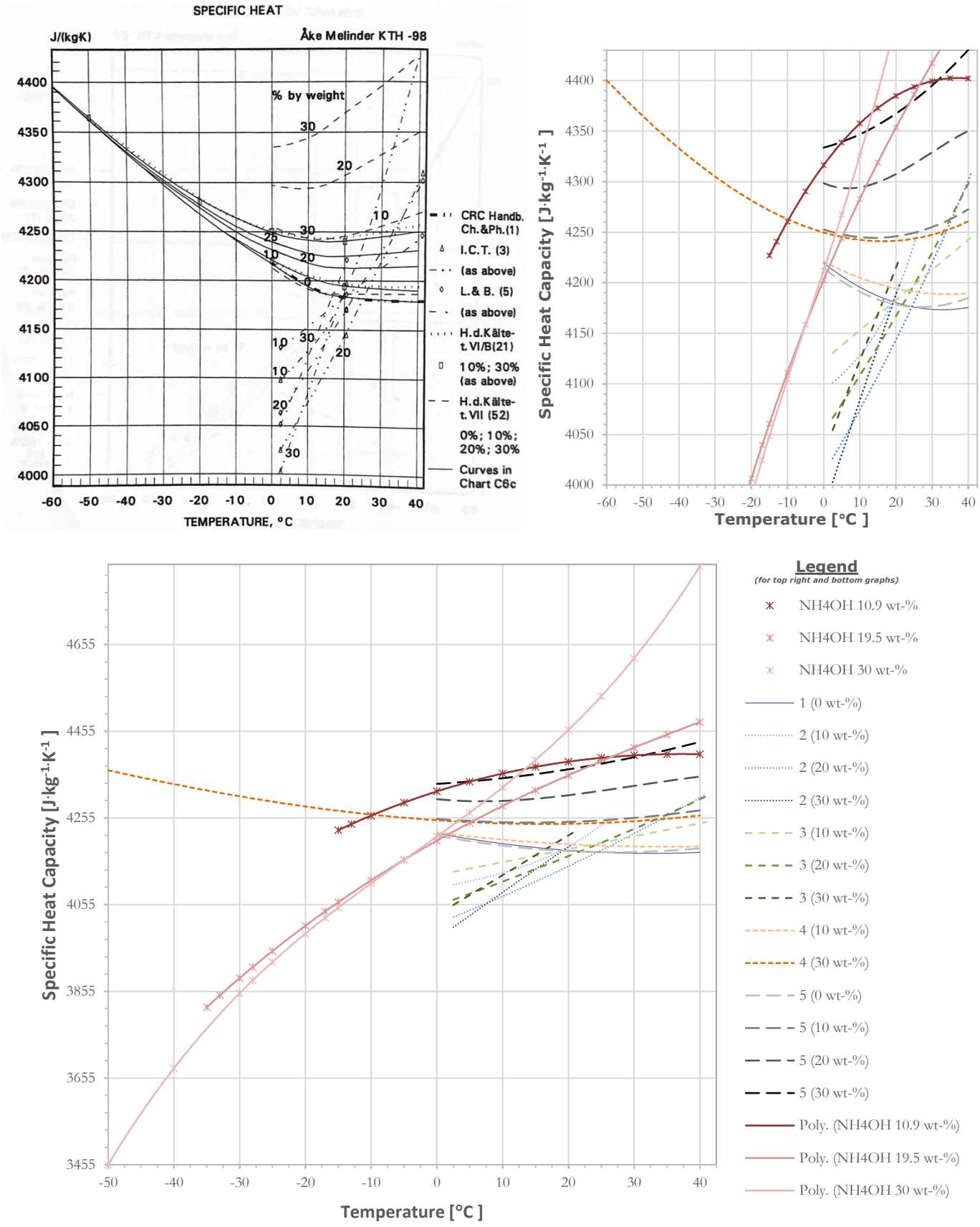

Figure 33: Comparison of reference data and new experimental data for specific heat capacity of aqua ammonia. The top left graph is a scan from Melinder (1998) with a digital recreation on the top right. The digital recreation shows values estimated from the original copy with trendlines, as well as new experimental values for three aqua-ammonia solutions (lines with the star markers). The bottom graph is the same as the top right with larger axis ranges to show the more complete experimental data in comparison with the reference values.

Table 8: Information for comparing Melinder (1998) data and new values for specific heat capacity.

Number	Melinder (1998) Ref. Number	Source	Year	Concentrations	Label in Graph
1	[1]	CRC Handbook of Chemistry and Physics, 67th Edition (1986-87)	1986	0 (water)	1 (0 wt-%)
2	[3]	International Critical Tables of Numerical Data, Physics, Chemistry, and Technology (1928-29)	1928	10 wt-%, 20 wt-%, 30 wt-%	2 (10 wt-%) 2 (20 wt-%) 2 (30 wt-%)
3	[5]	Landolt-Börnstein; Numerical Data and Functional Relationships in Science and Technology; Vol 1b (1977)	1977	10 wt-%, 20 wt-%, 30 wt-%	3 (10 wt-%) 3 (20 wt-%) 3 (30 wt-%)
4	[21]	Handbuch der Kältetechnik, VI/B; R. Plank (1988)	1988	10 wt-%, 30 wt-%	4 (10 wt-%) 4 (30 wt-%)
5	[52]	Handbuch der Kältetechnik, VII; R. Plank (1959)	1959	0 wt-%, 10 wt-%, 20 wt-%, 30 wt-%	5 (0 wt-%) 5 (10 wt-%) 5 (20 wt-%) 5 (30 wt-%)

3.6 Thermal Conductivity Results

The results for thermal conductivity deviate from the reference values, although not as significantly as for specific heat capacity. Figure 34 shows the results and reference values. The measured results for each solution are the points on the graph. Linear trendlines were applied to each in order to more accurately estimate the values outside of the measuring range of the instruments. Ammonia solutions are highly conductive, resulting in values that fluctuate highly between temperatures, which is the reason to display the data with trendlines. For every solution, the reference values are lower than the measured values. Similar to specific heat capacity, the 2 wt-% solution has higher thermal conductivity than water at lower temperatures. This is unexpected, as it has been assumed that any additive to water will decrease the thermal conductivity. The reference values in the graph, the dashed lines, all have the same slope as the reference line for water, which indicates that the reference values were estimated with the assumption that the thermal conductivity is affected by temperature in the same way as for water. The less steep slopes of the measured values prove that this was an incorrect assumption. Furthermore, the slope is nearly the same for all of the ammonia solutions. The largest difference between the reference and measured values is at -20°C for 30 wt-% solution with the measured value 13% higher than the reference.

The results for 17.7 wt-%, 19.5 wt-%, and 21 wt-% solutions show very similar values as well as some unexpected results. The reason for these overlapping trendlines could be due to degassing of samples during the experiment, resulting in inconsistent results. This especially applies to samples with higher ammonia concentrations and at higher temperatures, starting at 10°C. The results show that there is a higher discrepancy between experimental results and reference values for solutions at higher ammonia concentrations. There is also a gap in the results between 7.7 wt-% and 10.9 wt-% indicating a specific concentration where the thermal conductivity drops and lessens the gap between measured and reference values.

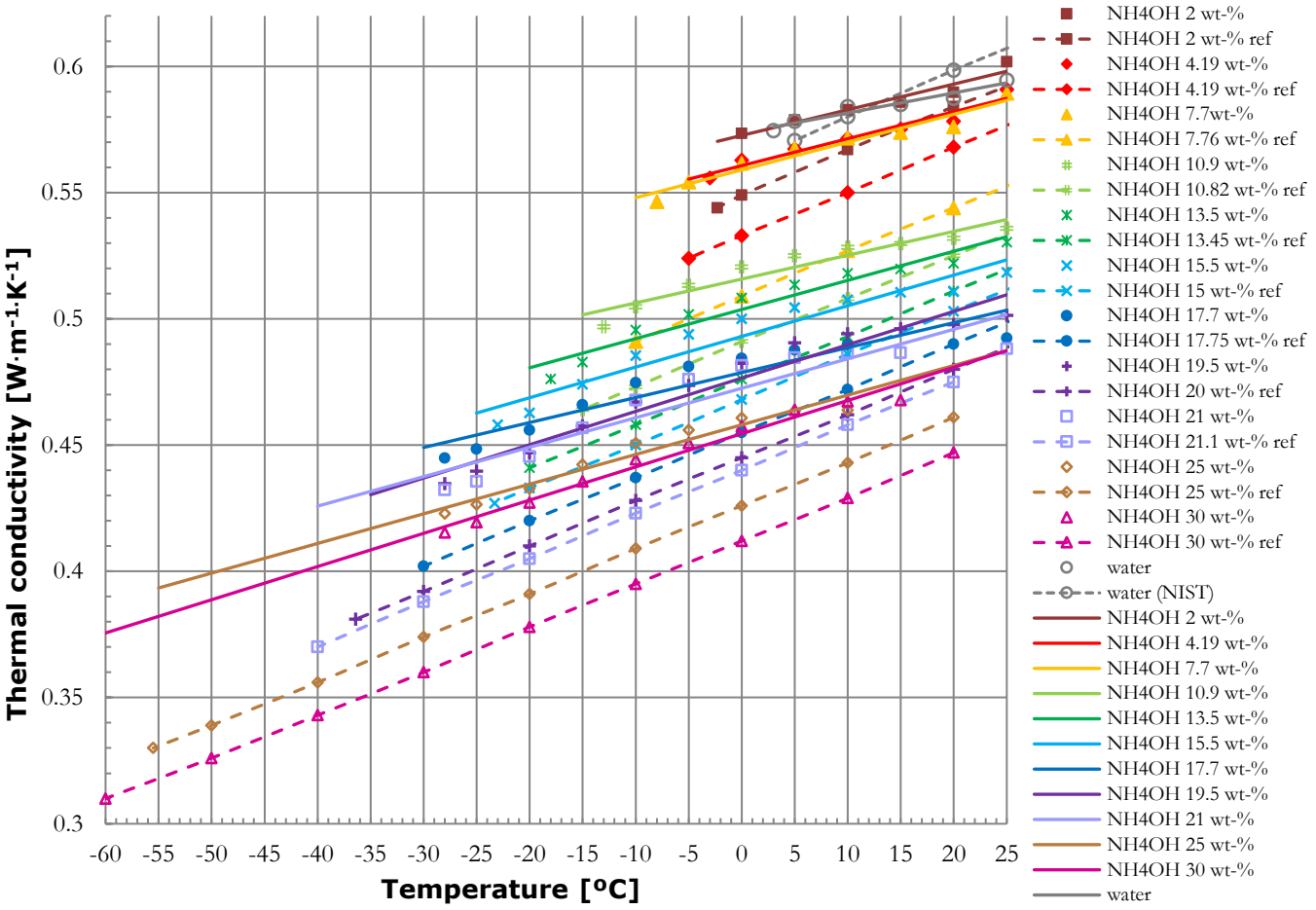

Figure 34: Thermal conductivity experimental results for ammonia solutions with reference values.

Figure 35 shows reference data from Melinder (1998) in the top left graph and the digital recreation in the top right graph. The digital version also includes experimental data from this project for easy comparison. The solid line curves shown in the scanned graph from Melinder (1998) were only generated from the two values indicated with a diamond at 8.9 wt-% and 26 wt-%. In addition to these measured values indicated with square markers, the bottom graph includes another source of measured thermal conductivity values for 15 wt-% and 20 wt-% indicated with circle markers.

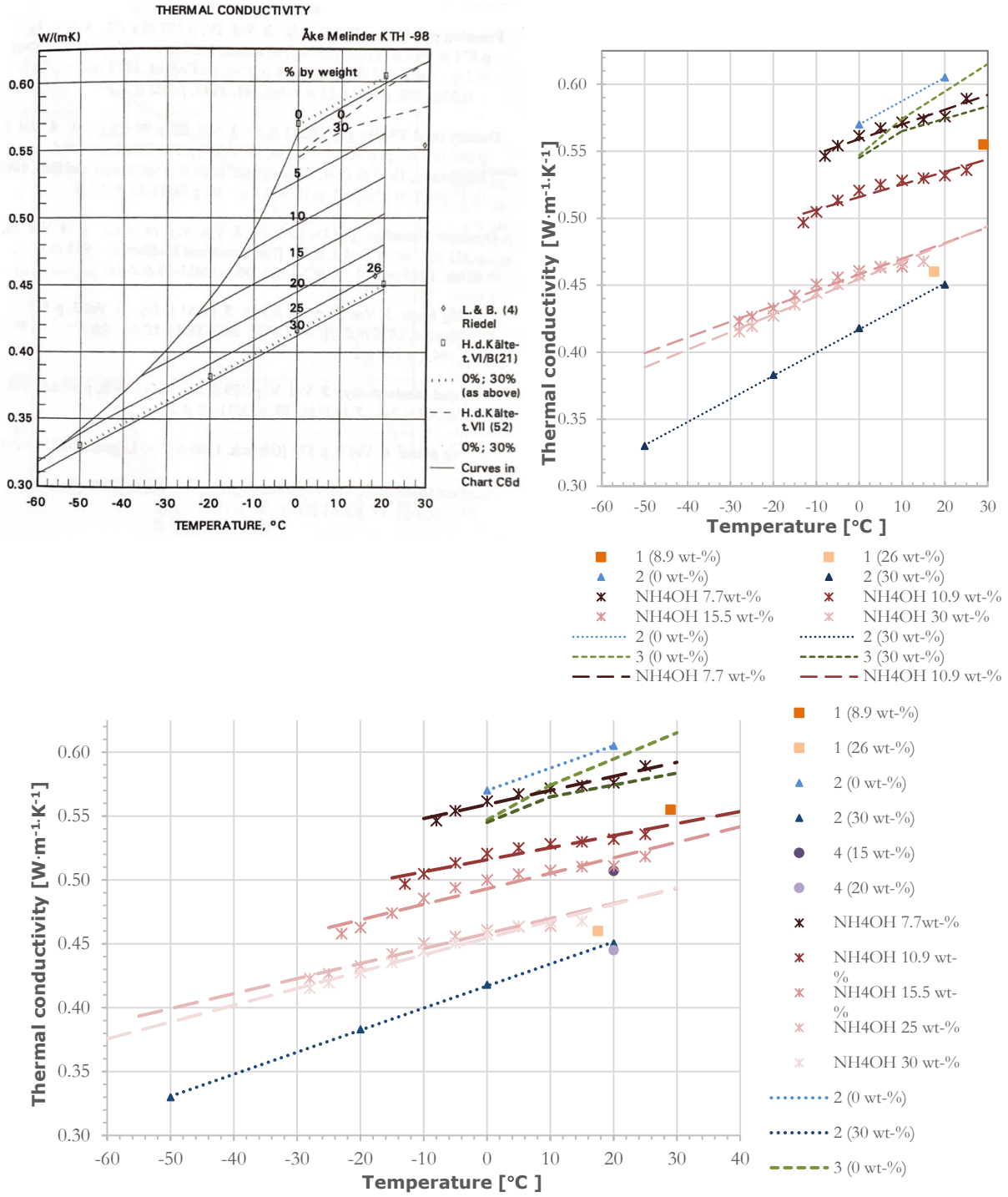

Figure 35: Comparison of reference data and new experimental data for thermal conductivity of aqua ammonia. The top left graph is a scan from Melinder (1998) with a digital recreation on the top right. The digital version shows values estimated from the original copy with trendlines, as well as new experimental values for four aqua ammonia solutions (lines with the star markers). The bottom graph is the same as the top right, with another source of measured data and new experimental data at an additional concentration.

These reference data are comparable to new experimental data at similar concentrations and temperatures, which somewhat validates the current results. However, these were the only measured values found and are from 1951 and 1960, which proves the need for more experimental results for thermal conductivity of ammonia solutions. Table 9 shows the references used to create the graph from Melinder (1998) along with the corresponding label for the two digital graphs in Figure 35.

Table 9: Information for comparing Melinder (1998) data and new values for thermal conductivity.

Number	Melinder (1998) Ref. Number	Source	Year	Concentrations	Label in Graph
1	[4]	Landolt-Börnstein; Eigenschaften der Materie in Ihren Aggregatzuständen (1960-1971)	1997	8.9 wt-%, 26 wt-%	1 (8.9 wt-%) 1 (26 wt-%)
2	[21]	Handbuch der Kältetechnik, VI/B; R. Plank (1988)	1988	0 wt-%, 30 wt-%	2 (0 wt-%) 2 (30 wt-%)
3	[52]	Handbuch der Kältetechnik, VII; R. Plank (1959)	1959	0 wt-%, 30 wt-%	3 (0 wt-%) 3 (30 wt-%)
4	N/A	Wärmeleitfähigkeitsmessungen an Mischungen verschiedener organischer Verbindungen mit Wasser; L. Riedel (1951)	1951	15 wt-%, 20 wt-%	4 (15 wt-%) 4 (20 wt-%)

3.7 Corrosion Results

Corrosion is a chemical reaction, often electrochemical, of a material that destroys its structure. Simply put, when a metal is placed in a corrosive solution, different areas of the surface act as anodes and cathodes, essentially creating a short-circuited galvanic cell. In the anodic regions, the metal is being oxidized and a loss of mass is observed. The oxygen in the solution is reduced at the cathodic regions (Ignatowicz, 2008). This loss of mass was used to determine corrosion rates according to the ASTM NACE TM0169/G31-12a standard, while the specimens were prepared and measured according to ASTM G1-03 (reapproved 2017) standard. The following graphs in Figure 36 show the corrosion rates of the different specimens for each aqua ammonia solution. The highest corrosion rates appear for copper at a maximum of 16.2 mm/year and the lowest rates appear for stainless steel at a maximum of 0.044 mm/year. There are some corrosion rates that are negative, specifically for aluminum. This means that passivation occurred instead of corrosion.

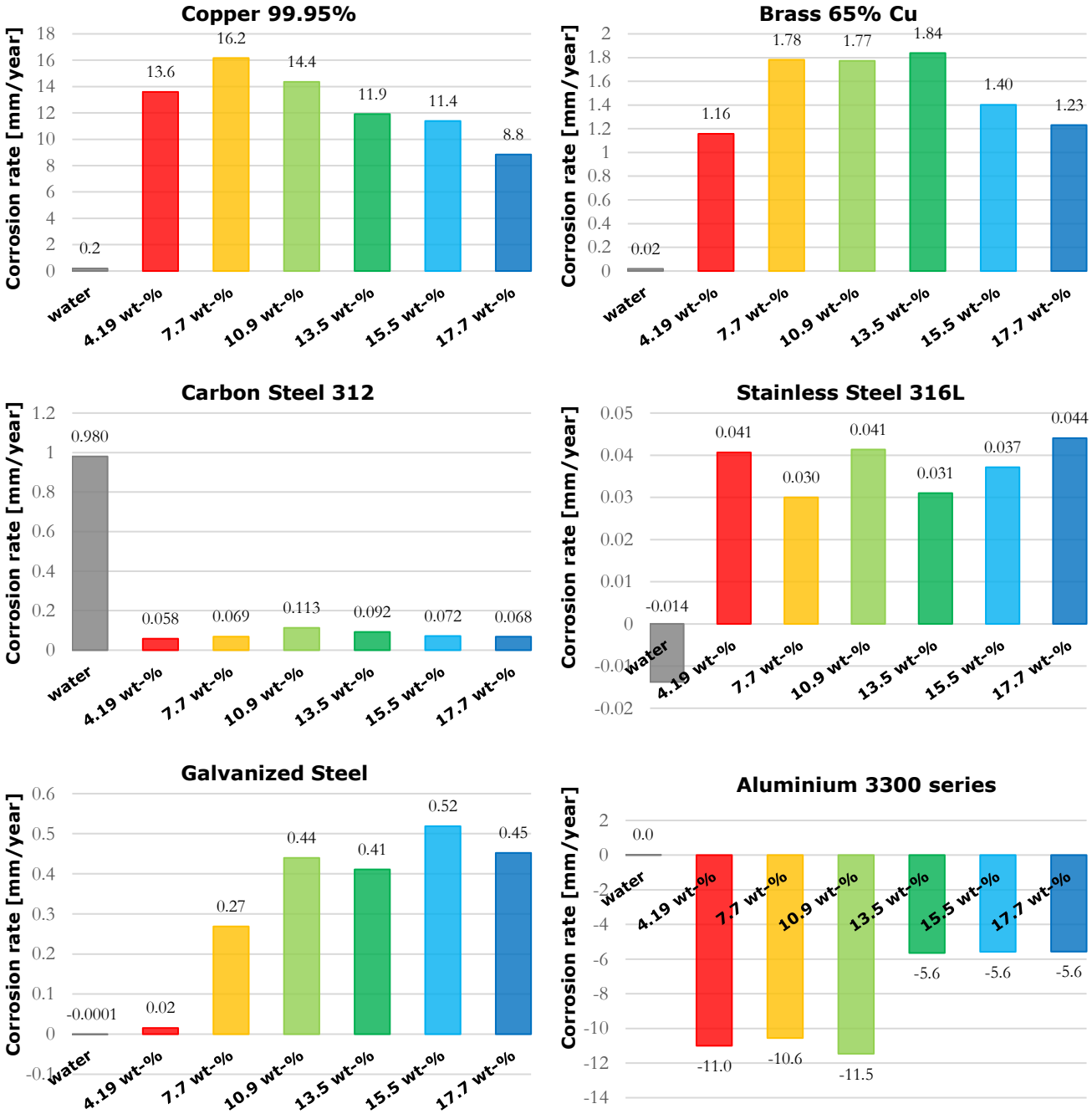

Figure 36: Corrosion rates, [mm/year], for copper, brass, carbon steel, stainless steel, galvanized steel, and aluminum in ammonia solutions from 4.19 wt-% to 17.7 wt-%.

Passivation is when an oxide film forms on the surface of the metal, essentially forming a protective layer against further corrosion (Ignatowicz, 2008). In these cases, the mass of the metal increases, resulting in negative corrosion rates. In either the case of corrosion or passivation, the results have peaks of corrosion rates versus the solution concentration. This means that an increase in solution concentration does not have a linear effect on corrosion. For each type of metal specimen, there is a certain concentration with the highest corrosion rates. This is due to the amount of oxygen present in the solution. There is a certain amount of oxygen that is ideal for corrosion to occur. This peak should be observed when designing a system to know which concentrations will result in higher corrosion rates.

In addition to metal samples, brass connections commonly used in industry were also tested and resulted in a corrosion rate of a maximum of 112.6 g/year, seen in Figure 38. Note that this result is in grams rather than millimeters due to the complex geometry of the connections. The copper and copper connection specimens after the test are shown in Figure 37.

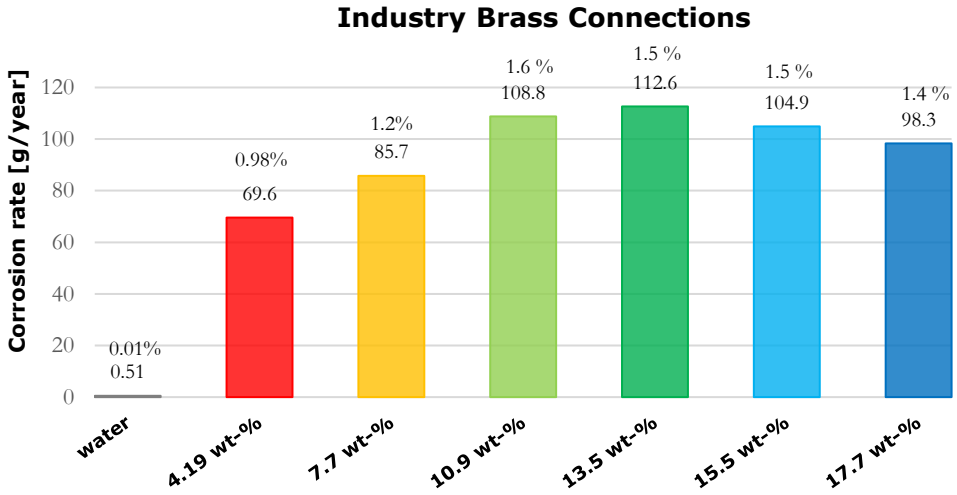

Figure 37: Corrosion rate, [g/year], of brass connection commonly used in industry.

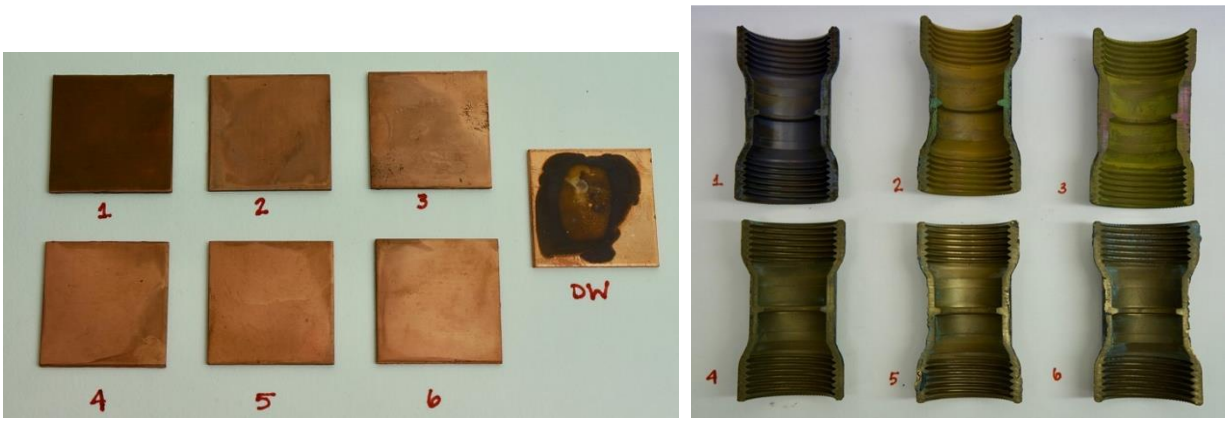

Figure 38: Pictures of completed corrosion tests for copper (left) and brass connections (right) in ammonia solutions ranging from 4.19 wt-% to 17.7 wt-%. The numbers are associated with the ammonia solution used for the test. Number 1 represents 4.19 wt-% and 6 represents 17.7 wt-%.

These corrosion rates are crucial knowledge in the conversion of existing systems to aqua ammonia systems because of the frequent use of such fittings during repairs. Knowing the corrosion rate of certain system components will help to predict if and when a leak will occur. The corrosion rate should also be used when designing a new system to avoid potential leaks. Furthermore, there is not much available data on these specific corrosion rates, which allows this data to be particularly helpful to the refrigeration sector. Based on these results, stainless steel and carbon steel are recommended as materials compatible with aqua ammonia, while copper and aluminum are not compatible.

4 Theoretical Comparative Study

4.1 Objectives

A study has previously been conducted in order to compare the performance of several common secondary fluids in ice rinks. The study compares a typical refrigeration system design at steady state and does not include analysis of investment or operation costs (Mazzotti, 2014). However, this study used the properties available, yet outdated, at the time for aqua ammonia as a secondary fluid. The study has been repeated using the tools developed by Mazzotti (2014) with the updated thermophysical properties for aqua ammonia, as well as the latest experimental results for the other secondary fluids, when available. This section will explain the theoretical model and discuss the new results in comparison with the previously generated results, as well as the other secondary fluids analyzed. Appendix B contains the equations used in the development of the tool used in this comparative study. Further details on the background information and assumptions made for this study can be found in the thesis completed by Mazzotti (2014).

4.2 Design of Comparative Study

In order to compare several secondary fluids, the calculations were carried out assuming a fixed, standard ice rink design. The controlled parameters of the ice rink design include the ice floor layout and piping arrangement, evaporator design, and the rink and piping dimensions. The primary refrigerant was chosen to be ammonia. Furthermore, heat loads and freezing points are fixed for each calculation but can be varied as needed before the start of the calculation. The tool operates by inputting a main variable, which could be one of the following: average temperature of the secondary fluid, ice temperature, and pump control (temperature difference). The outcome is a number of results that can be used to compare secondary fluids in terms of their thermophysical properties and overall refrigeration efficiency, identify optimum pump control, and compare the use of fluids with different freezing points. The secondary fluids included in this study are solutions of calcium chloride ($CaCl_2$), propylene glycol (PG), ethylene glycol (EG), aqua ammonia (NH_3), potassium acetate (K-acetate), and potassium formate (K-formate) in water. Figure 39 is a diagram of the calculation process of the model. For simplicity, throughout Section 5 the secondary fluids will be referred to by the additive to water as opposed to the additive with water. For example, aqua ammonia is actually NH_4OH but will be referred to as NH_3.

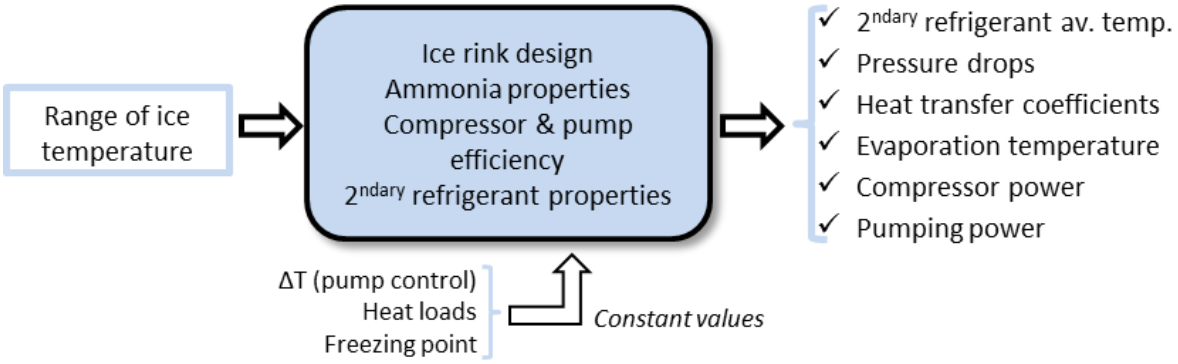

Figure 39: Diagram of calculation process of the theoretical model with ice temperature as the input values (Mazzotti, 2014).

The main tool of the study was developed in *Microsoft Excel* and utilized *Visual Basic* for programming. Additionally, *COMSOL Multiphysics* was used in order to develop both two- and three-dimensional models of the ice floor. The properties of the primary refrigerant (F-Chart Software, n.d.; Granryd et al., 2009) and secondary fluids (Melinder, 2010b) were used for the calculations (Mazzotti, 2014).

4.2.1 Evaporator Assumptions

Ice rink indirect refrigeration systems operate in a manner where the secondary fluid acts as a heat source for the evaporation of the primary refrigerant. Therefore, the evaporator acts as a heat exchanger between the fluids and is considered to be a plate heat exchanger (PHE) in this case. PHEs are commonly used due to their high efficiency, compact size, and cost (Huang, 2010).

It is necessary to assume the same PHE design for all secondary fluids in order to effectively compare their performance, which was determined based on literature studies and results from calculations in the *Alfa Laval* software (Mazzotti, 2014). The evaporator is chosen to be a flooded, single-pass counter-flow heat exchanger with corrugated plates, as shown in Figure 40. The plates are chevron-type and separate the primary and secondary fluids in this alternated flow distribution. Moreover, the evaporator is considered to be a flooded evaporator.

The plates are assumed to be made of titanium to ensure no corrosion with the ammonia or any of the secondary fluids. Titanium has many advantages with its main drawback being the high cost (Ignatowicz, 2008). The main features of the plates that are influential in the calculations include effective channel length and width, corrugation pitch, plate thickness, chevron angle, and pressing depth, which are illustrated in Figure 41. These factors directly impact the surface enlargement factor, hydraulic diameter, Reynolds number, and Nusselt number, whose definitions can be found in Appendix B. The geometry of the plates also dictates the amount of pressure drop on the secondary fluid side of the PHE.

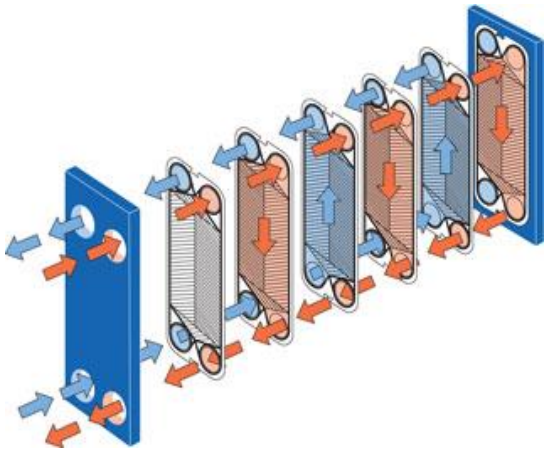

Figure 40: Flow configuration in a single-pass counter-flow PHE from Alfa Laval software (Mazzotti, 2014).

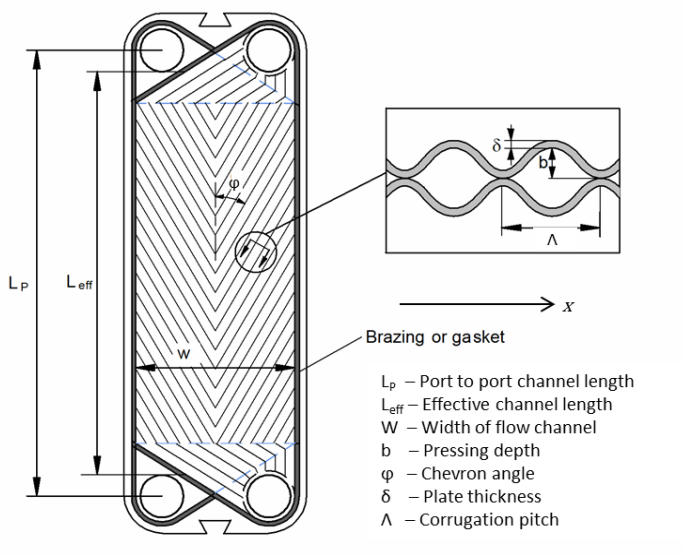

Figure 41: Geometry and features of a plate from a chevron-type PHE (Huang, 2010).

4.2.2 Evaporator Heat Transfer

Generally, heat transfer is characterized by a heat transfer coefficient that can be used to help determine the effectiveness of different secondary fluids. In the PHE, convective heat transfer occurs on the secondary fluid side of the plates while boiling heat transfer occurs on the primary refrigerant side. The determination of the heat transfer coefficients is affected by the Nusselt and Reynolds numbers, as shown in the explanation of the calculations in Appendix B. Both convective and boiling heat transfer coefficients are used to calculate the overall heat transfer coefficient. The overall heat transfer coefficient is the proportionality constant between the heat flux and temperature difference ("Heat Transfer Coefficient," 2019). In calculating the heat transfer coefficient, all of the heat transfer resistances within a plate of the PHE are considered. Typically, the resistance from fouling is accounted for in calculating the heat transfer coefficient. However, this correlation has not yet been well defined specifically for PHE and has been omitted from these calculations (Huang, 2010). The evaporator is also assumed to be isolated, which means all of the heat released from the secondary fluid is absorbed by the primary fluid. The assumed PHE design considering the pressure drop and heat transfer was confirmed with *Alfa Laval* (Mazzotti, 2014).

4.2.3 Ice Rink Design Assumptions

As mentioned, the ice rink refrigeration system is assumed to be a fully indirect system as described in Section 1. The indirect loop of the system interacts with two heat exchangers: the evaporator and the ice rink floor. The loop is insulted from the ground, eliminating any associated heat gains. The total cooling capacity of the indirect loop is a sum of the heat loads from the ice floor and the heat gains from the pumps,

headers, and distribution pipes. It is assumed that the heat loads account for 90% and the heat gains account for 10%. The distribution pipes connect the evaporator to the ice floor and are assumed to be 20 m long steel pipes with an inner diameter of 150 mm and roughness of 50 μm.

Pump control of the secondary fluid is imperative to the performance in terms of heat transfer and pressure drop. The pump controls the flow of the secondary fluid, which influences the heat transfer coefficient and total pumping power. Relations made by the Nusselt number show that a higher flowrate results in higher heat transfer coefficients. The flowrate also dictates the type of flow within the pipes: laminar or turbulent. Turbulent flow is favored as it results in higher heat transfer coefficients. Because the ice surface is required to have an even distribution of temperature, the pump in ice rink systems is most often controlled by maintaining the temperature difference of the secondary fluid (ΔT). This may, however, lead to a less-than-optimal pumping power.

The design and analysis of the refrigeration system within the ice rink is not the focus of the study and, therefore, calculations are based on a theoretical cycle using values from literature and the pressure-enthalpy (P-h) diagram for ammonia, shown in Figure 42. The assumptions made around the refrigeration cycle are as follows (Mazzotti, 2014):

- Ammonia is the primary refrigerant
- The compressor isentropic efficiency is constant at 0.65
- Isentropic expansion
- Constant evaporation and condensation pressures
- Low value of superheating at 1 K due to flooded evaporator
- Subcooling value of 5 K
- Boiling heat transfer calculation using a coefficient of 0.1121 for the flooded evaporator
- Constant condensation temperature of 20°C
- Evaporation temperature is dependent on the secondary fluid used and was determined by a polynomial approximation tool in *Microsoft Excel*
- Critical pressure of 113.33 bar

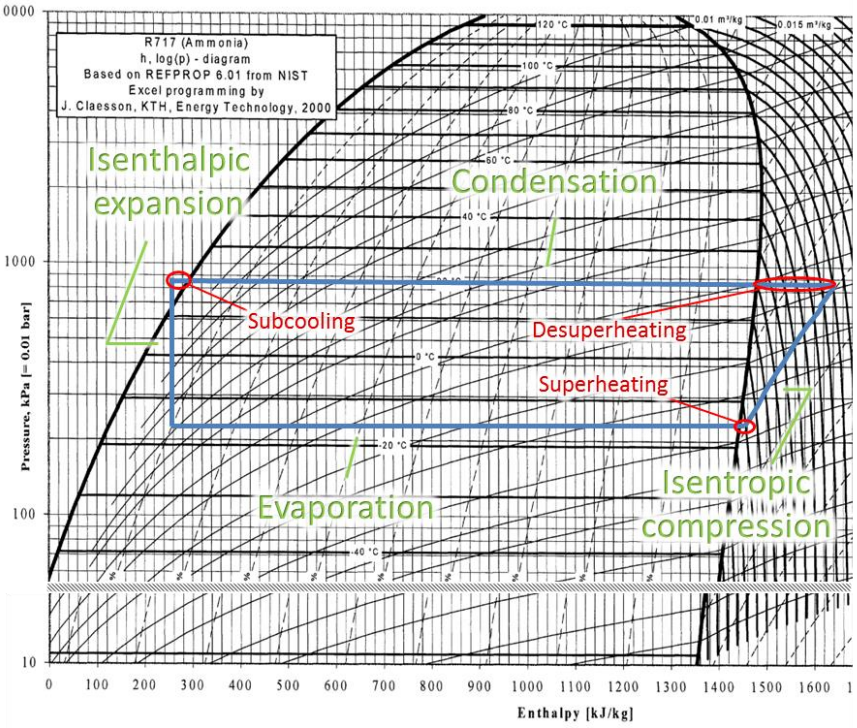

Figure 42: P-h diagram for ammonia with an example of a theoretical refrigeration system with constant evaporation and condensation pressures, isenthalpic expansion, and isentropic compression (Granryd et al., 2009). However, superheating is identified but has not been included in the assumptions for the refrigeration system to be modeled.

Hockey is assumed to be the main purpose of the ice rink, resulting in an ice floor that is 60 m by 30 m. The pipes that are located under the ice slab that transport the secondary fluid are U-shaped pipes that run the length of the ice rink floor with the header located along the short side, as displayed in Figure 43. The header is reverse-return, enabling for an evenly distributed flow. The pipes are located 10 cm apart in a concrete slab that is 15.5 cm thick. Below the concrete layer is 15 cm of insulation before the ground. The 3 cm ice slab is located on the concrete, as shown in Figure 44, along with the outer diameter and wall thickness of the U-pipes (12.5 mm and 2.3 mm, respectively). The total length of a U-pipe is around 120 m and there are assumed to be a total of 150 pipes.

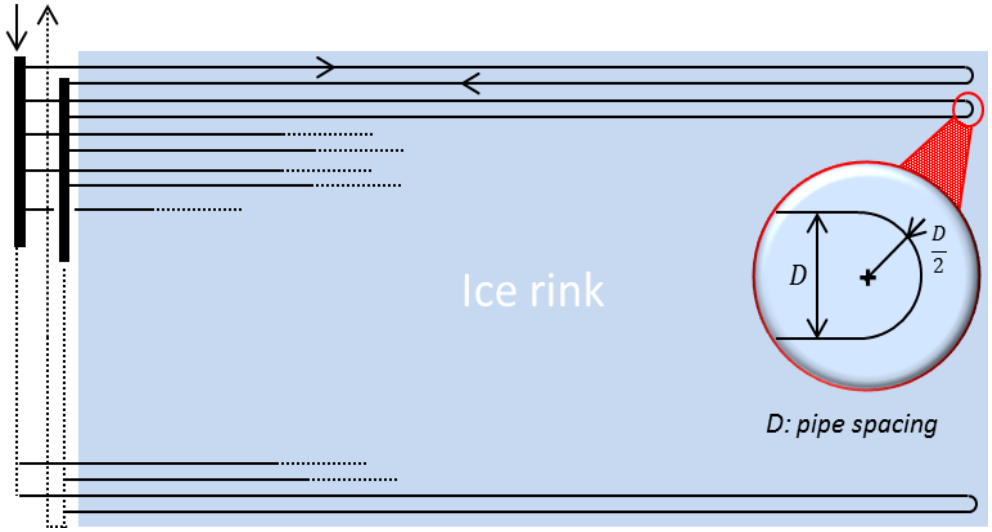

Figure 43: Example of U-pipe layout in the rink floor with a reverse-return header (Mazzotti, 2014).

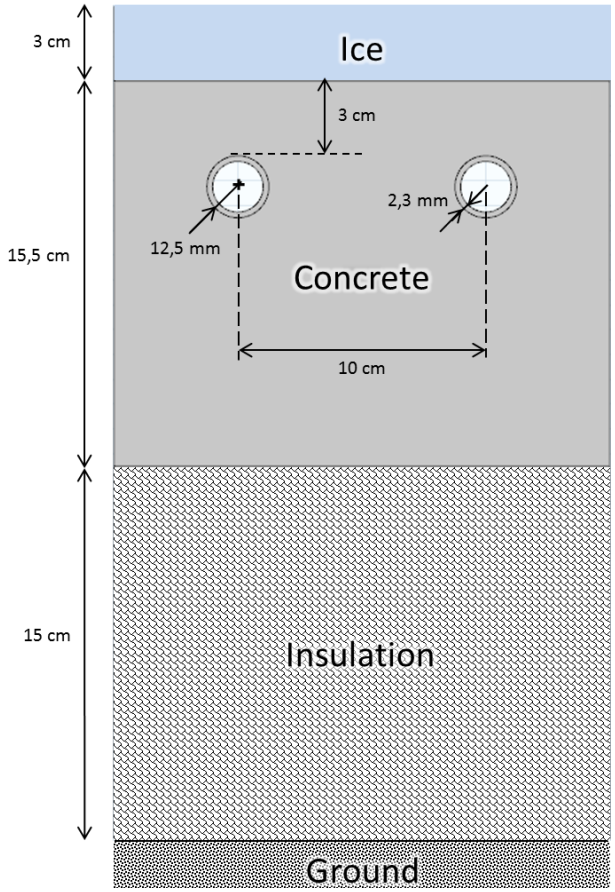

Figure 44: Ice rink floor cross section (Mazzotti, 2014).

Heat transfer within the ice rink floor is highly dependent on the type of flow through the pipes – turbulent or laminar. To account for this difference, multiple equations were used for varying ranges of the Reynolds and Prandtl numbers. A detailed description of equations used and estimation of heat transfer resistances in the pipes can be found in Appendix B. These equations lead to the possibility of calculating the total heat flow in the ice rink floor.

The pressure drop within the pipes is another important factor in the calculations. The type of flow also indicates which equation to use to calculate the friction factor, used in the equation for the total pressure drop. Minor losses within the system are neglected as they vary from system to system and only major losses are considered in order to create a tool that can be applicable to a wider range of rinks. The losses due to the bends in the pipes and in the headers are considered in this case. The correlations used to calculate pressure drop were based on literature regarding cooling coils with secondary fluids (Mazzotti, 2014).

4.2.4 Secondary Fluid Assumptions

The secondary fluids analyzed in the study include the most commonly used fluids or alternate fluids with the potential to be implemented. Typically, secondary fluids are used with a freezing point of -30°C. However, using fluids at lower concentrations, and higher freezing points, could lead to operational advantages. Such advantages could include lower viscosity, hence lower pumping power, and higher thermal conductivity. The study analyzes the potential advantages of using secondary fluids with a freezing point of -20°C instead of the ones with a freezing point of -30°C. The original study includes thermophysical properties for the pure fluids from Melinder (2010) at both temperatures analyzed (Mazzotti, 2014).

4.2.5 Calculation Process

The calculations were compiled into a program with several sub-functions written in *Visual Basic* from *Microsoft Excel* in order to quickly perform all calculations. The iterative calculations were completed using the *Solver* tool.

The pumping power is the sum of the individual power for the PHE and the ice rink floor, headers, and distribution pipes with a constant pump efficiency of 0.5. The compressor power was calculated based off literature data (Granryd et al., 2009). At a given condensation temperature, assumed to be 20°C, the data gave the isentropic compressor power versus evaporation temperature. The higher temperature difference between the condensation and evaporation temperature results in lower energy efficiency.

4.2.6 Comparative Study Limitations

The model is limited by assumptions made around the compressors and pumps, as well as the efficiency thereof, and the control strategies and modeling of superheat in the PHE. The model could be expanded to include all energy systems within an ice rink, not just the refrigeration. Furthermore, the study assumes steady state, but could also be adjusted for unsteady state. Limitations also exist since heat transfer, pumping power, and the resulting cooling capacity were the only factors investigated. The comparative study did not account for several long term factors including, corrosion, environmental aspects, and maintenance and operation.

4.3 Updated Model

As mentioned, the study was developed by Mazzotti (2014) and updated for this project. The main purpose for using this tool is to show how the updated properties of aqua ammonia and the other secondary fluids affect the performance and various parameters of ice rink refrigeration. A few changes were made to the original tool. First, the calculations were carried out at a freezing point of -25°C because -30°C is prevalently used in industry, but lower concentrations lead to better thermophysical properties (Mazzotti, 2014). The results from the original study were used with a freezing point of -30°C. As discussed later in the results, the difference in freezing temperature is considered when comparing the original results with the updated results. Nevertheless, the model was updated with the experimentally measured properties available for the secondary fluids. The new, measured values for aqua ammonia came from the work carried out for this project. The measurements for the glycols were extracted from a report for the Swedish Energy Agency (Ignatowicz et al., 2018), and the measurements for the potassium salts were taken from a conference paper (Ignatowicz et al., 2019). Since there were no measured results available for calcium chloride solution with

a freezing point of -25°C, the reference values used are from the same source as in the original calculations (Melinder, 2010b). The resulting outputs are considered the updated results. Additionally, the freezing points of -20°C and -30°C were used for the comparison of overall efficiency for different solution concentrations. Similarly, the properties for the secondary fluids were updated with the same sources as for a freezing point of -25°C. However, for calcium chloride, measured values for freezing point -30°C were used (Mazzotti, 2014).

Updated results were completed for cooling capacities of 100 kW, 200 kW, and 300 kW. The previous version of the study included analysis of ethyl alcohol (EA) but has been omitted in the updated results due to its lack of use in real systems. The value of ΔT was assumed to be 2.5 K, as in the original study. The results of the updated model were analyzed against the results of the original model, as well as again comparing aqua ammonia as a secondary fluid to other fluids included in the study.

4.4 Results

The results from the study allow for the comparison of secondary fluids, determination of optimum pump control, and the ideal freezing point temperature of the secondary fluid. The secondary fluids are compared by analyzing graphs displaying either convection heat transfer coefficients, overall efficiency, or pumping power for various input parameters. As an indicator of overall efficiency, the calculations give results for the coefficient of performance (COP), which is defined in this case as the ratio of the cooling capacity to the sum of the compressor and pumping power, (Equation 8. Graphs were also generated to compare optimum pump control at the different cooling capacities mentioned. The graphs at the different cooling capacities not mentioned in this section can be found in Appendix B. Finally, the model was used to compare freezing points by analyzing the change in COP with different secondary fluid concentrations. The overall results in each of the following sections are analyzed and compared to the previous results.

$$COP = \frac{\dot{Q}_2}{P_{comp} + P_{pump}} \qquad \textit{(Equation 8)}$$

$\dot{Q}_2$: cooling capacity [W]

P_{comp} : compressor power [W]

P_{pump} : pumping power [W]

4.4.1 Secondary Fluid Comparison – Convection Heat Transfer Coefficient

The heat transfer coefficients of the secondary fluids are compared first. The heat transfer coefficient in the U-pipes in the ice floor and in one plate of the PHE was calculated, with results shown in Figure 45 and Figure 46, respectively. For both coefficients, K-formate has the highest values for the entire temperature range, followed by NH_3 and $CaCl_2$. The sharp change in heat transfer values for aqua ammonia, for example, in both graphs is due to the change of flow type within the plate or pipe. Laminar flow results in lower heat transfer coefficients, seen at the lower temperatures before the drastic increase. The change from laminar to turbulent flow for NH_3 occurs around -12°C in the U-pipe and around -6°C in the PHE. In the U-pipes, PG, EG, and K-acetate have laminar flow for the entire temperature range and hence, insufficient heat transfer coefficients. The use of these secondary fluids in this particular system would be ineffective or inefficient. Furthermore, at temperatures lower than -12°C, the heat transfer coefficient of NH_3 in the U-pipe would about one sixth of the coefficient above -12°C. The case is similar for $CaCl_2$ but with the threshold at -9°C instead of -12°C. It can be observed that the convection heat transfer coefficients increase with increasing temperature in both the U-pipes and PHE, with the exception of laminar flow in the U-pipes. This would suggest that selecting a higher secondary fluid temperature would lead to better heat transfer performance. This would also lead to a higher evaporation temperature, therefore increasing overall system performance.

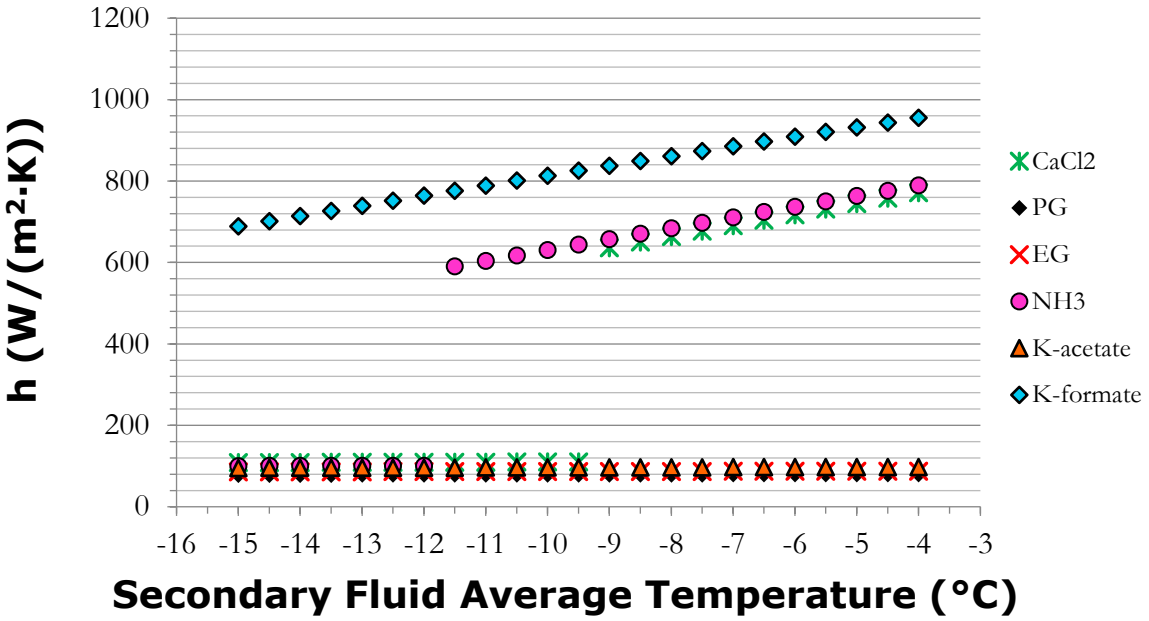

Figure 45: Convection heat transfer coefficient in a U-pipe vs. T_{av} (CC = 200 kW, T_f = -25°C, ⊿T = 2K).

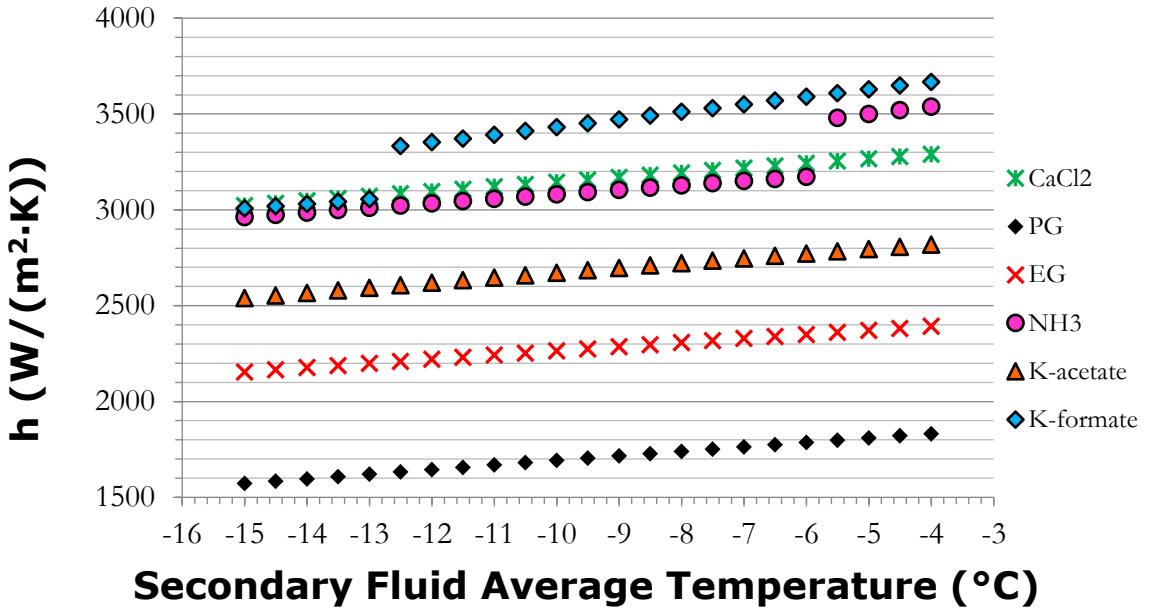

Figure 46: Convection heat transfer coefficient in a plate of the PHE vs. T_{av} (CC = 200 kW, T_f = -25°C, ⊿T = 2K).

These results can be compared to the graphs from the original study, shown in Figure 47 and Figure 48. The reference values were used in the graphs on the left side of the figures, while the measured values are used in the graph on the right (same as Figure 45 and Figure 46). The heat transfer coefficients calculated with measured values in both the U-pipes and plates of the heat exchanger are less than those calculated with reference values. An important difference in these calculations is the temperature at which flow regime changes. With the measured values, the flows of K-formate, NH_3, and $CaCl_2$ do not change from laminar to turbulent until higher temperatures in both cases. In fact, K-acetate does not reach turbulent flow for the entire temperature range with the measured values. Considering only the heat transfer coefficient in the U-pipe during turbulent flow, the difference in the results ranges from around a 17% to 27% decrease for K-formate and NH_3, respectively. The difference in results for the plate of the PHE range from around 8-9% (K-formate, NH_3, EG, and PG) to about 18% ($CaCl_2$), again comparing values from turbulent flow, where applicable. It should be noted that the calculations with the reference values assume a freezing point of -30°C, while for the measured values, the calculations assume a freezing point of -25°C. As mentioned

previously, a freezing point temperature of -25°C was chosen to more easily relate to real systems in operation or for the design of future systems. However, the trends in the change of thermophysical properties show that at higher concentrations, thermal conductivity and specific heat are lower and viscosity is higher. This suggests that the heat transfer coefficient would be greater for lower concentrations, which is not the case demonstrated here. With this theory, analysis of the convection heat transfer coefficient reveals that the reference values are overestimated in terms of advantageous thermophysical properties. Nevertheless, comparing the secondary fluids results in the same conclusions for both the original and updated calculations. Specifically, K-formate has the highest heat transfer coefficient in both the U-pipe and plate, followed by NH_3 and $CaCl_2$.

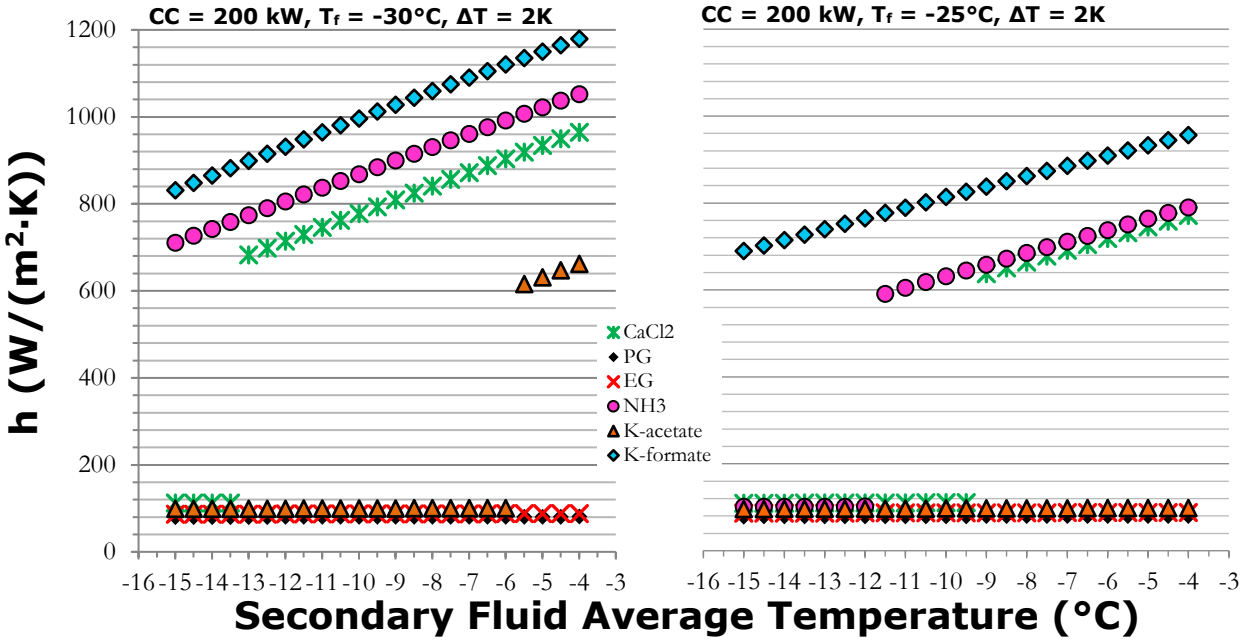

Figure 47: Comparison of the convection heat transfer coefficient in a U-pipe calculated with reference values (left) and measured values (right).

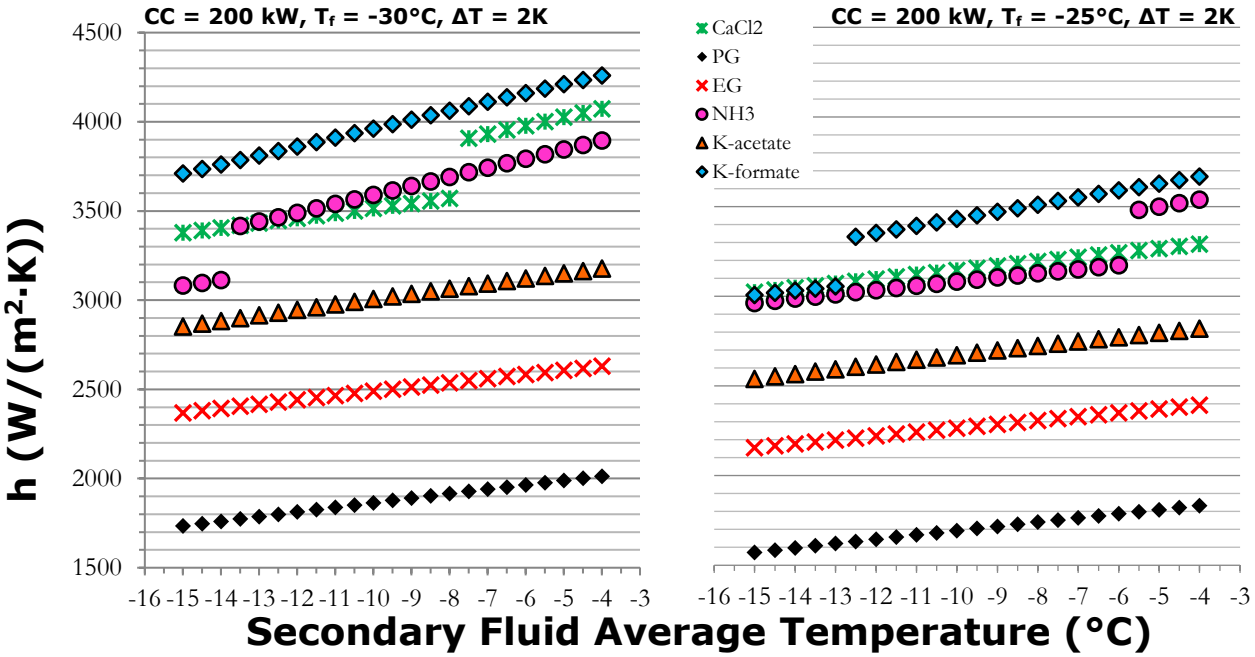

Figure 48: Comparison of the convection heat transfer coefficient in one plate of the PHE calculated with reference values (left) and measured values (right).

4.4.2 Secondary Fluid Comparison – Pumping Power

The required pumping power is also compared over a range of average temperatures of the secondary fluid, as shown in Figure 49. Viscosity increases at lower temperatures, which increases the pumping power required to circulate the secondary fluid. The results show that PG has the highest power at the full range of displayed temperatures and increases significantly with decreasing fluid temperature. A system with PG would require much more energy, and therefore a higher cost, to operate. The fluid with the lowest required pumping power is consistently NH_3. There is a break in the trend around -12°C where the flow changes from laminar to turbulent, which requires more pumping power. Above -11°C might require more pumping power, but the tradeoff would be the higher convection heat transfer coefficients than at lower temperatures.

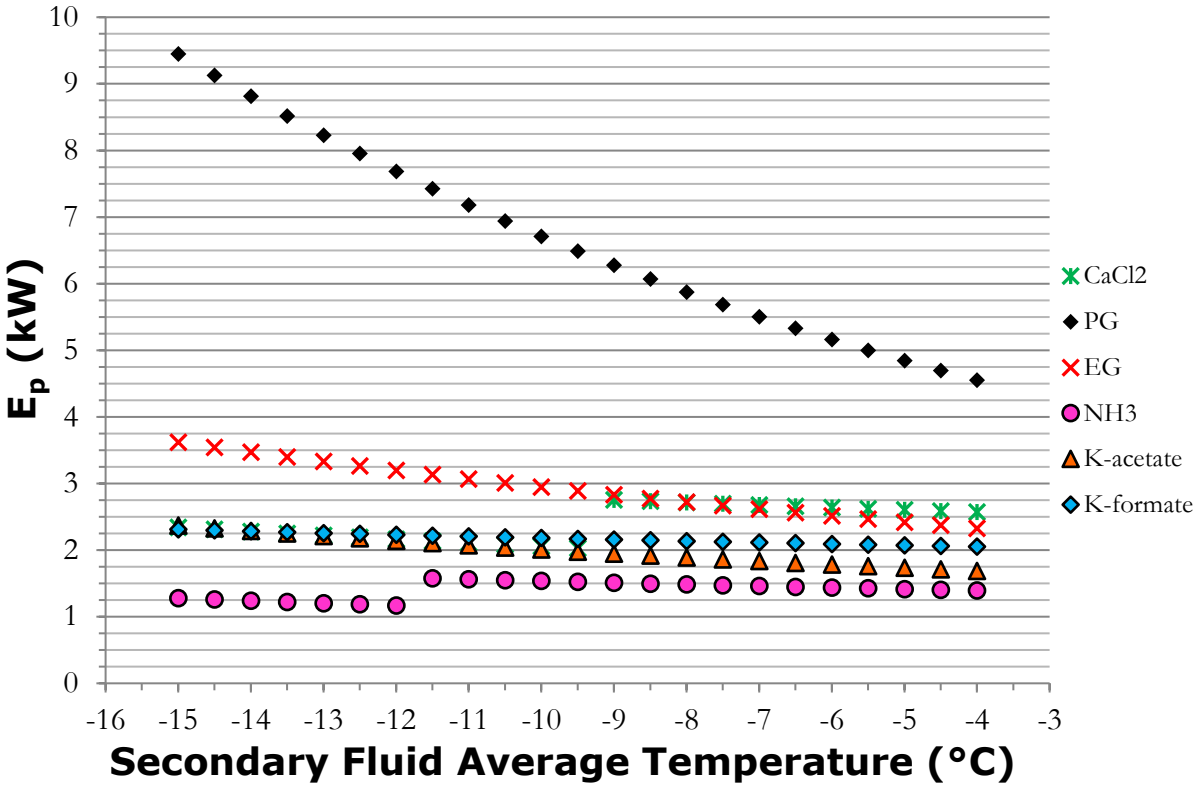

Figure 49: Pumping power vs. T_{av} (CC = 200 kW, T_f = -25°C, ⊿T = 2K).

When comparing the calculations using reference values and measured values in Figure 50, it is clear that the reference values result in higher pumping power for each of the secondary fluids, generally speaking. The trends of the pumping power for each fluid with varying temperature is also quite similar between the original and updated calculations; NH_3 requires the lowest pumping power while PG requires the highest by far. One change in the trends that can be observed is when, or if, the flow regime changes from laminar to turbulent, for example with NH_3 and $CaCl_2$. The significantly higher values, especially for PG, might be due to the freezing point selection for the calculations. Viscosity measurements are sensitive to the change in temperature, which could explain the approximately 55% increase for PG. Since NH_3 has a low viscosity, the change in temperature does not have as great of an effect on pumping power and the calculations at different freezing points do not result in values with a large difference. With measured values and a freezing point of -25°C, the secondary fluids are all within a smaller range of pumping power. Calculating pumping power can easily demonstrate if high viscosity of a secondary fluid will have a notable effect on the system, as with PG.

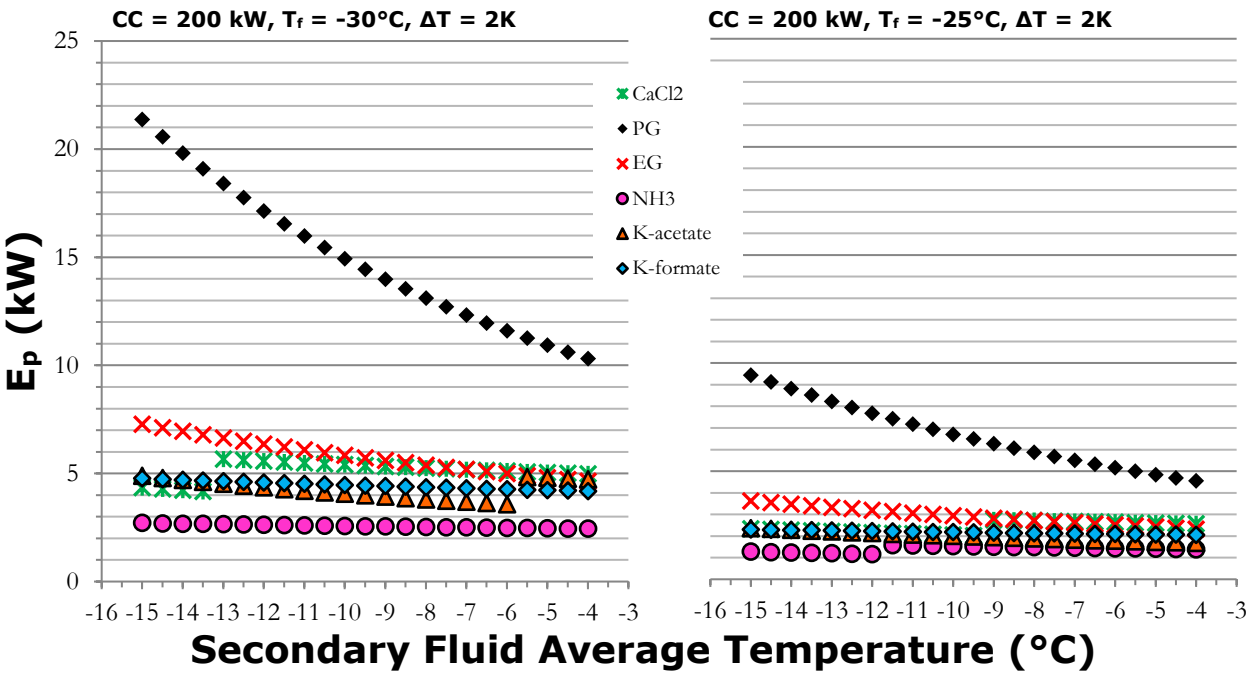

Figure 50: Comparison of the pumping power using reference values (left) and measured values (right).

For this project, perhaps the most noteworthy result is the lowest pumping power required with NH_3. This has a direct impact on system performance, as discussed in the following results sections. An argument for the use of aqua ammonia is the energy savings that come from lower pumping power. The cost of operation saved depends on the ice rink's current consumption and electricity prices.

4.4.3 Secondary Fluid Comparison – COP

The COP of a refrigeration system can be defined as the ratio of the total cooling capacity to the sum of the power demand, which comes from compressor and pumping power. COP is a measure of overall efficiency of a system and is useful because it allows secondary fluids to be compared based on their impact on overall system performance. Figure 51 shows the updated COP for the secondary fluids versus the temperature of the ice. Most of the secondary fluids have comparable COP values, with around an average of a 11% difference between NH_3 and EG while PG is about 25% lower than NH_3. COP increases slightly with increasing temperature, which can be a sign of the higher viscosity and pumping power at lower temperatures. The graph also demonstrates the change in flow type from laminar to turbulent for NH_3 around -12°C, while the other secondary fluids are within turbulent flow for the entire temperature range. The COP of a system decreases with increased cooling capacity due to the lower evaporation temperatures and can be observed in the graphs in Appendix B.

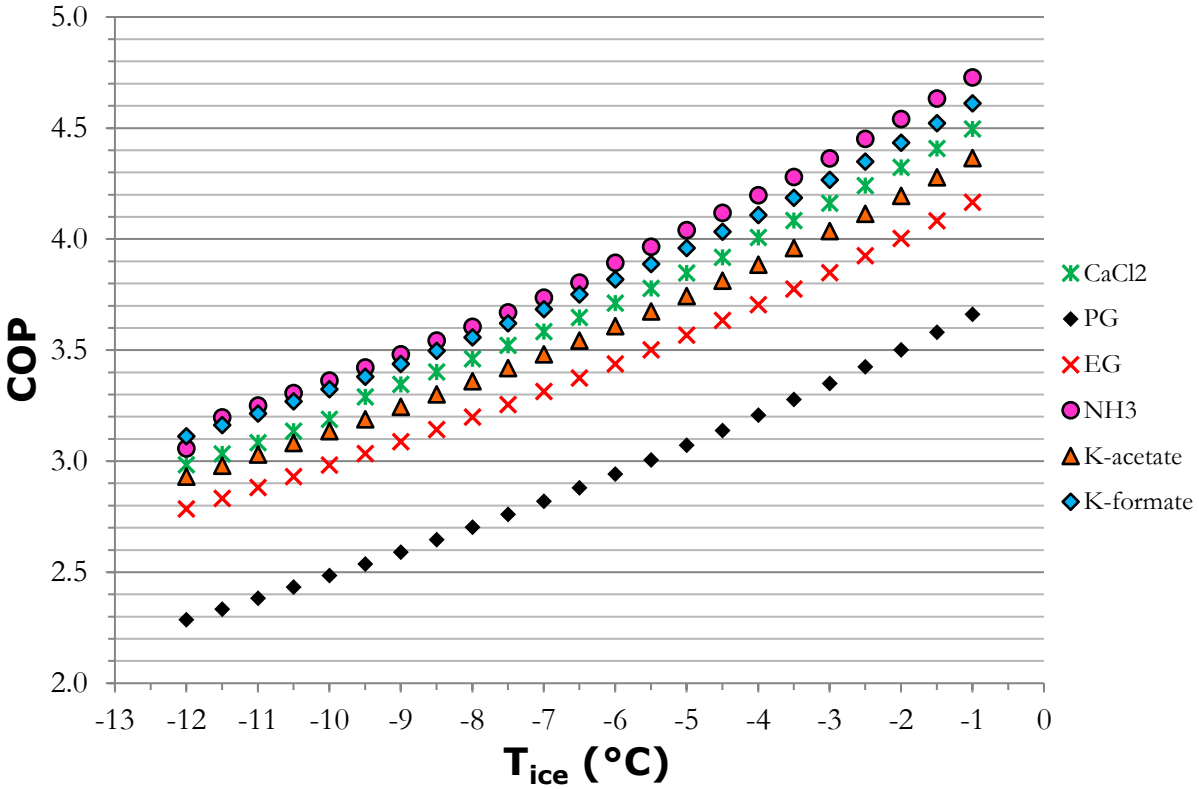

Figure 51: COP vs. T_{ice} (CC = 200 kW, T_f = -25°C, ⊿T = 2K).

Figure 52 shows the comparison of the original calculations of COP with reference values on the left with the updated calculations with measured values on the right. As shown, the cooling capacity used for the calculations in Figure 52 is 300 kW, not 200 kW as in Figure 51. This change in cooling capacity is reflected in lower COP values. For the secondary fluids with higher COP values, such as NH_3, the COP is almost the same at the lowest temperatures, but changes at different rates with an increase in ice temperature. The measured values demonstrate a slower increase in COP with ice temperature. The secondary fluid with COP values that vary the most, both between original and updated results and compared to other secondary fluids, is PG. The updated version of the study gives the same ranking of secondary fluids, apart from $CaCl_2$ and EG at temperatures above -7°C where COP is nearly the same for both. With the different freezing points, it could be expected that -25°C would result in higher COP values. However, this is not the case and indicates a greater difference between reference and measured values.

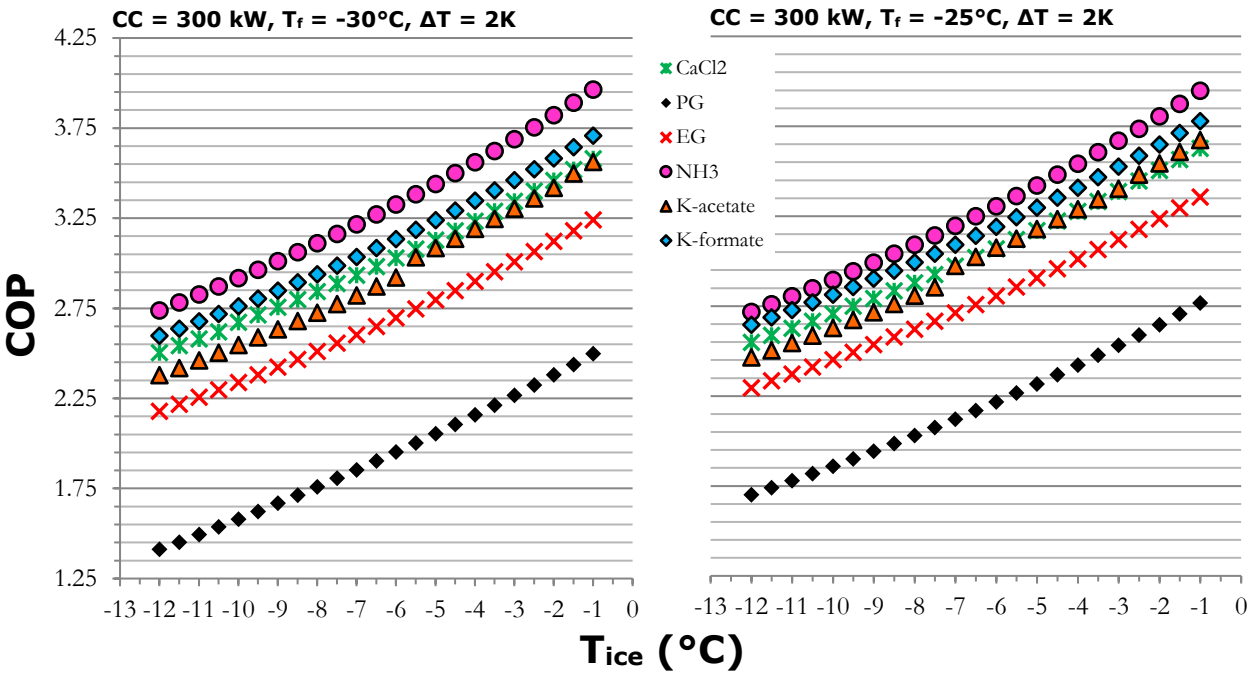

Figure 52: Comparison of COP vs. T_{ice} calculated with reference values (left) and measured values (right).

4.4.4 Optimum Pump Control Results

A method to control the circulation pumps is to operate them in order to maintain a constant temperature difference in the secondary fluid (ΔT). Lower pumping power, and therefore higher ΔT, increases performance because the fluid is flowing at a lower flowrate. However, decreasing the flowrate can also lead to laminar flow while increasing the compressor power. At a higher pumping power, the flowrate is increased but at the cost of higher energy consumption by the pump. Consequently, there is an optimal ΔT that results in more favorable COPs. Figure 53 shows how the COP is affected by changes in ΔT. For all the secondary fluids, there is a peak in the COP near a ΔT of 2-2.5 K. This low value ΔT is suitable for ice rinks because it allows for a more consistent temperature at the surface of the ice, which is preferred by the skaters. For NH_3, K-formate, and $CaCl_2$, it is clear where the flow switches from laminar at lower ΔT to turbulent. PG has the lowest COP values and the highest optimal ΔT.

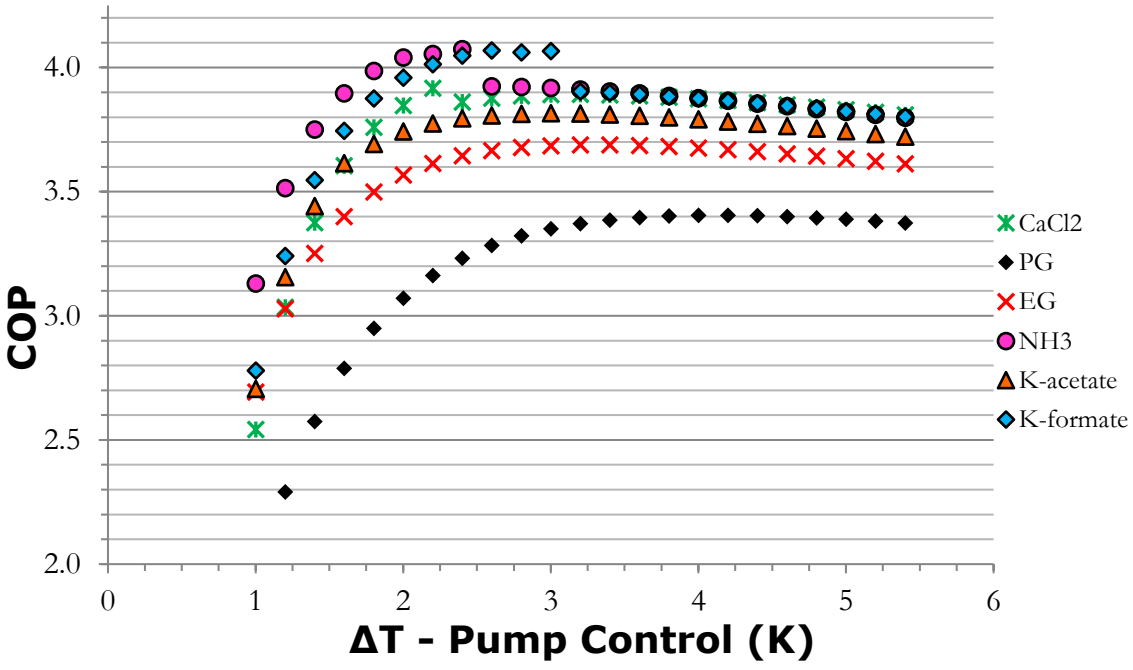

Figure 53: COP vs. ⊿T (CC = 200 kW, T_f= -25°C, T_{ice} = -5°C).

Figure 54 shows the comparison of the optimal pump control based on COP calculated with reference values used in the original study (left) and with updated measured values from this project (right). These results do not show much difference when analyzing optimal pump control. PG is the fluid that is most affected by the change in thermophysical properties and has a larger optimal pump control with the original calculation. For the rest of the secondary fluids, the optimal pump control is around 2-2.5 K for both cases. One difference in the results is when the change from laminar to turbulent occurs with NH_3, K-formate, and $CaCl_2$, which occurs at a higher pump control for the new results.

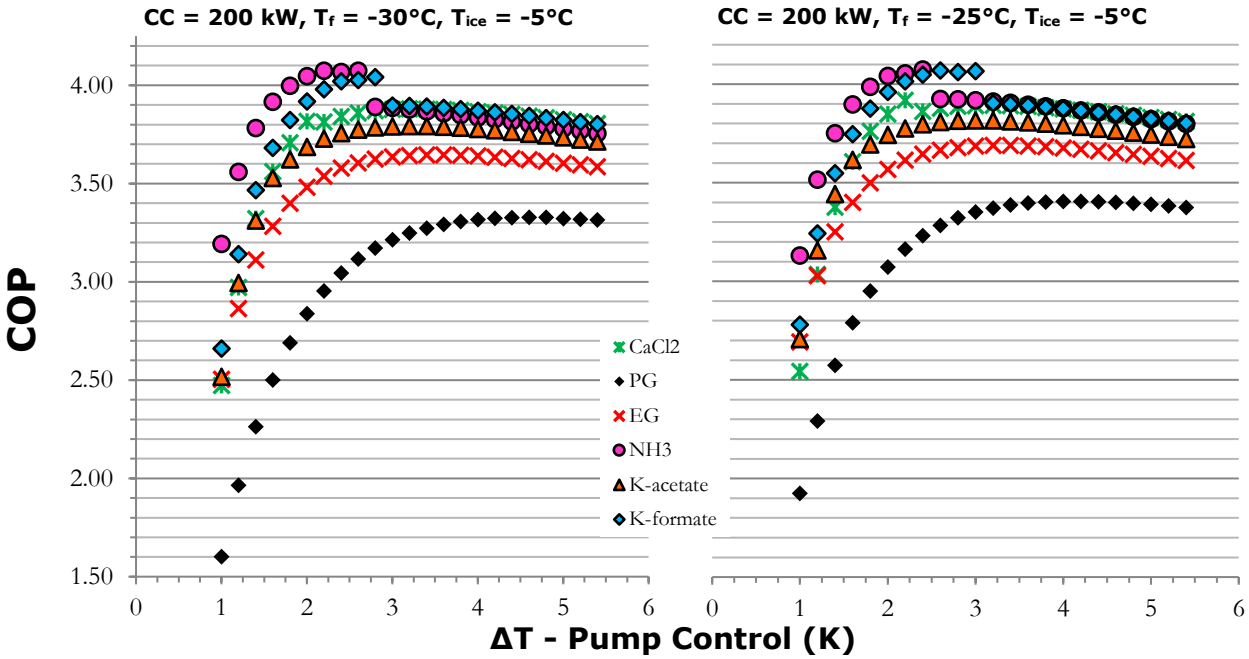

Figure 54: Comparison of COP vs. ⊿T calculated with reference values (left) and measured values (right).

In order to better analyze how the change in thermophysical properties affects the optimal pump control, the calculations were also completed for measured values of the fluids with a freezing point of -30°C. These results are compared to the results in Figure 53 and are shown in Figure 55 with the freezing point temperature of -25°C on the left and -30° on the right. The secondary fluids have the same trend and show nearly identical values for optimal pump control. The slight difference between these results is that the COP is higher for the secondary fluids with a freezing point temperature of -25°C, notably so for PG. The difference between the first turbulent value for each concentration of NH_3 is only about 0.75%. These results deduce that the updated thermophysical properties will not significantly change the optimal pump control. However, performance improvements can be made in systems that are not operating using this strategy or at these ideal temperature differences.

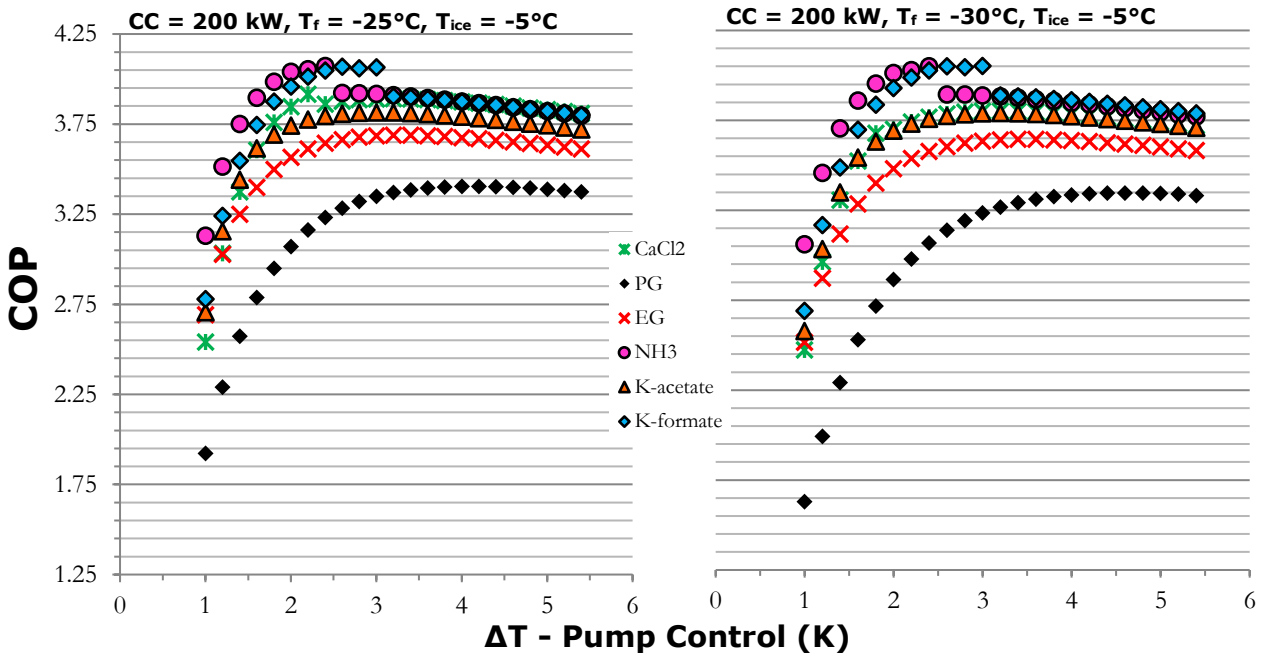

Figure 55: Comparison of COP vs. ΔT calculated with measured values for fluids with a freezing point of -25°C (left) and -30°C (right).

4.4.5 Impact of Secondary Fluid Concentration

The concentration of the secondary fluid chosen for a system determines the lowest possible operating temperature. The chosen secondary fluid should have a freezing point of around 10 K below the lowest operating temperature (Melinder, 2007). The higher the concentration of the secondary fluid, the lower achieved freezing point, but the thermophysical properties become less ideal when considering heat transfer and pressure drop. The commonly used freezing point in ice rinks is around -30°C but could theoretically be higher because operating temperatures do not tend to exceed -10°C (Mazzotti, 2014). In order to evaluate the system performance by using secondary fluids with lower concentrations, COP was calculated at various cooling capacities for fluids with freezing points of -20°C and -30°C. The percent change was calculated between the COP values for each fluid and is shown in Figure 56. The COP is higher for lower concentration solutions, defining the percent difference as the increase in COP at a -20°C freezing point compared the COP at a -30°C freezing point. Higher COP differences are reflected at higher cooling capacities, meaning it is more advantageous to use fluids with a higher freezing point, where possible, for systems with higher cooling capacities. The largest change in COP for all the cooling capacities is for PG, while the lowest percent change is for NH_3. Since aqua ammonia already has favorable thermophysical properties at many different freezing points and a relatively high COP, it makes sense that decreasing the solution concentration would only result in a slight increase in COP, the largest being around 2% for 400 kW cooling capacity. Although COP increase may not influence the use of lower concentration solutions when it comes to ammonia, safety concerns might steer designs away from its use at higher concentrations.

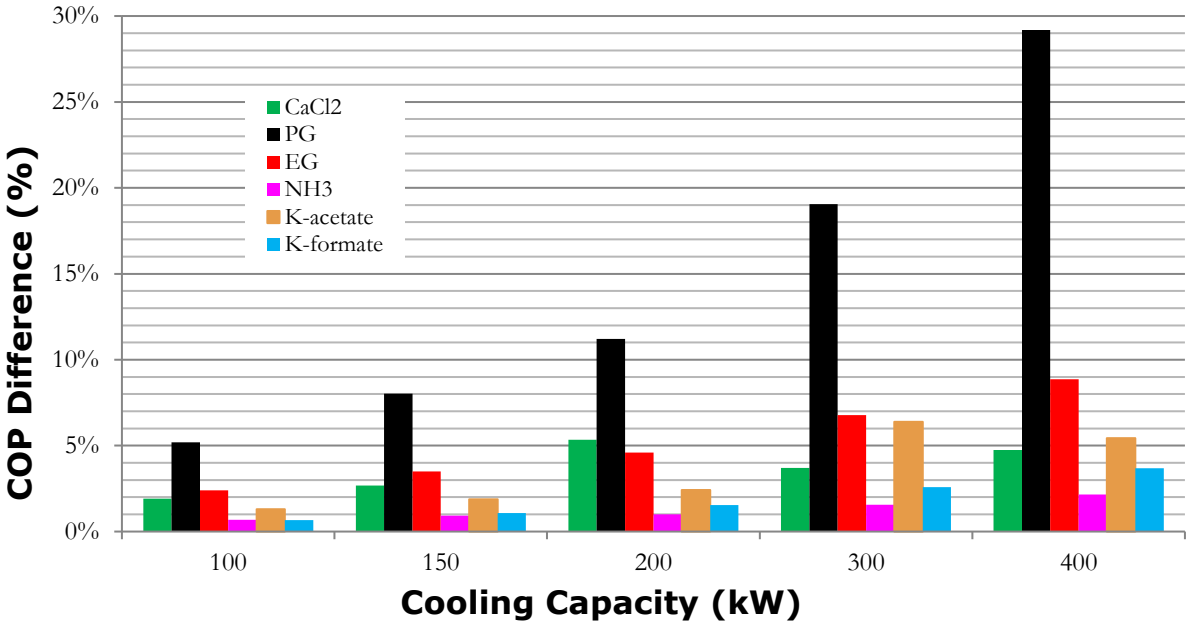

Figure 56: Percent increase in COP for fluids with a freezing point of -25 °C compared to fluids with a freezing point of -30 °C (T_{ice} = -5 °C, ⊿T = 2.5 K).

5 Conclusion

This project focused on aqua ammonia as a secondary fluid by primarily determining correct thermophysical properties and how use of the updated values impacts calculated operation parameters of the refrigeration system in ice rinks through a theoretical model. One of the main drivers of this project is the status of the reference values currently used for aqua ammonia thermophysical properties, including density, dynamic viscosity, specific heat capacity, and thermal conductivity. The reference values have not been experimentally measured or updated since the early 1900s. Specifically, specific heat capacity and thermal conductivity have the oldest and fewest reported values. The values used today have continuously been copied from previous resources, making the method of determination of these values unclear. These thermophysical properties have been experimentally measured for 11 solutions of aqua ammonia, ranging from 2 wt-% to 30 wt-% with freezing point temperatures from -2°C to -84°C. The new values were used in a theoretical model to determine the impact of the more realistic values on an ice rink refrigeration system. Furthermore, corrosion tests were completed for six of the aqua ammonia solutions (4.19 wt-% to 17.7 wt-%) for copper 99.95%, brass (65% copper), carbon steel 312, stainless steel 316L, galvanized steel, aluminum 3300 series, and a brass connection commonly used in ice rink refrigeration systems.

The first step in determining the thermophysical properties of aqua ammonia was to verify the solution concentration with freezing point and refractive index tests. The freezing point tests using a deep freezer resulted in values around the expected freezing points but were not at an acceptable level of precision. Then refractive index was tested to confirm the concentrations due to the fact that refractive index is highly sensitive to changes in solution concentration and could be compared to reliable reference values. The largest difference between the reference values and the results of the refractive index test was 0.28% for 25 wt-% solution.

The next step was to measure the remaining properties: density, dynamic viscosity, specific heat capacity, and thermal conductivity. Density results were as expected and similar to reference values, in both values and trends with increasing concentration and temperature. The results varied from 0.3% to 1.7% lower than the reference values. This shows a high level of agreement between reference values and new experimental values. Dynamic viscosity results show the same trend pattern for changing solution concentration and temperature. However, the values are higher than previously reported. This test has a measuring range from -17°C to 20°C. Over this range, the largest change in viscosity between the experimental data and references was 15% for 2 wt-% solution at 20°C. The smallest change was 2% for 15.5 wt-% solution at 20°C. The

difference in results at higher temperatures close to 20°C may be due to the limitation of the unit. The average change in viscosity is around 8-9%. Typically, the lower the temperature, the higher the viscosity, especially with higher concentration solutions.

Although viscosity showed some difference in the experimental values and the reference values, the results for specific heat capacity and thermal conductivity revealed more unexpected results, most drastically for specific heat capacity. The values and trends for this property were significantly different than theoretical reference values, specifically in Melinder (2010). The results clearly show an opposite trend with changing temperature and solution concentration. The reference values show increasing specific heat capacity for an increase in concentration of aqua ammonia and decrease in temperature. However, experimental results show the opposite. The values are similar for most solutions around -5°C to 5°C, where the trendlines cross. The largest observed difference, for temperatures down to -40°C, is 18% lower than the reference for 30 wt-% at -40°C. Although larger differences are observed at lower temperatures, the average difference is 6%, which indicates that the impact of new specific heat values depends on the temperature or freezing point being used.

Thermal conductivity results show similar trends to the reference values, but with less variance with changing temperature. The values are higher than expected and still decrease with decreasing temperature, but to a lesser degree. The largest increase in the experimental values was 12% for 30 wt-% at -20°C. The lab instrument is capable of measuring down to -28°C. While specific heat capacity results were lower than values currently used, thermal conductivity results were higher. This may balance the impact on ice rink refrigeration systems, but to determine the effects, a theoretical model was implemented.

A tool developed during a previous master's thesis project was utilized to determine the impact of the updated thermophysical properties. The purpose of the model was to compare multiple secondary fluids for use in a standard ice rink. In this project, the model was utilized with updated thermophysical values, where possible, for the secondary fluids. The secondary fluids analyzed are calcium chloride ($CaCl_2$), propylene glycol (PG), ethylene glycol (EG), aqua ammonia (NH_3), potassium acetate (K-acetate), and potassium formate (K-formate). The results show that aqua ammonia is favorable with high COP and low pumping power, and therefore low pressure drop. At a cooling capacity of 200 kW and a ΔT of 2 K, the pumping power for NH_3 is 45% lower than that for $CaCl_2$ at a secondary fluid temperature of -9°C. Aqua ammonia is most comparable to $CaCl_2$ and K-formate when observing coefficients of heat transfer, but has higher COP, followed by potassium formate. The COP of a system using NH_3 at a cooling capacity of 200 kW to maintain an ice temperature of -5°C is 4.7% higher than that of using $CaCl_2$.

Another purpose of the model was to see how using updated thermophysical properties impacts the calculation results, specifically for aqua ammonia. The change in COP due to the updated properties, when T_{ice} is -5°C, was only 0.55% lower for aqua ammonia at 300kW cooling capacity. When comparing COP with a pump control of 2K, the decrease in COP was 0.22% at 200kW. The change in heat transfer coefficient was more significant, with a 27% decrease in the U-pipe at a secondary fluid temperature of -10°C. The difference in one plate of the heat exchanger was calculated at a secondary fluid temperature of -5°C to compare turbulent flow in both cases and the difference was 9% lower with experimental values. Even though, these heat transfer coefficient values are lower than previously calculated, the required pumping power is also lower: 40% lower at a secondary fluid temperature of -10°C. Even though the change in heat transfer coefficients is larger with experimental values, the 0.22% impact on COP is minimal.

The last experiment of this project was to determine corrosion rate of different metals. The most corrosive metal was copper, followed by brass, with maximum corrosion rates of 16.2 mm/yr and 1.84 mm/yr, respectively. The most compatible specimen was stainless steel, followed by carbon steel, with maximum corrosion rates of 0.041 mm/yr and 0.11 mm/yr, respectively. Brass connections commonly used in industry were also tested and resulted in corrosion rates ranging from 69.6 g/yr to 112 g/yr for 4.19 wt-% and 13.5 wt-% solutions, respectively. This accounts for about 1% and 1.5% of the connections' total weight, respectively, lost per year.

To condense these results into general suggestions for implementation of aqua ammonia as a secondary fluid in ice rink refrigeration, a system would operate at a higher COP and lower pressure drops with aqua ammonia. The system should not contain any copper or brass and ideally only have stainless steel or carbon steel components.

6 Future Work

The proposal for this project contained many other areas to explore and research in relation to aqua ammonia as a secondary fluid in ice rinks. The following list summarizes those areas:

- Field measurement analysis – collect data in order to evaluate energy performance, especially of retrofitted systems, in order to quantify advantages to switching to an ammonia system

- Experimental tests of thermophysical properties – complete additional tests to further verify the results presented in this thesis, especially for those with more sensitive methods, including specific heat capacity and thermal conductivity

- Retrofit – complete interviews and/or visits of real cases to help determine and develop guidelines for cleaning procedures and requirements, standard steps to follow and how they differ with ammonia systems, and how to avoid leakages

- Degassing – determine if degassing is necessary and any long term affects it might have on the system, as well as estimate the cost for commonly used or offered equipment on the market

- Safety – outline the codes and regulations present and how to deal with leakages should they occur in order to minimize fear and hesitation towards use of aqua ammonia

- Leakages – how to predict and repair leakages and determine if common leak-sealing products on the market are sufficient

References

Ammonia, anhydrous—Substance Information—ECHA. (n.d.). Retrieved September 27, 2019, from https://echa.europa.eu/substance-information/-/substanceinfo/100.028.760

ASHRAE Refrigeration Committee. (2017). ASHRAE Position Document on Ammonia as a Refrigerant. ASHRAE. https://www.ashrae.org/File%20Library/About/Position%20Documents/Ammonia-as-a-Refrigerant-PD-2017.pdf

Didier, C., Jean-Luc, D., & Valentin, M. (2017). 35th Informatory Note on Refrigeration Technologies: The impact of the refrigeration sector on climate change (p. 17). International Institute of Refrigeration. http://www.iifiir.org/userfiles/file/publications/notes/NoteTech_35_EN_uz7bwths.pdf

European Commission. (2016, November 23). EU legislation to control F-gases [Text]. Climate Action - European Commission. https://ec.europa.eu/clima/policies/f-gas/legislation_en

F-Chart Software. (n.d.). EES Property Calculator Software.

Garry, M. (2018, December 3). Curling rink gets North America's first aqua ammonia system. Ammonia21. http://www.ammonia21.com/articles/8711/curling_rink_gets_north_americas_first_aqua_ammonia_system1543850136

Granryd, E., Ekroth, I., Lundqvist, P., Melinder, Å., Palm, B., & Rohlin, P. (2009). Refrigeration Engineering. US-AB.

Heat transfer coefficient. (2019). In Wikipedia. https://en.wikipedia.org/w/index.php?title=Heat_transfer_coefficient&oldid=913724835

Huang, J. (2010). PERFORMANCE ANALYSIS OF PLATE HEAT EXCHANGERS USED AS REFRIGERANT EVAPORATORS [Doctoral]. University of Witwatersrand.

Ignatowicz, M. (2008). Corrosion aspects in indirect systems with secondary refrigerants [Master, KTH, The Royal Institute of Technology, Division of Applied Thermodynamics and Refrigeration]. urn:nbn:se:kth:diva-65569

Ignatowicz, M., Barcarolo, L., Melinder, Å., Molinaroli, L., & Palm, B. (2019). Cesium and ammonium salts as low temperature secondary fluids. 8. https://doi.org/10.18462/iir.icr.2019.1185

Ignatowicz, M., Melinder, Å., & Palm, B. (2018). Adsorption corrosion inhibitors, green corrosion inhibitors and alternative secondary fluids for indirect refrigeration system (No. P03; EffsysExpand, p. 69). Swedish Energy Agency.

IIHF Facilities Committee. (2016). IIHF Ice Rink Guide (H. Bogomoloff, Ed.). IIHF. https://iihfstorage.blob.core.windows.net/iihf-media/iihfmvc/media/downloads/projects/ice%20rink%20guide/iihf_ice_rink_guide_web_pdf.pdf

Karampour, M. (2011). Measurement and Modelling of Ice Rink Heat Loads [Master, KTH, The Royal Institute of Technology, Division of Applied Thermodynamics and Refrigeration]. urn:nbn:se:kth:diva-61330

Linde. (n.d.). R717 (Ammonia). Linde Gas. Retrieved September 27, 2019, from http://www.linde-gas.com/en/products_and_supply/refrigerants/natural_refrigerants/r717_ammonia/index.html

Mazzotti, W. (2014). Secondary Fluids Impact on Ice Rink Refrigeration System Performance [Master, KTH, The Royal Institute of Technology, Division of Applied Thermodynamics and Refrigeration]. http://urn.kb.se/resolve?urn=urn:nbn:se:kth:diva-140602

Melinder, Å. (1998). Thermophysical properties of liquid secondary refrigerants: A critical review on literature references and laboratory measurements [Engineering Licentiate Thesis, KTH, The Royal Institute of Technology, Division of Applied Thermodynamics and Refrigeration]. http://urn.kb.se/resolve?urn=urn:nbn:se:kth:diva-816

Melinder, Å. (2007). Thermophysical Properties of Aqueous Solutions Used as Secondary Working Fluids [Doctoral, KTH, The Royal Institute of Technology, Division of Applied Thermodynamics and Refrigeration]. http://urn.kb.se/resolve?urn=urn:nbn:se:kth:diva-4406

Melinder, Å. (Ed.). (2010a). Handbook on indirect refrigeration and heat pump systems. Svenska Kyltekniska Föreningen.

Melinder, Å. (2010b). IIR -- Properties of Secondary Working Fluids for Indirect Systems (Secondary Refrigerants or Coolants, Heat Transfer Fluids) (2nd ed.). International Institute of Refrigeration (IIR). https://www.techstreet.com/standards/iir-properties-of-secondary-working-fluids-for-indirect-systems-secondary-refrigerants-or-coolants-heat-transfer-fluids?product_id=1737807

Montreal Protocol. (2019). In Wikipedia. https://en.wikipedia.org/w/index.php?title=Montreal_Protocol&oldid=910565366

Nieto, D. (2015, September 26). What are the Differences between Dynamic and Kinematic Viscosities? RheoSense. https://blog.rheosense.com/what-are-the-differences-between-dynamic-and-kinematic-viscosities

Pearson, A. (2008). Refrigeration with ammonia. International Journal of Refrigeration, 31(4), 545–551. https://doi.org/10.1016/j.ijrefrig.2007.11.011

Plank, R. (1959). Handbuch der Kältetechnik, Band VII (Vol. 7). Springer Berlin.

Refrigerant Management. (2017, February 7). Drawdown. https://www.drawdown.org/solutions/materials/refrigerant-management

Riffat, S. B., Afonso, C. F., Oliveira, A. C., & Reay, D. A. (1997). Natural refrigerants for refrigeration and air-conditioning systems. Applied Thermal Engineering, 17(1), 33–42. https://doi.org/10.1016/1359-4311(96)00030-0

Rogstam, J, Bolteau, S., Pomerancevs, J., & Grönqvist, C. (2019). Aqua Ammonia as secondary refrigerant in ice rink applications. 8. https://doi.org/10.18462/iir.icr.201.1129

Rogstam, Jörgen. (2017, November 10). Ice rinks with R744 as refrigerant [Guest Lecture]. Advanced Refrigeration and Heat Pump Technology, Stockholm.

Rumble, J. R. (Ed.). (2019). Concentrative Properties of Aqueous Solutions: Density, Refractive Index, Freezing Point Depression, and Viscosity. In CRC Handbook of Chemistry and Physics: Vol. Internet Version 2019 (100th ed.). CRC Press/Taylor & Francis.

SETARAM Instrumentation. (2014). Technical Note TN 320, Liquid heat capacity vessel (S60/1599). KEP Technologies.

Shan K. Wang. (2001). REFRIGERANTS, REFRIGERATION CYCLES, AND REFRIGERATION SYSTEMS. In Handbook of Air Conditioning and Refrigeration, 2/e (2nd ed.). McGraw-Hill Education. https://www.accessengineeringlibrary.com/content/book/9780070681675/chapter/chapter9

Steiss, A. (Ed.). (2018). Annual Report (July 2017-June 2018; p. 142). International Ice Hockey Federation. https://www.iihf.com/IIHFMvc/media/Downloads/Annual%20Report/AnnualReport2018.pdf

Steyer, T. (2017). Drawdown: The Most Comprehensive Plan Ever Proposed to Reverse Global Warming (P. Hawken, Ed.; First Edition edition). Penguin Books.

SWEP. (n.d.). 5.8 Secondary refrigerants. SWEP. Retrieved September 20, 2019, from https://www.swep.net/refrigerant-handbook/5.-refrigerants/sd/

Timmermans, J. (1960). The physico-chemical constants of binary systems in concentrated solutions. Interscience.

UNFCCC. (2017). What is the Paris Agreement? | UNFCCC. https://unfccc.int/process-and-meetings/the-paris-agreement/what-is-the-paris-agreement

US EPA, O. (2016, January 12). Understanding Global Warming Potentials [Overviews and Factsheets]. US EPA. https://www.epa.gov/ghgemissions/understanding-global-warming-potentials

Appendix A

Additional Experiment Details

- Viscosity – graph displaying all experimental results and reference values

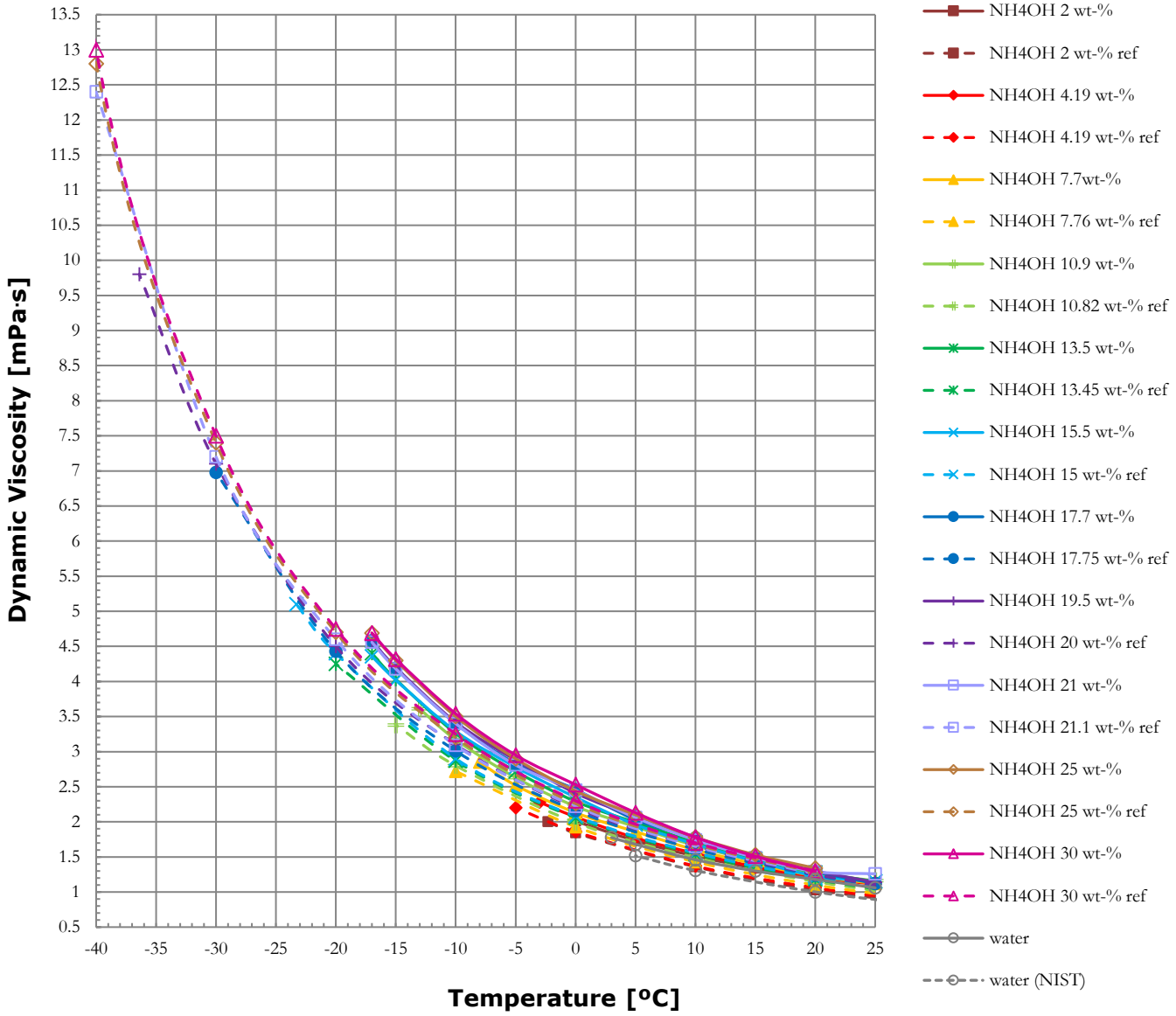

- TPS – pictures of eroded sensors

Aqua ammonia is highly corrosive to some materials, one of them being the coating and materials used in the sensors used during the TPS tests. Higher concentration solutions were more corrosive to the sensors. The following pictures show damage to the multiple sensors used. Early on in the testing, the sensor was switched from Kapton to Teflon.

This top left image shows a useable sensor that has already been used for a couple tests. The black around the end of the sensor is the start of corrosion of the adhesive used in construction of the sensor. The other three pictures are of a damaged, unusable sensor. All sensors in these images are Teflon, which last much longer than Kaplan sensors.

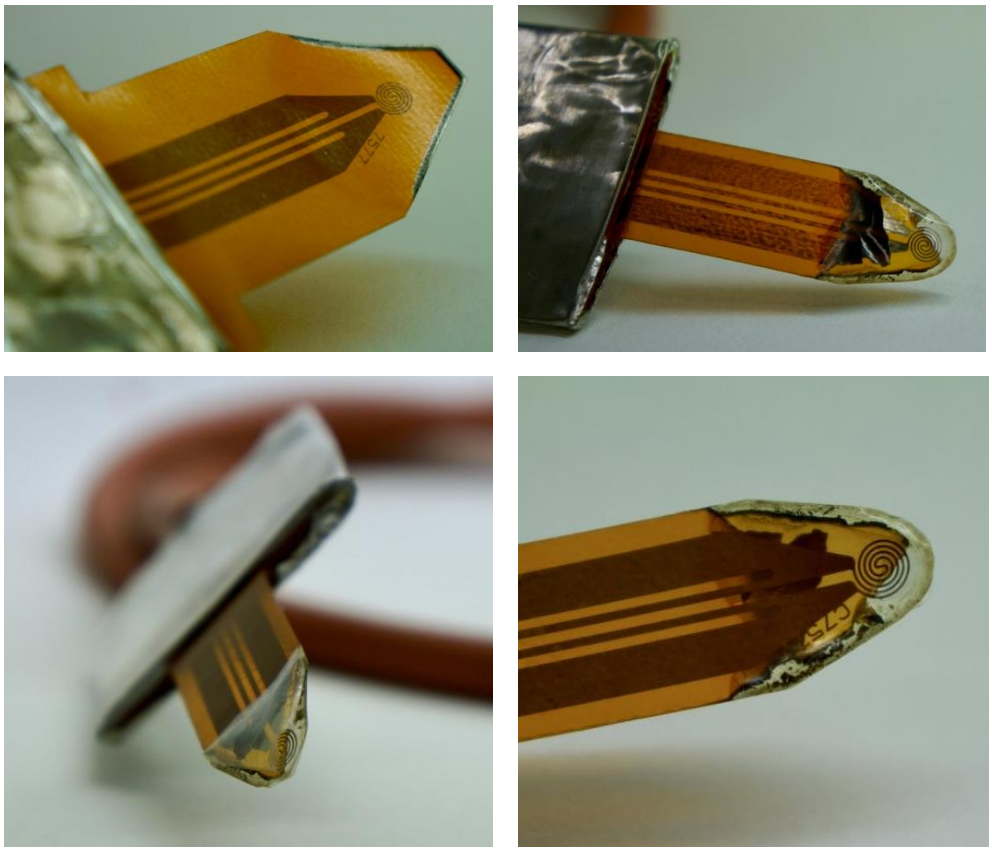

- Corrosion – pictures of final results

Copper

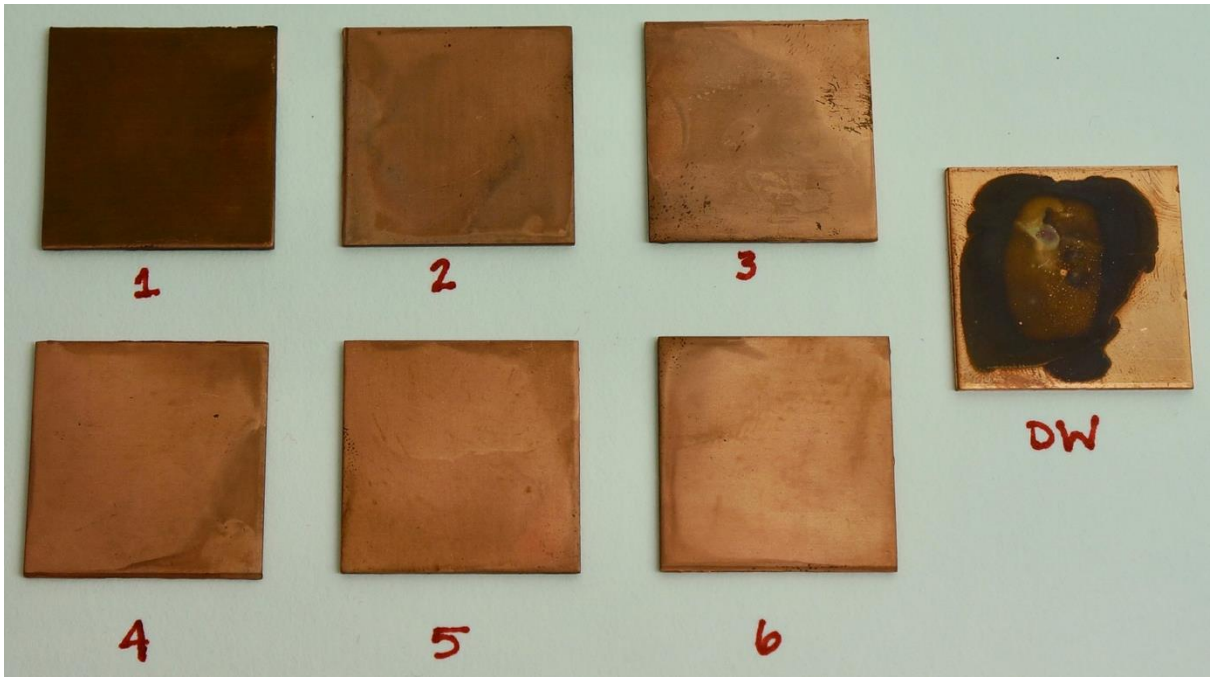

Brass

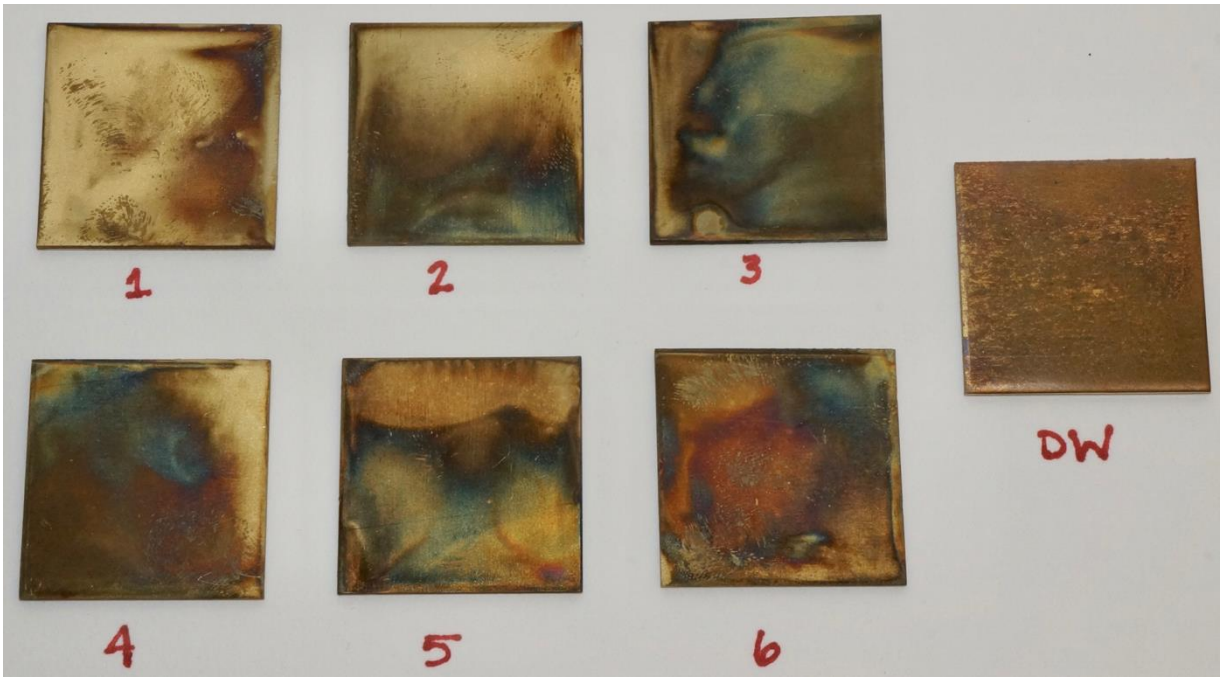

Carbon Steel

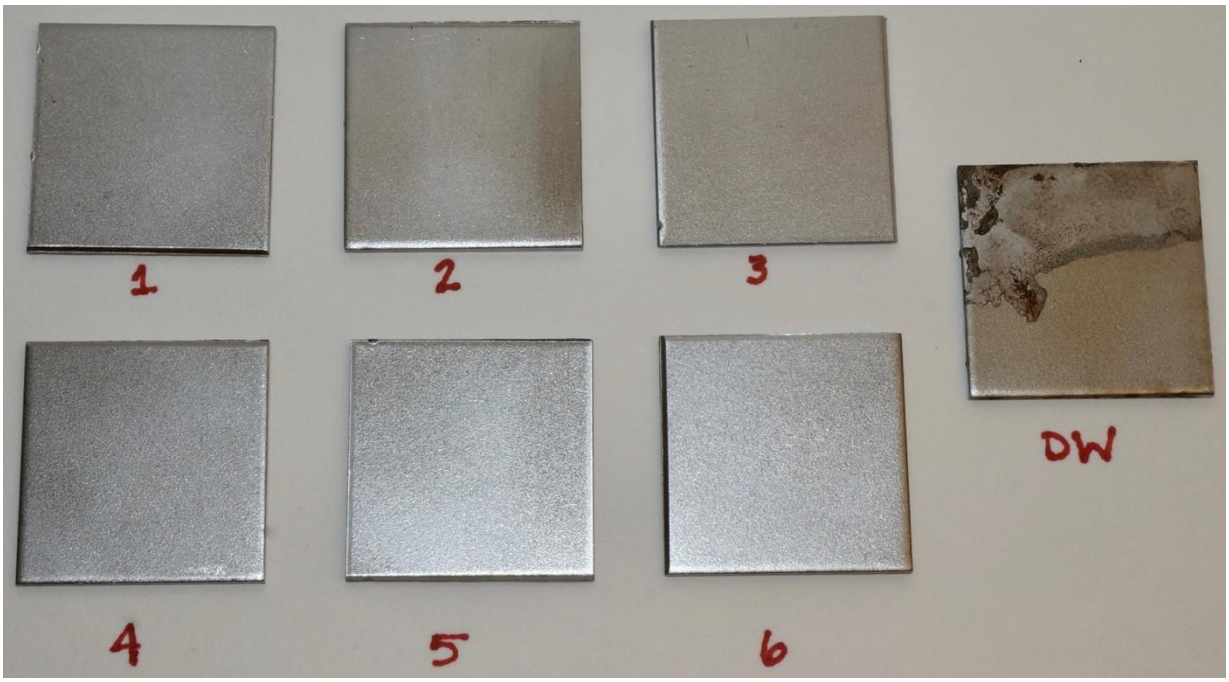

Stainless Steel

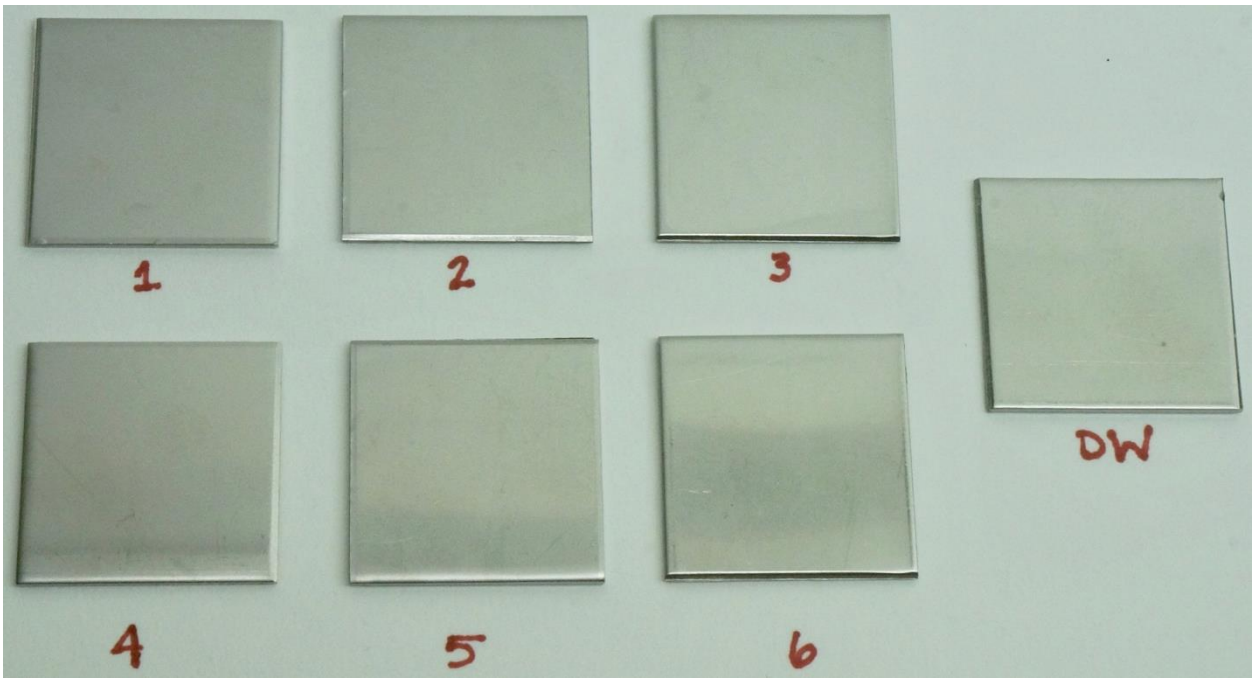

Galvanized Steel

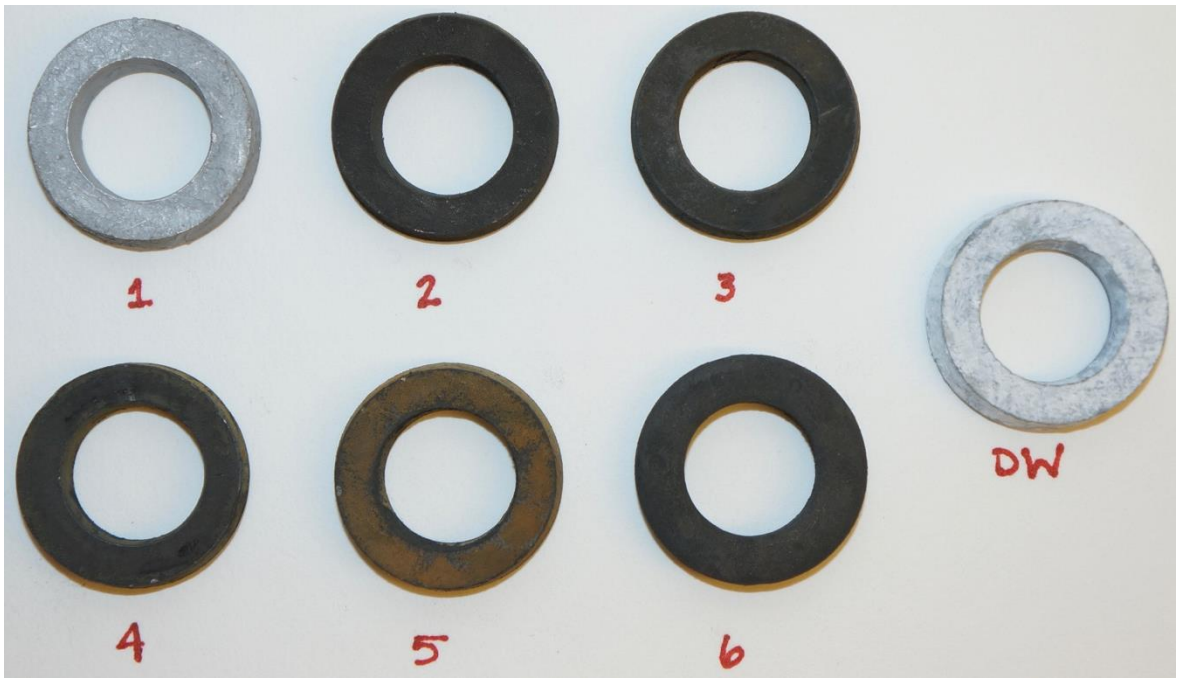

Aluminum

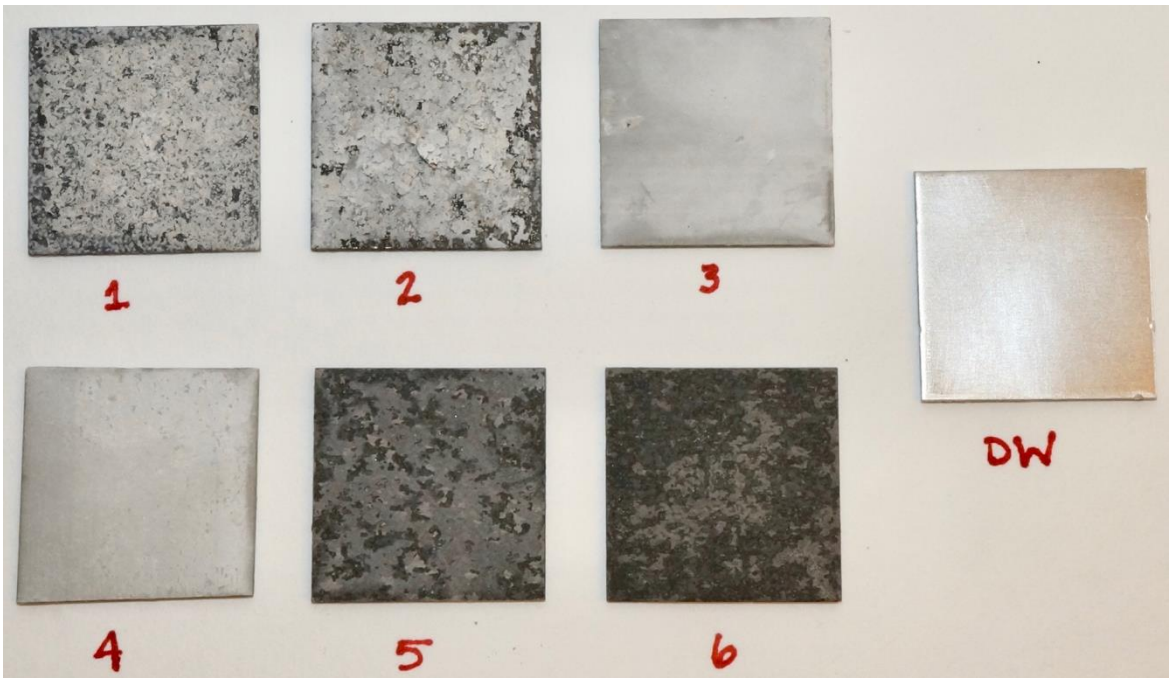

Closeup of Aluminum Results

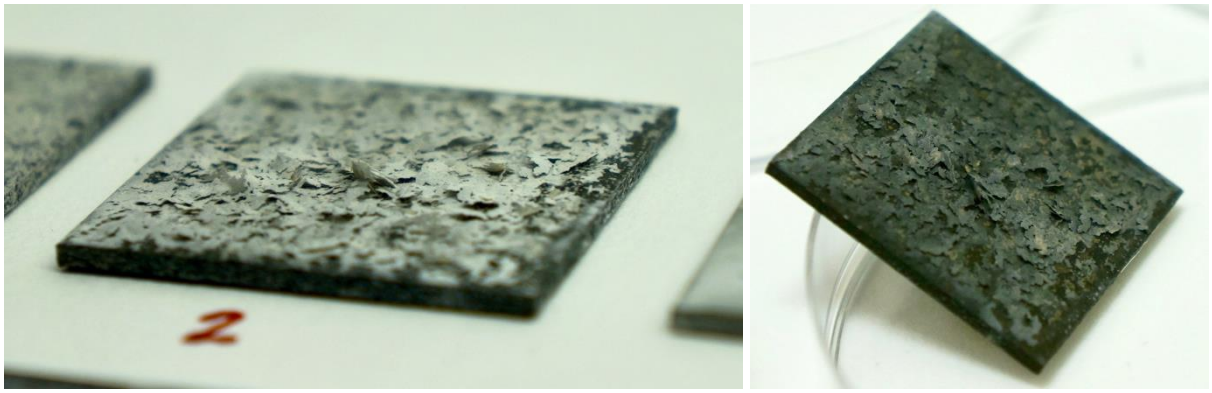

Brass Connections

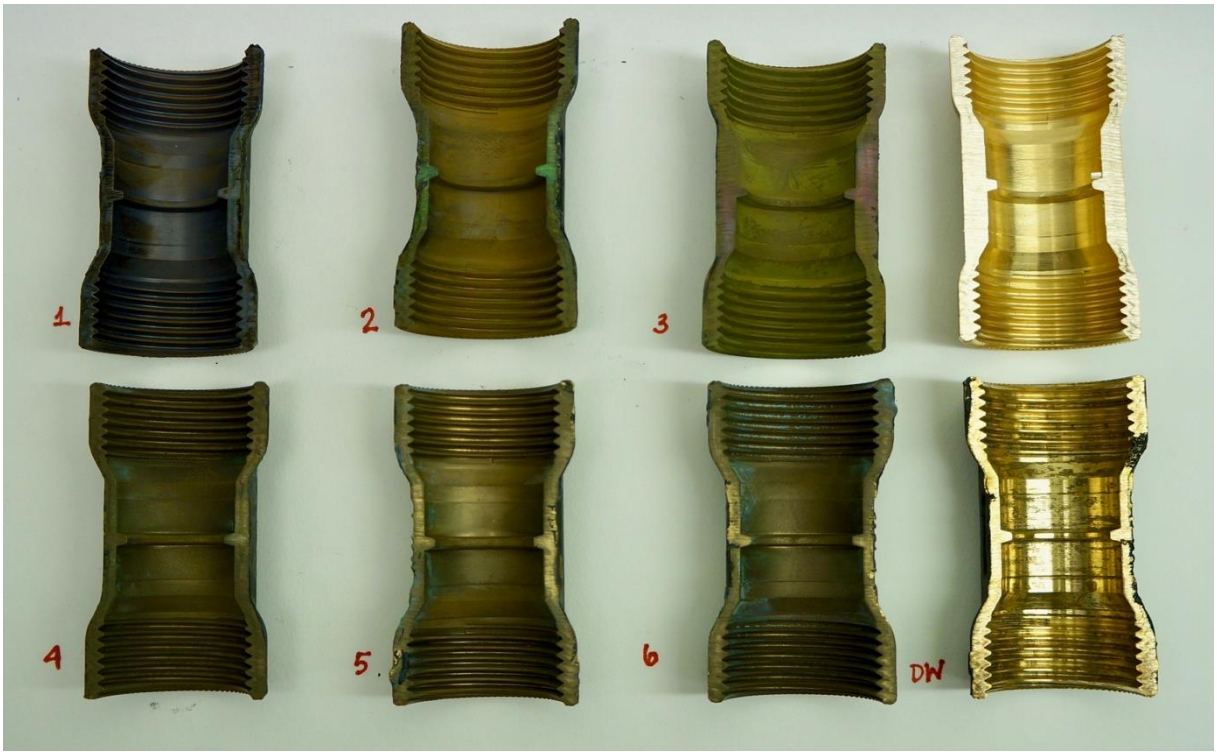

Appendix B

Calculation Details used in Theoretical Comparative Study

This Appendix lists the calculations used in the performance study part of this project. The calculations were developed for a previous master's thesis project (Mazzotti, 2014).

Contents:

Equations for Evaporator Side

- Evaporator design
- Dimensionless numbers: Reynolds, Nusselt, and Prandtl numbers and Moody friction factor
- Convective heat transfer of the secondary fluid in the evaporator
- Pressure drop of the secondary fluid side of the evaporator
- Boiling heat transfer phenomena (ammonia)
- Overall heat transfer coefficient and thermal resistance

Equations for Ice Rink Calculations

- Total volumetric flowrate at a given cooling capacity
- Range of the Reynolds number inside the evaporator
- Range of the Reynolds number inside the distribution pipes in the ice rink floor
- Variables for the functions of input data of the secondary fluids versus temperature
- Primary refrigerant mass flow
- Reynolds number used for the heat transfer on the boiling side
- Number of U-pipes in the ice rink floor
- Total heat transfer in the ice rink floor
- Pressure drop characterization in the distribution pipes

Equations for Evaporator Side

- Evaporator Design
  - The number of plates does not include the two outermost plates:

$$N_C = N_P + 1$$

N_C : number of channels

N_P : number of plates

  - Geometric features of the plate are used to calculate the surface enlargement factor (Φ):

$$\Phi = \frac{2}{\Lambda}\int_0^{\frac{\Lambda}{2}} \sqrt{1 + \left(\frac{d}{dx}\big(y(x)\big)\right)^2}\, dx$$

Λ : corrugation pitch [m]

y : corrugation function

x : x-axis along plate width

  - Hydraulic diameter (d_h [m]) within the evaporator:

$$d_h = 4 \cdot \frac{A}{P} = \frac{2 \cdot b}{\Phi}$$

A : cross-sectional area [m²]

P : wet perimeter [m]

b : pressing depth [m]

Φ : surface enlargement factor [-]

  - Heat transfer area for one plate (A_{ht} [m²]):

$$A_{ht} = W \cdot \Phi \cdot L_{eff}$$

W : width of the plate [m]

Φ : surface enlargement factor [-]

L_{eff} : effective plate length [m]

- All features chosen for evaporator calculations:

PHE feature	Formula	Value	Unit
Pressing depth	b	0,003	m
Surface enlargement factor	Φ	1,18	-
Hydraulic diameter	d_h	5,08E-03	m
Number of plates	N_P	121	-
Number of channels	N_C	122	-
Chevron angle	ϕ	60	°
Reverse chevron angle	β	30	°
Corrugation pitch	Λ	0,012	m
Plate width	W_{plate}	0,4	m
Plate length (port to port)	L_{plate}	0,8	m
Heat transfer effective length	L_{eff}	0,64	m
Average heat transfer area (for one plate)	A_{ht}	0,30208	m^2
Plate thickness	δ	0,0005	m
Thermal conductivity of plate material	k_{plate}	21,9	$W.m^{-1}.K^{-1}$
Port diameter	D_{port}	0,1	m

- Dimensionless numbers: Reynolds, Nusselt, and Prandtl numbers and Moody friction factor
  - Reynolds number (Re)

$$Re = \frac{G \cdot d_h}{\mu} = 2 \cdot \frac{\dot{m}_{tot}}{W \cdot b \cdot N_C} \cdot \frac{d_h}{\mu}$$

G : mass flux [$kg \cdot m^{-2} \cdot s^{-1}$]

d_h : hydraulic diameter [m]

μ : dynamic viscosity [Pa·s]

$\dot{m}_{tot}$: total mass flow of fluid [$kg \cdot s^{-1}$]

W : plate width [m]

b : pressing depth [m]

N_C : number of channels

d_h : hydraulic diameter [m]

  - Nusselt number (Nu)

$$Nu = \frac{h \cdot d_h}{k}$$

h : convection heat transfer coefficient [$W \cdot m^{-2} \cdot K^{-1}$]

d_h : hydraulic diameter [m]

k : thermal conductivity [$W \cdot m^{-1} \cdot K^{-1}$]

- Prandtl number (Pr)

$$Pr = \frac{C_p \cdot \mu}{k}$$

C_p : specific heat capacity [J·kg^{-1}·K^{-1}]

μ : dynamic viscosity [Pa·s]

k : thermal conductivity [W·m^{-1}·K^{-1}]

- Moody friction factor (f)

$$f = 2 \cdot \frac{\Delta p \cdot d_h}{\rho \cdot u^2 \cdot L}$$

Δp : specific heat capacity [J·kg^{-1}·K^{-1}]

d_h : hydraulic diameter [m]

ρ : density [kg·m^{-3}]

u : fluid velocity [m·s^{-1}]

L (L_{eff}) : length of channel [m]

- Convective heat transfer of the secondary fluid in the evaporator
  - Correlations for Nusselt number (Nu) estimation in PHEs for Reynolds values from 400 to 10,000 and for values less than 400:

$$Nu = 0{,}122 \cdot Pr^{\frac{1}{3}} \cdot \left(\frac{\mu}{\mu_w}\right)^{\frac{1}{6}} \cdot (f \cdot Re^2 \cdot \sin(2 \cdot \varphi))^{0{,}374} \qquad (Re = 400\text{-}10{,}000)$$

$$Nu = 0{,}44 \cdot \left(\frac{\varphi}{30}\right)^{0{,}38} \cdot Re^{0{,}5} \cdot Pr^{\frac{1}{3}} \cdot \left(\frac{\mu}{\mu_w}\right)^{0{,}14} \qquad (Re = <400)$$

Pr : Prandtl number [-]

μ : bulk viscosity [Pa·s]

μ_w : viscosity at wall temperature [Pa·s]

f : friction factor [-]

Re : Reynolds number [-]

φ : chevron angle [°]

- Pressure drop of the secondary fluid side of the evaporator
  - Pressure drop (Δp) on one channel, including geometric definitions of PHE, with all variables previously defined

$$\Delta p = f \cdot \frac{G^2 \cdot L_{eff}}{2 \cdot \rho \cdot d_h} \quad \text{where, } G = \rho \cdot u$$

  - To calculate the friction factor dependent on the chevron angle and Reynolds number

$$\frac{1}{\sqrt{f}} = \frac{\cos(\varphi)}{\sqrt{0{,}18 \cdot \tan(\varphi) + 0{,}36 \cdot \sin(\varphi) + \frac{f_0}{\cos(\varphi)}}} + \frac{1 - \cos(\varphi)}{\sqrt{3{,}8 \cdot f_{1{,}0}}}$$

where

$$f_0 = \begin{cases} {}^{64}/_{Re} & if\ Re < 2000 \\ (1{,}8 \cdot \log(Re) - 1{,}5)^{-2} & if\ Re \geq 2000 \end{cases}$$

$$f_{1,0} = \begin{cases} {}^{597}/_{Re} + 3{,}85 & if\ Re < 2000 \\ {}^{39}/_{Re^{0{,}289}} & if\ Re \geq 2000 \end{cases}$$

- Pressure drop in the inlet and outlet ports of each plate (Δp_{ports})

$$\Delta p_{ports} = 1{,}5 \cdot \left(\frac{G^2}{2 \cdot \rho}\right)_{inlet} \cdot N_{pass}$$

G_{inlet} : mass flux at inlet port [kg·m^{-2}·s^{-1}]

ρ : density [kg·m^{-3}]

N_{pass} : number of passes (typically 1 for evaporators)

- Boiling heat transfer phenomena (ammonia)
  - Heat transfer (h) on the boiling side

$$h = 0{,}025 \cdot C \cdot \left(\frac{k_l}{d_h}\right) \cdot \left(\frac{Re_l^2 \cdot h_{lg}}{L_{eff}}\right)^{0{,}4124} \cdot \left(\frac{P}{P_{crit}}\right)^{0{,}12} \cdot \left(\frac{65}{\beta}\right)^{0{,}35}$$

where

$$C = \begin{cases} 0{,}1121 & \text{for flooded evaporators} \\ 0{,}0675 & \text{for dry expansion (DX)} \end{cases}$$

k_l : thermal conductivity of the liquid [W·m^{-1}·K^{-1}]

d_h : hydraulic diameter [m]

Re_l^2 : Reynold number (liquid-state viscosity) [-]

h_{lg} : latent heat [J·kg^{-1}]

L_{eff} : effective length of one channel [m]

P : evaporation pressure [bar]

P_{crit} : critical pressure [bar]

β : complementary angle to chevron angle [°]

- Overall heat transfer coefficient and thermal resistance
  - Heat transfer coefficient (UA) in PHEs

$$\dot{Q} = UA \cdot \Delta T_{LMTD}$$

$\dot{Q}$: heat flow or cooling capacity [W]

ΔT_{LMTD} : log mean temperature difference [K]

  - Ammonia, the primary refrigerant, is an azeotropic mixture with a constant temperature if superheating in the evaporator is neglected, resulting in the following definition of the log mean temperature difference (ΔT_{LMTD}):

$$\Delta T_{LMTD} = \frac{T_{sec.fl.-in} - T_{sec.fl.-out}}{\ln\left(\frac{T_{sec.fl.-in} - T_{evap}}{T_{sec.fl.-out} - T_{evap}}\right)}$$

- The resistance (R) is defined as:

$$R = \frac{1}{UA}$$

- The heat transfer of a plate in the PHE is one-dimensional and similar to that of a plane wall, shown in the thermal resistance diagram, below. The total heat transfer resistance is the sum of the resistances and will be equivalent for each plate since they are in parallel in the PHE. To determine the overall heat transfer coefficient (UA):

$$UA = A \cdot \frac{N_P}{\frac{1}{h_{boil}} + \frac{\delta}{k} + \frac{1}{h_{sec.fl.}}}$$

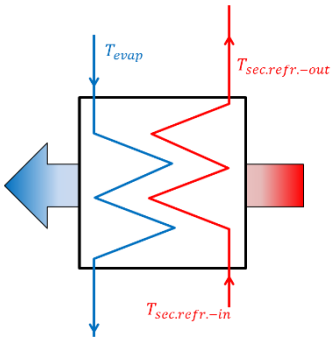

A : heat transfer area (single plate surface) [m²]

N_P : total number of plates in PHE

h_{boil} : boiling heat transfer coefficient [W·m^{-2}·K^{-1}]

δ : plate thickness [m]

k : thermal conductivity of plate [W·m^{-1}·K^{-1}]

$h_{sec.fl.}$: secondary fluid convective heat transfer coefficient [W·m^{-2}·K^{-1}]

Equations for Ice Rink Calculations

- Calculating the total volumetric flowrate ($\dot{V}_{tot}$) at a given cooling capacity:

$$\dot{V}_{tot} = \frac{\dot{Q}}{\Delta T \cdot \rho \cdot C_p}$$

$\dot{Q}$: cooling capacity [W]

ΔT : secondary fluid temperature difference [K]

ρ : density [kg·m^{-3}]

C_p : specific heat capacity [J·kg^{-1}·K^{-1}]

- The flowrate allows for the range of the Reynolds number (Re) inside the evaporator to be calculated:

$$Re = 4\frac{\dot{V}_{tot} \cdot \rho}{\pi \cdot d_h \cdot \mu}$$

$\dot{V}_{tot}$: volumetric flowrate [m^3·s^{-1}]

ρ : density [kg·m^{-3}]

d_h : hydraulic diameter [m]

μ : dynamic viscosity [Pa·s]

- The flowrate allows for the range of the Reynolds number (Re) inside the distribution pipes in the ice rink floor to be calculated:

$$Re = 4\frac{\dot{V}_{tot} \cdot \rho}{N_{U-pipes} \cdot \pi \cdot d_h \cdot \mu}$$

$\dot{V}_{tot}$: volumetric flowrate [$m^3 \cdot s^{-1}$]

ρ : density [$kg \cdot m^{-3}$]

$N_{U-pipes}$: number of U-pipes

d_h : hydraulic diameter [m]

μ : dynamic viscosity [Pa·s]

- The polynomial approximation tool in *Excel* was used to obtain functions of input data of the secondary fluids versus temperature. These functions were then used to determine evaporation temperature. The variables needed for the calculations are as follows:
  - h_l and h_g : enthalpies at the saturated liquid and vapor states [$J \cdot kg^{-1}$]
  - v_l : specific volume at saturated liquid state [$m^3 \cdot kg^{-1}$]
  - k_l : thermal conductivity at saturated-liquid state [$W \cdot m^{-1} \cdot K^{-1}$]
  - μ_l : dynamic viscosity at saturated-liquid state [Pa·s]
  - P : evaporation pressure (absolute) [bar]
  - COP_{is} : isentropic coefficient of performance [-]
  - $h_{superheat}$: enthalpy of superheated fluid after evaporation [$J \cdot kg^{-1}$]
  - $h_{subcool}$: enthalpy of subcooled (saturated) fluid after condensation [$J \cdot kg^{-1}$]
  - The enthalpies of the superheated fluid and subcooled fluid were determined using *EES Property Calculator Software*.

- The cooling capacity is used to calculate the primary refrigerant mass flow ($\dot{m}$):

$$\dot{m} = \frac{\dot{Q}}{h_{superheat} - h_{subcool}}$$

$\dot{Q}$: cooling capacity [W]

$h_{superheat}$: enthalpy of superheated fluid [$J \cdot kg^{-1}$]

$h_{subcool}$: enthalpy of subcooled (saturated) fluid [$J \cdot kg^{-1}$]

- Reynolds number (Re_{lo}) used for the heat transfer (h) on the boiling side (all variables previously defined with the mass flow and viscosity referring to the primary refrigerant, ammonia):

$$Re_{lo} = \frac{G \cdot d_h}{\mu_l} = 2 \cdot \frac{\dot{m}}{W_{plate} \cdot b \cdot N_C} \cdot \frac{d_h}{\mu_l}$$

- The number of U-pipes ($N_{U-pipes}$) in the ice floor:

$$N_{U-pipes} = \frac{W_{ice}}{D_{spacing}}$$

W_{ice} : ice pad width [m]

$D_{spacing}$: distance between two consecutive pipes [m]

- The total heat transfer in the ice rink floor has both convection and conduction mechanisms. Depending on the type of flow, turbulent or laminar, different equations are used.
    - When the flow is turbulent and the Reynolds number (Re) is greater than 2300, the Nusselt number (Nu) is calculated:

$$Nu = \frac{\frac{f}{8} \cdot (Re - 1000) \cdot Pr}{1 + 12{,}7 \cdot \left(\frac{f}{8}\right)^{0{,}5} \cdot \left(Pr^{\frac{2}{3}} - 1\right)}$$

f : friction factor [-]

Pr : Prandtl number [-]

when the flow is fully developed with a maximum entry length ($x_{fd,max}$) for turbulent flow calculated by:

$$x_{fd,max} = 60 \cdot D_{in}$$

D_{in} : pipe inner diameter [m]

    - For laminar flow, the Nusselt number (Nu) with calculated with:

$$Nu = 3{,}66 + \frac{0{,}0668 \cdot Gz}{1 + 0{,}04 \cdot Gz^{\frac{2}{3}}}$$

where the Graetz number (Gz) is:

$$Gz = \left(\frac{D_{in}}{L}\right) \cdot Re \cdot Pr$$

D_{in} : pipe inner diameter [m]

L : pipe length [m]

Re : Reynolds number [-]

Pr : Prandtl number [-]

assuming a constant surface temperature of the inner wall and maximum entry length ($x_{fd,h}$) of:

$$x_{fd,h} = Re \cdot D_{in} \cdot 0{,}05$$

D_{in} : pipe inner diameter [m]

    - Conduction equivalent resistance (R_{cond}) in the ice floor is calculated using:

$$R_{cond} = \frac{\Delta T}{\Phi}$$

ΔT : temperature difference between the averages of the top of the ice and inner pipe wall [K]

Φ : heat flow [W·m^{-1}]

    - The total heat transfer resistance ($R_{ice-floor}$) is calculated using:

$$R_{ice-floor} = \frac{R_{cond} + \frac{1}{h \cdot \pi \cdot D_{in}}}{L \cdot N_{U-pipes}}$$

R_{cond} : conduction resistance [m·K·W^{-1}]

h : convection heat transfer coefficient [W·m^{-2}·K^{-1}]

D_{in} : pipe inner diameter [m]

L : U-pipe length [m]

$N_{U-pipes}$: total number of U-pipes

- In the ice rink floor, the heating loads are less than the cooling capacity, so a different equation is used to calculate the log mean temperature difference:

$$\Delta T'_{LMTD} = \frac{T_{sec.refr.-in} - T'_{sec.refr.-out}}{\ln\left(\frac{T_{sec.refr.-in} - T_{evap}}{T'_{sec.refr.-out} - T_{evap}}\right)}$$

- Pressure drop characterization in the distribution pipes
  - The friction factor (f) for turbulent flow, Reynolds number greater than 2300:

$$f = (0{,}79 \cdot \ln(Re) - 1{,}64)^{-2}$$

  - The friction factor (f) for laminar flow, also known as Poiseuille's law:

$$f = \frac{64}{Re}$$

  - Weisbach's formula is used to calculate pressure drop and determines the minor loss coefficient (K) of any bend with:

$$K = \left(\left(0{,}131 + 1{,}847 \cdot \left(\frac{D_{in}}{2 \cdot r}\right)^{3{,}5}\right) \cdot \frac{\theta}{90}\right)$$

D_{in} : pipe inner diameter [m]

r : bend radius of curvature [m]

θ : bend angle [°]

  - The pressure drop is calculated in the supply and return pipes and must consider the pumping power associated at the inlet ($\left(\Delta p_f \cdot \dot{V}\right)_{in}$), outlet ($\left(\Delta p_f \cdot \dot{V}\right)_{out}$), and with minor losses ($\left(\Delta p_s \cdot \dot{V}_{in}\right)$) from the T-junction. The total pumping power ($E_{p,header}$) is the sum of the pumping power requires for each motif. For each motif, i:

$$\left(E_{p,header}\right)_i = \frac{\left(\Delta p_{header} \cdot \dot{V}\right)_i}{e_{pump}}$$

where

$$\left(\Delta p_{header} \cdot \dot{V}\right)_i = \left(\Delta p_f \cdot \dot{V}\right)_{in,i} + \left(\Delta p_f \cdot \dot{V}\right)_{out,i} + \left(\Delta p_s \cdot \dot{V}_{in}\right)_i$$

e_{pump} : pump efficiency [-]

Δp_f : major head loss [Pa]

Δp_s : minor head loss [Pa]

$\dot{V}$: secondary fluid flowrate [$m^3 \cdot s^{-1}$]

  - The header has as many motifs as there are U-pipes. The minor loss coefficient can be calculated by:

$$K_i = \lambda_1 + (2 \cdot \lambda_2 - \lambda_1)\left(\frac{\dot{V}_{out,i}}{\dot{V}_{in,i}}\right)^2 - 2 \cdot \lambda_2 \cdot \left(\frac{\dot{V}_{out,i}}{\dot{V}_{in,i}}\right) \cdot \cos(\alpha')$$

where

$$\lambda_1 = \begin{cases} 0{,}0712 \cdot \alpha^{0{,}7141} + 0{,}37 & for\ \alpha < 22{,}5° \\ 1 & for\ \alpha \geq 22{,}5° \end{cases}$$

$$\lambda_2 = \begin{cases} 0{,}0592 \cdot \alpha^{0{,}7029} + 0{,}37 & for\ \alpha < 22{,}5° \\ 0{,}9 & for\ \alpha \geq 22{,}5° \end{cases}$$

$$\alpha' = 1{,}41\alpha - 0{,}00594\alpha^2$$

- The total pumping power for the header ($\left(\dot{E}_{p,header}\right)_{tot}$) is expressed as:

$$\left(\dot{E}_{p,header}\right)_{tot} = \frac{\left(\Delta p \cdot \dot{V}\right)_{tot}}{e_{pump}}$$

where

$$\left(\Delta p \cdot \dot{V}\right)_{tot} = 8 \cdot \frac{\rho}{\pi^2} \cdot \frac{1}{d_h^4} \cdot \left(\frac{\dot{V}_{tot}}{150}\right)^3 \left\{ \frac{L}{d_h} \sum_{j=1}^{150} \left(f'_{in,j} \cdot j^3\right) + 0{,}37 \cdot \frac{150 \cdot 151}{2} \right\}$$

ρ : density [kg·m^{-3}]

d_h : hydraulic diameter [m]

$\dot{V}_{tot}$: total secondary fluid volumetric flowrate [m^3·s^{-1}]

L : length of one motif [m]

$f'_{in,j}$: friction factor of inlet section, *j* [-]

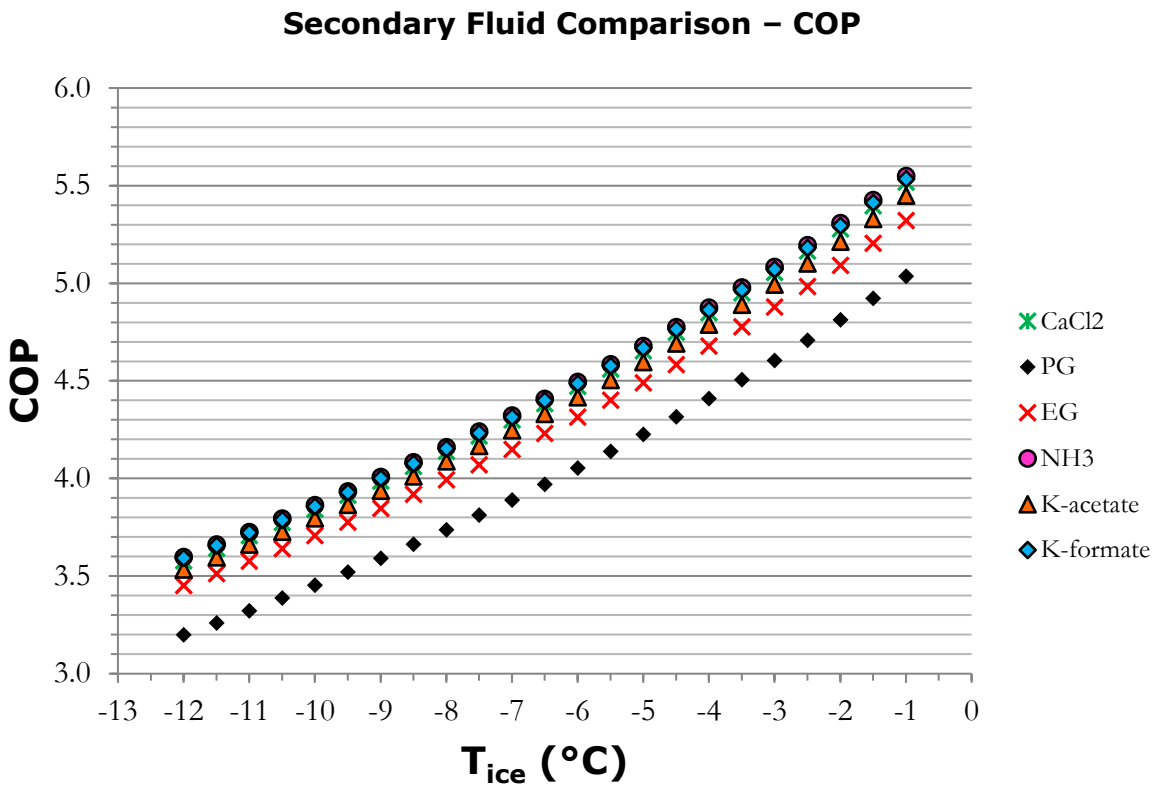

Figure 57: COP vs. T_{ice} (CC = 100 kW, T_f = -25°C, ⊿T = 2K).

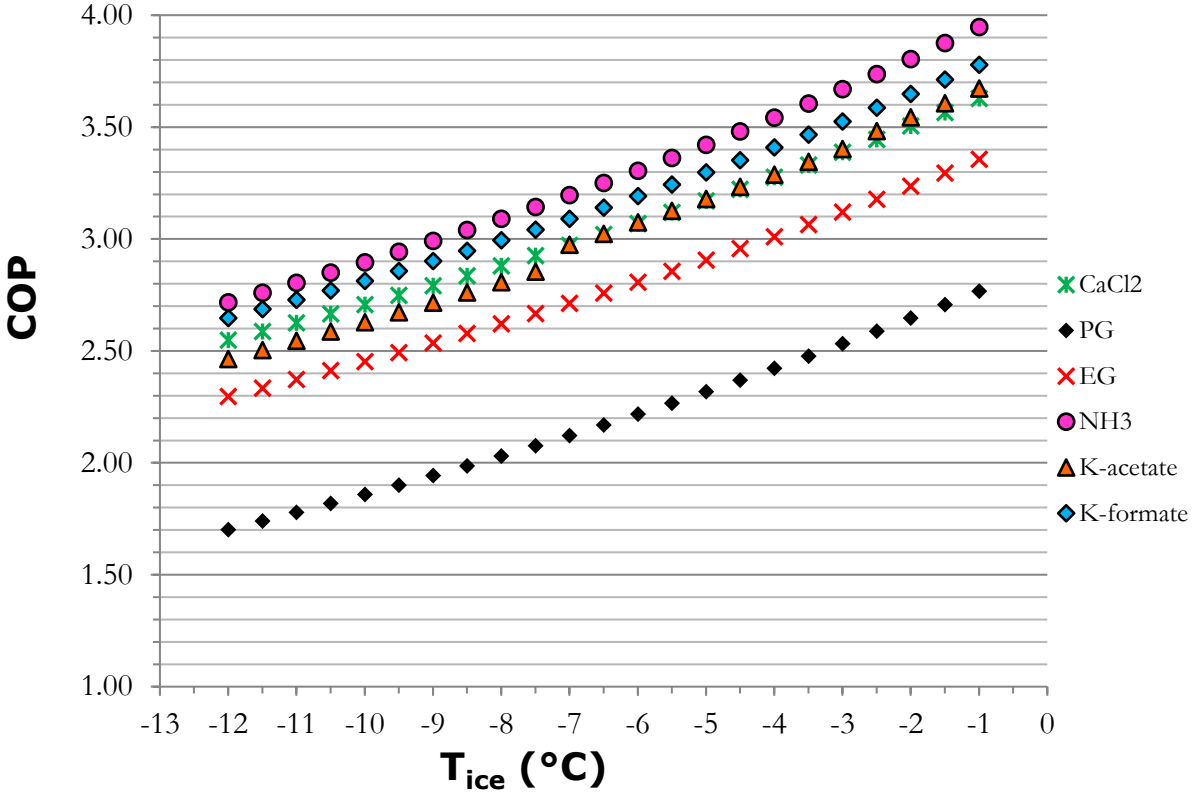

Figure 58: COP vs. T_{ice} (CC = 300 kW, T_f = -25°C, ⊿T = 2K).